Title
Therapeutic Manipulation of Central T cell Tolerance

Permalink
https://escholarship.org/uc/item/7wc5n3v9

Author
Khan, Imran Saeed

Publication Date
2014

Peer reviewed|Thesis/dissertation

Therapeutic Manipulation of Central
T cell Tolerance

by

Imran S. Khan

DISSERTATION

Submitted in partial satisfaction of the requirements for the degree of

DOCTOR OF PHILOSOPHY

in

Biomedical Sciences

in the

GRADUATE DIVISION

of the

UNIVERSITY OF CALIFORNIA, SAN FRANCISCO

Acknowledgements

I begin by thanking Mark Anderson, my thesis advisor, for his ongoing support and guidance throughout my tenure in his lab. His optimistic outlook and positive attitude have contributed to a wonderful lab environment where everyone is eager to contribute their ideas and always willing to collaborate. I would also like to thank Abul Abbas and Mark Ansel, members of my thesis committee, for providing critical feedback throughout my thesis research and for helping guide my work to its completion. I also thank Lukas Jeker for the privilege of working with him on Chapters 2 and 3 of this work. Lukas has been a valuable mentor to me throughout my tenure in the lab and I have benefited substantially from his wisdom, his guidance, and his critical eye in evaluating scientific data.

I thank members of the Anderson Lab for their intellectual contributions and technical assistance throughout my time in the lab. More importantly, I thank them for creating a friendly work environment such that I look forward to coming to work each day. In particular, I thank Maria Mouchess, with whom I have had the pleasure of collaborating with on the data presented in Chapter 2 of this work. I also thank Todd Metzger, who mentored me when I first joined the lab and taught me many secrets of the thymic stromal preparation protocol.

I also thank my parents and siblings for their steady encouragement throughout my dissertation. Lastly, I thank my wife for her unwavering love and support throughout my time in the lab. Her constant reinforcement and optimistic outlook have carried me through both high and low, and this work would not have been possible without her unconditional support.

Contributions of Co-authors to the Presented Work:

Chapter 2 of this dissertation is based largely on work that has been prepared and submitted as a manuscript entitled "Enhancement of an anti-tumor immune response by transient blockade of central T cell tolerance". This project was performed in full collaboration with Maria Mouchess[1], who contributed equally to the entirety of this work. The other co-authors of this manuscript include Meng-Lei Zhu[2], Bridget Conley[2], Kayla J. Fasano[1], Yafei Hou[3,4], Larry Fong[3,4], and Maureen A. Su[2]. Meng-Lei Zhu, Bridget Conley, and Maureen A. Su assisted with and supervised the initial tumor studies in TRP-1 mice. Kayla J. Fasano performed the H&E staining and autoantibody assays. Yafei Hou and Larry Fong assisted with and supervised tumor studies in B6 mice and tumor cell injections. Mark S. Anderson[1] supervised the entirety of this work.

Chapter 3 of this dissertation was published as "Canonical microRNAs in thymic epithelial cells promote central tolerance" in *European Journal of Immunology*. 2014 Feb 10; Epub ahead of print. Co-authors of this study include Ruth T. Taniguchi[1] and Kayla J. Fasano[1]. Ruth T. Taniguchi assisted with immunization and tetramer-pulldown assays. Kayla J. Fasano performed the H&E staining and autoantibody assays. Both Mark S. Anderson[1] and Lukas T. Jeker[1,4,5] supervised the entirety of this work.

Chapter 4 of this dissertation was prepared as a manuscript entitled "miR-205 is Highly Expressed in Medullary Thymic Epithelial Cells but its Role in the Postnatal Thymus Remains Unclear". Co-authors of this study include Chong Y. Park[1,6], Anastasia Mavropoulos[1,4], Nikki Shariat[1,6,7], Joshua L. Pollack[4], David J. Erle[4], and Michael T. McManus[1,6,7]. Chong Y. Park, Nikki Shariat and Michael T. McManus performed and supervised work pertaining to the generation of miR-205 targeted mice and the initial characterization of lacZ staining. Anastasia Mavropoulos assisted with *in situ* hybridizations. Microarray analysis was performed by the UCSF Sandler Center Functional Genomics Core Facility and data was analyzed by Joshua L. Pollack and David J. Erle. Both Mark S. Anderson[1] and Lukas T. Jeker[1,4,5] supervised the entirety of this work.

[1]UCSF Diabetes Center, University of California, San Francisco, CA.

[2]Department of Pediatrics and Microbiology/Immunology, School of Medicine, and Lineberger Comprehensive Cancer Center, University of North Carolina at Chapel Hill, Chapel Hill, NC.

[3]Division of Hematology/Oncology, University of California, San Francisco, CA.

[4]Department of Medicine, University of California, San Francisco, CA.

[5]Department of Pathology, University of California, San Francisco, CA.

[6]WM Keck Center for Noncoding RNAs, University of California, San Francisco, CA.

[7]Department of Microbiology and Immunology, University of California, San Francisco, CA.

Therapeutic Manipulation of Central

T cell Tolerance

Imran S. Khan

Abstract

Thymic central tolerance is a critical process that prevents autoimmunity, but also presents a challenge to the generation of anti-tumor immune responses. Medullary thymic epithelial cells (mTECs) eliminate self-reactive T cells by displaying a diverse repertoire of tissue-specific antigens (TSAs) that are also shared by tumors. Therefore, while protecting against autoimmunity, mTECs simultaneously limit the generation of tumor-specific effector T cells by expressing tumor self-antigens. This ectopic expression of TSAs largely depends on autoimmune regulator (Aire), which is expressed in mature mTECs. Thus, therapies to deplete *Aire*-expressing mTECs represent an attractive strategy to increase the pool of tumor-specific effector T cells. Recent work has implicated the TNF family members RANK and RANK-Ligand (RANKL) in the development of *Aire*-expressing mTECs. Here, we show that *in vivo* RANKL blockade selectively and transiently depletes *Aire* and TSA expression in the thymus to create a window of defective negative selection. Further, we demonstrate that RANKL blockade can rescue melanoma-specific T cells from thymic deletion and that persistence of these tumor-specific effector T cells promoted increased host

survival in response to tumor challenge. These results indicate that modulating central tolerance through RANKL can alter thymic output and potentially provide therapeutic benefit by enhancing anti-tumor immunity. Finally, in an effort to identify novel genes and signaling pathways required for thymic function, we demonstrate that canonical microRNAs (miRNAs) are required in TECs to maintain proper thymic architecture and to support the maintenance of central tolerance. By understanding which miRNAs are important for these functions, we hope to uncover new targets and regulatory pathways for therapeutic intervention in the thymus.

Table of Contents

Chapter 3

Canonial microRNAs in Thymic Epithelial Cells Promote Central Tolerance

Chapter 4

miR-205 is Highly Expressed in Medullary Thymic Epithelial Cells but its Role in the Postnatal Thymus Remains Unclear

Chapter 5

Discussion and Concluding Remarks

Appendix

Selected Protocols

List of Figures

Chapter 4

Chapter 5

Chapter 1: Introduction

T cells play a critical role in supporting the immune system's ability to defend against invading pathogens. A major hallmark of T cell function is the genetically-encoded specificity by which T cells encounter and recognize their cognate antigens. This specificity, however, creates a unique challenge for the production of a diverse T cell repertoire that is sufficient to protect our bodies against the broad range of infectious agents that we may encounter in our lifetime. To meet this challenge, random recombination events take place during T cell development which ensure the generation of T cell receptors (TCRs) capable of recognizing a limitless number of pathogens. While this process enables the potential recognition of a vast array of foreign antigens, many T cells will also come to bear TCRs that can recognize self-antigens and provoke autoimmune disease. To solve this dilemma, the thymus imposes central tolerance, a process by which self-reactive T cells are either purged from the developing T cell repertoire or recruited into the regulatory T cell lineage.

As we begin to understand more about central tolerance, it is clear that that T cell development depends on the integrity of the thymic stromal microenvironment. Cortical and medullary thymic epithelial cells (TECs) mediate the positive and negative selection of developing thymocytes, respectively, to ensure the production of both functional and self-tolerant T cells. Understanding the regulation of TEC function is essential for the

development of therapeutic interventions to modulate thymic function in order to improve outcomes in disease. In the context of autoimmunity and organ transplantation, boosting thymic function could be applied as an intervention to "re-impose" self-tolerance on a T cell repertoire that is mediating tissue destruction. In aging and bone marrow transplantation, promoting TEC regeneration could help produce new T cells and limit the morbidity and mortality associated with opportunistic infections during periods of compromised immunity. On the other hand, transiently suppressing central tolerance could be applied as a strategy to enhance the anti-tumor immune response by rescuing tumor self-antigen specific T cells from deletion in the thymus and allowing them to escape into the periphery. Given the current interest in manipulating peripheral tolerance for cancer immunotherapy, it is of great interest to determine whether combination therapies targeting both central and peripheral tolerance could further enhance anti-tumor immune responses. Furthermore, understanding the genes and pathways important for regulating TEC function represents an essential step towards successful manipulation of thymic function.

Positive and negative selection of thymocytes

T cells are derived from hematopoietic precursors which originate in the bone marrow and migrate to the thymus to undergo maturation [1]. Within the thymus, thymocyte development is a two-step process in which positive selection takes place in the cortex and negative selection subsequently occurs

in the medulla [1, 2]. In the cortex, early T cell precursors receive instructive signals from the resident stromal population which includes cortical thymic epithelial cells (cTECs) [1, 2]. As these T cell precursors commit to the αβ T cell lineage, they undergo maturation in the cortex by first rearranging a functional TCR β-chain and then the TCR α-chain [3, 4]. The αβ TCR heterodimer is expressed on the cell surface along with both CD4 and CD8 co-receptors during the double positive (DP) stage of thymocyte development [1]. DP thymocytes with TCRs capable of recognizing peptide-major histocompatibility complex (MHC) complexes on cTECs receive survival signals and are positively selected, while those unable to recognize self-MHC or with overly strong affinity for self-MHC undergo apoptosis [1, 5, 6]. This process of positive selection is necessary to ensure the generation of functional TCR signaling complexes and also to restrict the T cell repertoire to T cells capable of recognizing self-MHC haplotypes.

After completing positive selection and committing to either the CD4 or CD8 single-positive lineage (SP), SP thymocytes migrate to the medulla and undergo negative selection [2]. Negative selection is mediated by the direct or indirect presentation of tissue specific antigens (TSAs) by medullary thymic epithelial cells (mTECs) and dendritic cells, respectively [7-10]. Through recognition of these TSAs, whose expression is normally limited to peripheral tissues, autoreactive T cells are either negatively selected from the pool of developing thymocytes or recruited into the T regulatory cell lineage [11-19]. This process of negative selection eliminates thymocytes with self-reactivity

and is necessary to maintain self-tolerance within the T cell repertoire. The importance of this process is highlighted by mice deficient for either RelB or TRAF6, as these mice show defects in the formation of the thymic medulla and develop severe multi-organ autoimmunity [20-25]. Thus, both positive selection in the cortex and negative selection in the medulla are necessary to ensure the development of both a functional and self-tolerant repertoire of T cells capable of protecting against infectious agents and preventing autoimmune disease.

Aire drives tissue-specific antigen expression in the thymus

The transcriptional activator autoimmune regulator (Aire) was originally identified as the causative gene in the monogenic autoimmune disease Autoimmune Polyglandular Syndrome type 1 (APS1), also known as Autoimmune Polyendocrinopathy-Candidiasis-Ectodermal Dystrophy (APECED) [26, 27]. Patients with APS1 develop multi-organ autoimmunity including hypoparathyroidism, adrenal insufficiency, chronic mucocutaneous candidiasis, and ectodermal dystrophy [28]. The expression of Aire was mapped primarily to the thymic medulla which suggested that Aire might play a role in T cell tolerance [29, 30]. Similar to APS1 patients, Aire-deficient mice also develop multi-organ autoimmunity, which further supports a role for Aire in maintaining T cell tolerance [31, 32].

Since these early studies, many groups have shown that ectopic TSA expression in the thymus is largely dependent on Aire [11, 32]. Several studies have shown that the Aire-dependent expression of individual self-antigens in

the thymus is necessary to prevent organ-specific autoimmunity [13-15, 17, 33]. Within the thymus, Aire is expressed in a mature subset of mTECs which are characterized by high levels of both MHC II and the co-stimulatory molecule CD80 (Figure 1.1A) [34-36]. BrdU incorporation and lineage tracing studies have together shown that Aire is expressed during the terminal stages of mTEC maturation [34, 37, 38]. As mTECs undergo maturation, they upregulate MHC II and Aire such that they begin their development as mTEC^{lo} (MHC II^{lo} Aire^{-}) cells and transition through the mTEC^{hi} (MHC II^{hi}, Aire^{-}) stage and eventually become Aire^{+} (MHC II^{hi}, Aire^{+}) cells [34-36]. Interestingly, recent work has identified a post-Aire stage of mTEC maturation which is characterized by intermediate levels of MHC II and TSA expression, but the functional role of these cells remains unclear [37-39].

Thymocyte-mTEC crosstalk regulates thymic development

Much of the focus on T cell development and central tolerance induction revolves around the instructive signals provided by the thymic stromal microenvironment to facilitate the survival, differentiation or deletion of developing thymocytes. Recent work, however, illustrates a much more complex interplay by which thymocytes provide reciprocal interactions to help maintain the thymic medulla. Early evidence for this relationship was observed in mice lacking TCRα or ZAP-70, whereby thymocyte maturation is impaired prior to the DP stage and the resulting thymic medulla contains limited clusters of mTECs [40-43]. Interestingly, mice with defects in CCR7 or CCR7 ligands

have impaired migration of SP thymocytes from the cortex to the medulla and show similar defects in mTEC development and negative selection [44-46]. The latter of these observations suggests that even when positive selection is maintained, the migration of SP thymocytes to the medulla is necessary to maintain mTEC cellularity and proper negative selection.

More recent studies have found that in addition to promoting positive selection, TCR signaling in thymocytes also drives the expression of a number of TNF super-family (TNFSF) cytokines including RANK ligand (RANKL), CD40 ligand (CD40L) and lymphotoxin (LT) [47-50]. Interestingly, the expression of these cytokines is higher in SP thymocytes compared to DP thymocytes, and their cognate receptors such as RANK and CD40 are expressed preferentially in mTECs compared to cTECs [47-49, 51]. Furthermore, mice deficient for RANK or RANKL show defects in mTEC development, while forced expression of RANKL in the absence of positive selection can rescue defects in the mTEC compartment [47, 52, 53]. Interestingly, mTECs also express Osteoprotegerin (OPG), a soluble decoy receptor for RANKL which regulates RANK-RANKL signaling, and OPG-deficient mice show increased mTEC cellularity [47]. Proper embryonic development of the thymic medulla also depends on RANKL signals provided by lymphoid tissue-inducer (LTi) cells and invariant γδ-T cell progenitors, as evidence by the reduction of Aire[+] mTECs in RORγ-deficient mice which lack LTi cells [51, 52, 54].

The importance of these reciprocal interactions is highlighted by the breakdown in central tolerance and subsequent autoimmunity in mice deficient

for these signaling components. For example, both RANK and CD40 signal downstream through the nonclassical NF-κB pathway, and mice deficient for RelB or TRAF6 show impaired mTEC development and develop autoimmunity [20-25]. Together, these studies suggest a model in which the development and maintenance of the thymic medulla is dependent on TNFSF cytokine signals provided by positively selected thymocytes and LTi cells. Proper embryonic development of mTECs requires RANKL production by LTi cells while maintenance of the post-natal thymus likely depends on continuous input from positively selected thymocytes in the form of RANKL, CD40L and LT (Figure 1.1A). However, the majority of work implicating the TNFSF cytokines has focused on thymic development, and thus the exact role of these pathways in maintaining the post-natal mTEC compartment remains unclear.

Dynamic turnover and recovery in the thymus

The thymus is a highly dynamic organ which undergoes involution in response to both physiologic and pathologic conditions of stress [55, 56]. Across many vertebrate species, the thymus undergoes gradual age-associated involution in a manner that is partially dependent on sex hormones [56, 57]. Similarly, pregnancy hormones have been associated with transient periods of thymic involution accompanied by decreased thymocyte and TEC proliferation [58, 59]. In more dramatic fashion, however, the thymus also undergoes acute thymic involution in response to infection, inflammatory cytokines, irradiation, and stress hormones [60-65]. In many of these more

acute examples, thymic involution comes at the expense of DP thymocyte apoptosis [60, 62, 66, 67]. Given the critical role of SP thymocytes in maintaining the mTEC compartment, it seems likely that DP thymocyte depletion can also disrupt the mTEC compartment by reducing the availability of cytokine crosstalk signals from positively selected thymocytes.

Remarkably, the thymus also has robust regenerative potential which enables it to rebound from many periods of transient involution. Recent work has shown that the both mTECs and cTECs represent a highly dynamic population with continuous cycling and turnover in the postnatal thymus [34, 37, 62, 68]. A combination of BrdU incorporation and lineage tracing studies has estimated that the turnover of mTECs in the adult thymus is roughly 7-10 days [34, 37, 38]. Other groups have utilized TEC-specific ablation models to show that both mTECs and cTECs can rapidly proliferate to repopulate their thymic niche [37, 62, 69]. Given the wide variety of insults that can cause thymic involution, it is of great interest to identify signaling pathways that could aid in the recovery of TECs from thymic injury. Of note, one recent study found that IL-22 production by thymic LTi cells was necessary for both TEC and thymocyte recovery following sub-lethal doses of irradiation [61]. Similarly, keratinocyte growth factor (KGF) is required for recovery following hematopoietic bone marrow transplantation, and KGF can be administered exogenously to drive TEC proliferation and speed up the recovery of thymopoiesis following bone marrow transplantation [70, 71]. Taken together, these findings demonstrate the remarkable ability of the thymus to respond to

environmental stimuli and suggest that targeting thymic function can be harnessed to improve outcomes in human disease.

Furthermore, recent work has begun to characterize a putative TEC progenitor population in the adult thymus with properties reminiscent of the slow-cycling, quiescent stem cell population recently characterized in skin epithelium [72-75]. These reports suggest that a pool of TEC progenitors resides within the immature MHC II^{lo} TEC population, and they provide evidence that these progenitors can give rise to mature mTEC and cTEC lineages *in vitro* [73, 75]. Earlier work confirmed the existence of a bi-potent TEC progenitor cell in the fetal thymus, and these recent studies have expanded these observations to the post-natal thymus [76, 77]. Further work is necessary to demonstrate the bi-potent differentiation potential of these TEC progenitor cells through *in vivo* thymic grafting studies. It also remains unclear whether these progenitor cells are required in TECs for recovery from thymic damage. Understanding how these pools of progenitor cells are maintained and the signals which drive their differentiation will be critical in developing novel therapies to manipulate thymic function.

MicroRNA regulation of thymic function

MicroRNAs (miRNAs) are ~22 nucleotide noncoding RNAs that mediate post-transcriptional repression of genes in a sequence-dependent manner [78, 79]. Primary miRNA transcripts are processed by the DROSHA /DGCR8 complex to generate ~60-80nt hairpin precursor miRNAs [80]. These hairpins

are further processed in the cytoplasm by Dicer to produce mature miRNAs. Mature miRNAs contain a "seed sequence" at nucleotide positions 2-8, and this seed sequence mediates repression through complementary base-pairing within the 3'-untranslated region (UTR) of target mRNAs. Each miRNA can target hundreds of mRNAs, and each mRNA can in turn be regulated by many miRNAs [79, 80]. Thus, miRNAs represent key regulators of gene networks and can be exploited to discover novel pathways.

Recent work by our group and others has shown that miRNA-deficiency in TECs causes a severe disruption of thymic function which leads to the breakdown of central tolerance [81-84]. However, the individual miRNAs responsible for these phenotypes and their precise mechanisms of action remain largely unknown. Identifying the specific miRNAs which are important for TEC biology will allow us to investigate novel networks of genes that are important for establishing and maintaining central tolerance. Understanding these novel pathways will provide new insight into the regulation of the thymic microenvironment and will contribute to the discovery of therapeutic targets to modulate thymocyte development and central tolerance.

Summary

The thymus plays an essential role in producing a diverse, functional T cell repertoire while maintaining self-tolerance to prevent autoimmunity. There is ongoing interest however, to discovery ways in which we can manipulate thymic function to improve outcomes in human disease. For example, although

central tolerance provides protection against autoimmunity, this process also represents a challenge for anti-tumor immunity [16, 85]. Since many of the TSAs expressed in the thymus are also expressed in tumors, high-affinity effector T cells capable of recognizing tumor self-antigens may normally be deleted in the thymus [86-89]. Transiently suppressing central tolerance by depleting mTECs or modulating *Aire* expression may provide a therapeutic window for the generation of T cells capable of recognizing tumor self-antigens. Modulating central tolerance requires an understanding of key biologic pathways that play an important role in regulating TEC function. Chapter 2 of this work explores the therapeutic implications of suppressing central tolerance by targeting RANK-RANKL interactions that are necessary to maintain mTEC function in the thymus. The contribution of TNFSF signaling in the thymus has been well described, but prior to this work it remained unclear whether these cytokine networks were required in the post-natal thymus and whether they could be manipulated *in vivo*. Chapters 2 and 3 of this work take a discovery approach to identify novel genes and networks that play an important role in regulating TEC function. Specifically, Chapter 2 focuses on the contribution of canonical miRNAs in TEC function, and Chapter 3 addresses a candidate miRNA, miR-205, in its ability to regulate mTEC function. Finally, the overall findings of this work are discussed in Chapter 5 along with some suggestions for further areas of investigation.

Figure 1.1. Current model of mTEC maturation

(A) Under the current model of mTEC maturation, immature mTECs upregulate levels of MHC II and CD80 before reaching the mature Aire$^+$ stage of maturation. RANKL signals are provided by LTi cells, invariant γδ-T cell progenitors during embryonic development and are necessary for the induction and maintenance of Aire+ mTECs. In the post-natal thymus, positively selected thymocytes maintain this cytokine signaling to support the maintenance of the mature mTEC population. Figure is adapted from Tykocinski, L. *et al*. [90]

Figure 1.1

A)
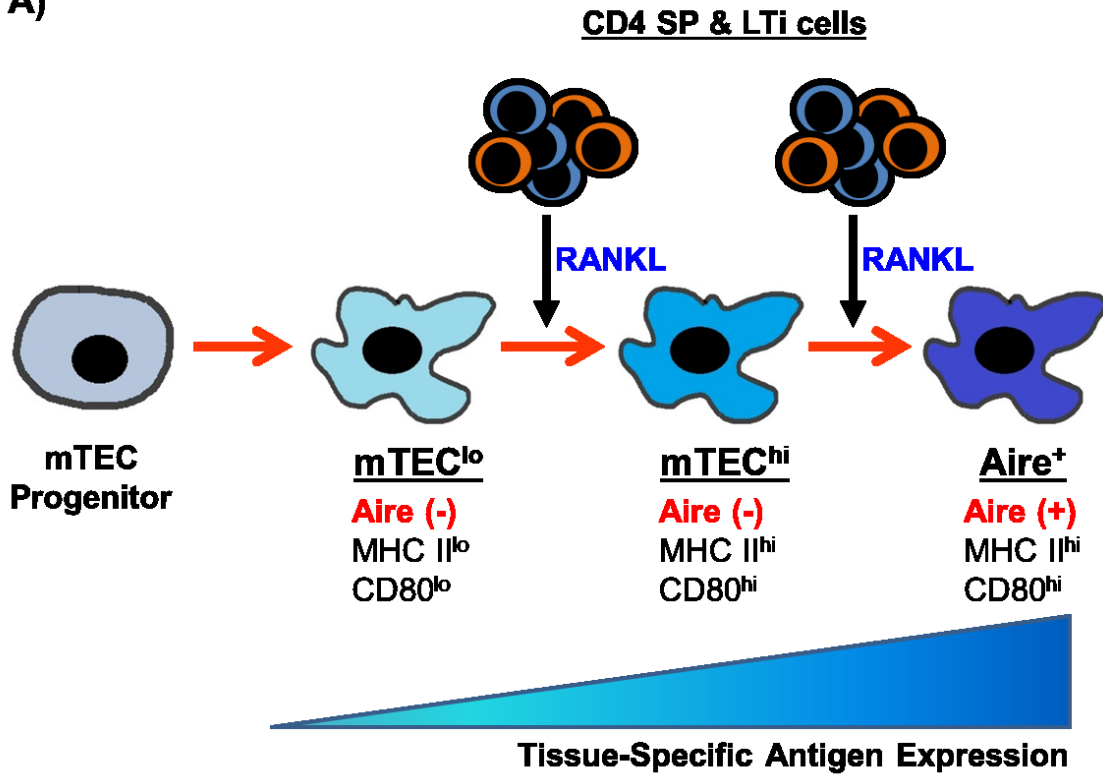
Chapter 2: Enhancement of an Anti-tumor Immune Response by Transient Blockade of Central T cell Tolerance

<u>Abstract</u>

Thymic central tolerance is a critical process that prevents autoimmunity, but also presents a challenge to the generation of anti-tumor immune responses. Medullary thymic epithelial cells (mTECs) eliminate self-reactive T cells by displaying a diverse repertoire of tissue-specific antigens (TSAs) that are also shared by tumors. Therefore, while protecting against autoimmunity, mTECs simultaneously limit the generation of tumor-specific effector T cells by expressing tumor self-antigens. This ectopic expression of TSAs largely depends on autoimmune regulator (Aire), which is expressed in mature mTECs. Thus, therapies to deplete *Aire*-expressing mTECs represent an attractive strategy to increase the pool of tumor-specific effector T cells. Recent work has implicated the TNF family members RANK and RANK-Ligand (RANKL) in the development of *Aire*-expressing mTECs. Here, we show that *in vivo* RANKL blockade selectively and transiently depletes *Aire* and TSA expression in the thymus to create a window of defective negative selection. Further, we demonstrate that RANKL blockade can rescue melanoma-specific T cells from thymic deletion and that persistence of these tumor-specific effector T cells promoted increased host survival in response to tumor

challenge. These results indicate that modulating central tolerance through RANKL can alter thymic output and potentially provide therapeutic benefit by enhancing anti-tumor immunity.

Introduction

Medullary thymic epithelial cells (mTECs) contribute to self-tolerance through the ectopic expression of tissue-specific antigens (TSAs) in the thymus [13, 18, 32, 91]. This TSA expression in mTECs is largely dependent on autoimmune regulator (Aire), which is expressed in mature mTECs [34, 35, 91]. Through the recognition of TSAs, developing autoreactive T cells are either negatively selected from the pool of developing thymocytes or recruited into the regulatory T cell lineage [11-16]. The overall importance of this process is underscored by the development of a multi-organ autoimmune syndrome in patients or mice with defective *AIRE* expression [26, 27, 32].

Although central tolerance provides protection against autoimmunity, this process also represents a challenge for anti-tumor immunity [16, 85]. Since many of the TSAs expressed in the thymus are also expressed in tumors, high-affinity effector T cells capable of recognizing tumor self-antigens may normally be deleted in the thymus [86-89]. Transiently suppressing central tolerance by depleting mTECs or modulating *Aire* expression may provide a therapeutic window for the generation of T cells capable of recognizing tumor self-antigens. Many current cancer immune therapies rely on activating relatively weak tumor-specific T cell responses through modulating peripheral tolerance [92, 93]. In

contrast, manipulation of central tolerance has the potential to increase the pool and affinity of effector T cells that can recognize and contribute to effective anti-tumor responses. Furthermore, such high-affinity, self-reactive T cells may be more resistant to peripheral tolerance mechanisms that typically restrain an anti-tumor response [93]. Thus, the development of methods that selectively and transiently deplete *Aire*-expressing mTECs may be an attractive method to enhance tumor-specific immune responses.

Previous work has identified agents that can inhibit the growth and development of thymic epithelial cells (TECs) such as corticosteroids, cyclosporine, and some inflammatory cytokines [60, 62, 64]. Despite their clear inhibitory effects on TECs, however, these agents do not appear to have selectivity for blocking mTEC development. Interestingly, recent studies have demonstrated a role for TNF family member pairs RANK-RANKL and CD40-CD40L in the embryological development of Aire[+] mTECs [47, 48, 52-54]. Recent work has also demonstrated that mTECs in particular have a relatively fast turnover in adult mice with an estimated half-life of approximately two weeks [34, 35, 37]. Given these findings, we speculated that *in vivo* blockade of RANKL in adult hosts could both selectively and transiently inhibit the development and turnover of mTECs with potential to alter central T cell tolerance. To this end, we performed *in vivo* RANKL blockade in adult mice and investigated its effects on both TECs and developing thymocytes. We show that anti-RANKL treatment not only depleted mTECs, but could also be used

therapeutically to break central tolerance and as a result, increase the generation of tumor-specific T cells.

Results and Discussion

Depletion of medullary thymic epithelial cells with RANKL blockade

The RANK-RANKL signaling pathway is important for medullary thymic epithelial cell (mTEC) development, but it remains unclear what impact perturbation of this pathway might have on the adult thymus. Previous work has linked the RANK-RANKL pathway to the development of *Aire*-expressing mTECs [47, 48, 52-54], and we hypothesized that treating mice with blocking anti-RANKL antibody would decrease Aire$^+$ mTECs. We treated wildtype mice with either anti-RANKL or isotype control antibody for 2 weeks and harvested their thymi for analysis. Interestingly, while mice treated with anti-RANKL showed only a modest loss of cTEC cellularity, they exhibited a severe depletion of over 80% of mTECs (Figure 2.1A). Using MHC II and Aire as markers of mTEC maturation [34, 35], we further analyzed the immature mTEC^{lo} (MHC II^{lo} Aire$^-$), intermediate mTEC^{hi} (MHC II^{hi} Aire$^-$) and mature Aire$^+$ mTEC subsets (MHC II^{hi} Aire$^+$). The relative mTEC composition in anti-RANKL treated mice revealed a substantial loss of Aire$^+$ and mTEC^{hi} cells along with enrichment of the remaining mTEC^{lo} cells (Figure 2.1B). Although absolute numbers of mTECs were decreased across all mTEC subsets, mTEC depletion was mostly due to the loss of over 90% of all Aire$^+$ and mTEC^{hi} cells (Figure 2.1B). Immunostaining revealed a slight decrease in the density of keratin-5$^+$

(K5) cells in the medulla of anti-RANKL-treated mice while Aire$^+$ cells were nearly undetectable (Figure 2.1C and data not shown). Importantly, staining for keratin-8 (K8) and K5 showed that the overall corticomedullary thymic architecture was preserved despite the loss of mature mTECs (Figure 2.1C). Furthermore, consistent with the loss of the Aire$^+$ and mTEC^{hi} subsets, Aire-dependent tissue-specific antigen (TSA) gene expression in sorted mTECs was decreased in anti-RANKL-treated mice (Figure 2.1D).

Next, we characterized the impact of anti-RANKL mediated mTEC depletion on thymocyte selection. In the polyclonal T cell repertoire of wildtype mice treated with anti-RANKL, we observed a modest increase in frequencies of both CD4 single-positive (SP) and CD8 SP thymocytes, consistent with a lack of negative selection (Figure 2.1E). Importantly, anti-RANKL treated mice showed only a slight reduction in the frequency of double-positive thymocytes while absolute numbers were maintained, confirming normal positive selection. In addition, total thymocyte numbers were also maintained in mice treated with anti-RANKL (Figure 2.1E). Furthermore, anti-RANKL-treated mice showed a 50% reduction of Foxp3$^+$ Tregs within the CD4 SP subset (Figure 2.1F).

Given the dramatic impact of RANKL blockade on mTECs, we sought to determine whether this effect could be reversed in the context of increased RANK signaling. Osteoprotegerin (OPG;Tnfrsf11b) is a soluble decoy receptor for RANKL and its role as a negative regulator of RANK signaling has been well described in bone physiology [94]. Interestingly, in sorted wildtype mTECs, OPG expression was upregulated in MHC II^{hi} mTECs when compared to MHC

II^{lo} mTECs (Figure 2.2A). To test whether OPG negatively regulates RANK-RANKL signaling in mTECs, we analyzed thymi from $OPG^{-/-}$ mice. While cortical thymic epithelial cell (cTEC) cellularity was increased 3-fold in $OPG^{-/-}$ mice, mTEC cellularity was increased by nearly 10-fold when compared to $OPG^{+/+}$ mice (Figure 2.2B). Although absolute numbers of all mTEC subsets were increased in $OPG^{-/-}$ mice, we observed an enrichment of Aire$^+$ mTECs and a proportional loss of the mTEC^{lo} subset (Figure 2.2C). Immunostaining of K8 and K5 showed that $OPG^{-/-}$ thymi maintained their corticomedullary thymic architecture despite these changes in TEC cellularity and mTEC composition (Figure 2.2D).

Thymocyte analysis of $OPG^{-/-}$ mice showed a trend toward increased total thymic cellularity (Figure S2.1A). Further analysis of these thymocytes revealed an increase in both the relative frequency and absolute number of CD8 SP thymocytes while the DP, CD4 SP and DN subsets remained comparable in both frequency and absolute number to littermate controls (Figure S2.1A). Within the CD4 SP thymocytes, however, we observed a nearly two-fold increase in both the frequency and absolute numbers of Foxp3+ Tregs in $OPG^{-/-}$ mice (Figure S2.1B)

Taken together, these data suggest that RANK-RANKL-OPG interactions regulate both TEC cellularity and mTEC maturation, and are particularly important for the induction of Aire$^+$ mTECs. Furthermore, anti-RANKL treatment selectively targeted mature mTECs and altered negative selection without affecting the development of new thymocytes. Lastly, these

data suggest a strong correlation between thymic Treg induction and Aire[+] mTECs in that the ablation of Aire[+] mTECs led to a decline in thymic Treg while the expansion of the Aire[+] subset in *OPG^{-/-}* mice was associated with an increase in thymic Tregs.

Regeneration of medullary thymic epithelial cells after withdrawal of anti-RANKL

We next examined the kinetics of mTEC recovery following withdrawal from anti-RANKL blockade. After a 2-week treatment window, we harvested mice at 2-week intervals and observed gradual recovery of the mTEC[hi] and Aire[+] subsets (Figure 2.3A-B). By 10 weeks we observed the complete recovery of all mTEC subsets and a normal level of *Aire* expression after anti-RANKL-treatment (Figure 2.3B). Interestingly, the pattern of mTEC recovery appeared consistent with published reports of mTEC^{lo} cells giving rise to mTEC^{hi} cells prior to the induction of Aire[+] mTECs (Figure 2.3B) [34, 35, 52]. Notably, thymi from anti-RANKL and isotype-treated mice at 10 weeks were indistinguishable by immunostaining (Figure 2.3C). Thus, anti-RANKL mediated mTEC depletion is a transient phenomenon with return of normal thymic composition following withdrawal of antibody treatment.

The ability of the mTEC compartment to recover following RANKL blockade is consistent with previous reports by both our group and others demonstrating the robust regenerative potential of mTECs and cTECs in the adult thymus [37, 62, 68, 69, 95]. Furthermore, recent work has identified a

putative TEC progenitor population which parallels the slow-cycling, quiescent stem cell population of the skin epithelium [72-74]. These reports suggest that the mTEC progenitor pool resides within the phenotypic mTEC^{lo} population, which is enriched with RANKL blockade and is perhaps required for the proper recovery of mTECs following the withdrawal of anti-RANKL.

Manipulation of thymic negative selection with RANKL blockade

To further characterize the impact of anti-RANKL treatment on negative selection, we first employed the *OT-II* CD4^{+} TCR *x RIP-mOVA* double transgenic mouse model. *RIP-mOVA* transgenic mice express a membrane form of ovalbumin (OVA) under the control of the rat insulin promoter which results in its expression in both the pancreatic islets and in mTECs [12, 96]. When the *OT-II* CD4^{+} TCR transgenic line is crossed to the *RIP-mOVA* transgenic line, OVA-specific OT-II T cells are deleted in the thymus [12, 96]. We treated both *OT-II* and *OT-II x RIP-mOVA* mice with either anti-RANKL or isotype control antibody and performed thymocyte analysis. Consistent with previous reports, *OT-II x RIP-mOVA* mice treated with control antibody showed a significant reduction in the proportions of CD4 SP thymocytes and also had decreased frequencies and numbers of *OT-II*$^{+}$ T cells (Figure 2.4A-B) [12, 96]. In contrast, thymocyte profiles of anti-RANKL treated *OT-II x RIP-mOVA* mice were indistinguishable from that of *OT-II* mice, demonstrating that RANKL blockade prevented thymic deletion of *OT-II* T cells (Figure 2.4A-B). We also observed a loss of thymic Treg development in these mice, which suggested a

loss of cognate antigen (OVA) expression from mTECs within the thymus (Figure 2.4C). These data further support the effect of RANKL blockade to deplete mature mTECs with a functional impact on the negative selection of antigen-specific effector cells and generation of Treg cells.

Importantly, long-term recovery of previously-treated *OT-II x RIP-mOVA* mice showed that thymic selection returned to normal following withdrawal of anti-RANKL blockade (Figure S2.2A-B). These data further support the notion that mTECs can fully recover following antibody withdrawal and that the suppression of central tolerance is a transient phenomenon which can be harnessed for therapeutic purposes.

To expand these observations to the polyclonal T cell repertoire, we analyzed the development of Aire-dependent autoreactive T cells using a tetramer enrichment protocol. Previously, we had shown that T cells specific for the self-antigen IRBP are deleted in thymus of *Aire*^{+/+} mice, whereas these cells escape deletion in *Aire*^{-/-} mice and cause autoimmune uveitis [13, 15]. Through the use of an IRBP peptide-class II tetramer, P2-I-A[b], such autoreactive CD4+ T cells can be detected in *Aire*^{-/-} mice. Given both the severe depletion of Aire[+] mTECs and the loss of thymic *IRBP* expression in anti-RANKL treated mice, we hypothesized that P2-I-A[b]-specific T cells could be detected in treated mice. After treating wildtype mice with anti-RANKL antibody, we immunized mice with a MHC II-binding IRBP peptide epitope (P2) to expand T cells for detection. Ten days after immunization, lymph nodes and spleen were pooled for the enumeration of CD4^{+} P2-I-A[b]-specific T cells by flow cytometry. Consistent with

the loss of Aire^{+} mTECs, tetramer analysis of anti-RANKL treated mice revealed an expansion of CD4^{+} P2-I-A[b]-specific T cells (Figure 2.4D). Overall, these data show a clear defect in negative selection associated with the loss of Aire^{+} mTECs in anti-RANKL treated mice.

To evaluate the functional impact of these negative selection defects, we treated wildtype NOD mice for two weeks with anti-RANKL antibody shortly after weaning and harvested the mice after 9 weeks. Anti-RANKL-treated mice showed evidence of increased splenic cellularity and increased frequencies of CD4^{+} T cells with a CD62L^{lo} CD44^{hi} activated-memory phenotype (Figure S2.3A-C). We performed hematoxylin and eosin (H&E) staining on various tissues to look for evidence of autoimmunity. Interestingly, anti-RANKL treated mice did not develop significantly increased autoimmunity as evidenced by immune infiltrates (Figure S2.3D). We next treated *Aire*[GW/+] mice which have a dominant negative mutation in *Aire* that predisposes mice towards developing autoimmunity [96]. Compared to isotype-treated mice, anti-RANKL-treated *Aire*[GW/+] mice showed increased splenic cellularity and increased activated-memory CD4^{+} and CD8^{+} T cells. (Figure S2.3A-C). Despite the further increase in peripheral T cell activation, these mice still developed comparable disease to isotype-treated mice (Figure S2.3D). Since antibody treatment did not commence until weaning, we speculated that perhaps the perinatal window of *Aire* expression was sufficient for central tolerance induction to Aire-dependent antigens [81, 84, 97]. These results lead us to speculate that although RANKL blockade is sufficient to cause a breakdown in central tolerance, peripheral

tolerance mechanisms may be sufficient to prevent the onset of spontaneous autoimmunity.

Treatment with anti-RANKL enhances anti-tumor immunity

Given its ability to selectively block mTECs and central tolerance, we next sought to determine whether anti-RANKL treatment could be employed to therapeutically enhance anti-tumor immunity. Previous work has shown that many tumor self-antigens are expressed by mTECs as TSAs, and that high-affinity T cells capable of recognizing these tumor self-antigens are efficiently deleted in the thymus [86-88]. To test whether anti-RANKL treatment could rescue tumor self-antigen specific T cells from thymic deletion, we utilized the *TRP-1* CD4$^+$ TCR transgenic mouse model which generates T cells specific for the melanoma antigen TRP-1 (Tyrp1) [98]. TRP-1 is expressed in B16 melanoma cells, and *TRP-1* T cells are efficacious against established B16 melanoma tumors [98, 99]. Importantly, mTECs endogenously express *TRP-1* in in an Aire-dependent manner, such that TRP-1 specific T cells are deleted in the thymi of *Aire*-sufficient, *TRP-1*-sufficient hosts [88, 98]. In contrast, Aire-deficient mice have decreased thymic expression of *TRP-1* that allows for the escape of *TRP-1* T cells [88]. Given the depletion of Aire$^+$ mTECs and loss of thymic *TRP-1* expression in anti-RANKL treated mice (Figure 2.1D), we hypothesized that anti-RANKL treatment could rescue *TRP-1* T cells from thymic deletion. To prevent endogenous TCR rearrangements, we crossed the *TRP-1* TCR transgene onto the *RAG1$^{-/-}$* background. We then treated *RAG1$^{-/-}$ x*

TRP-1 TCR transgenic mice with either anti-RANKL or control antibody and harvested their thymi and spleens for analysis. Consistent with previous reports, isotype-treated mice showed efficient deletion of CD4 SP T cells in the thymus (Figure 2.5A) [88, 98]. In contrast, anti-RANKL treatment prevented deletion of CD4 SP cells and also resulted in a much higher percentage of Vβ14$^+$ T cells (Figure 2.5A). *TRP-1* T cells were also detectable in the spleens of anti-RANKL treated mice and also expressed higher levels of the Vβ14 TCR (Figure 2.5B).

As a functional readout of *TRP-1* T cells escaping into the periphery, we next looked for evidence of vitiligo in anti-RANKL treated *RAG1$^{-/-}$ x TRP-1* TCR transgenic mice. We harvested ear tissue for qPCR analysis and observed a sharp decline in both Tyrosinase and Tyrp1 expression in anti-RANKL treated mice (Figure S2.4A). Thus, these results appear consistent with melanocyte depletion as a consequence of *TRP-1* T cells escaping thymic deletion in anti-RANKL treated mice.

Next, we challenged anti-RANKL treated *RAG1$^{-/-}$ x TRP-1* mice with B16 melanoma to determine whether a limited break in central tolerance could improve overall survival. We observed a statistically significant increase in the survival of anti-RANKL treated mice compared to the isotype-treated cohort (Figure 2.5C). We also found evidence of an enhanced T cell response in anti-RANKL treated mice by measuring CD3$^+$ T cell infiltrates within the tumors of these mice (Figure 2.5D). Furthermore, to exclude potential effects of anti-RANKL antibody on the tumor microenvironment, we performed adoptive

transfer studies in which splenocytes from antibody-treated *RAG1^-/- x TRP-1* mice were transferred into *RAG1^-/-* mice. When challenged with B16 melanoma, recipients of splenocytes from anti-RANKL treated donors again showed a statistically significant increase in survival (Figure 2.5E). Furthermore, the recipients of splenocytes from anti-RANKL treated donors showed clinical signs of vitiligo as evidenced by the emergence of white hair following the adoptive transfers (Figure S2.4B-C).

To extend these findings to the polyclonal T cell repertoire, we treated B6 wildtype mice with either anti-RANKL or control antibody and similarly challenged the mice with B16 tumors. Similar to our findings in the *TRP-1* model, we observed a statistically significant increase in the survival of mice treated with anti-RANKL (Figure 2.6A). Given the modest increase in overall survival, however, we hypothesized that combining anti-RANKL treatment with peripheral tolerance blockade might yield an even greater survival benefit [92, 93, 100]. To test this hypothesis, we administered B16 tumors to B6 wildtype mice treated with anti-RANKL in combination with GVAX (vaccination with irradiated, GM-CSF secreting B16 cells) and anti-CLTA4 [101, 102]. Consistent with our results in B6 wildtype mice, treatment with anti-RANKL and GVAX was able to extend the survival of mice challenged with melanoma when compared to those given GVAX alone (Figure 2.6B). Furthermore, the addition of anti-CTLA4 to this treatment regimen proved to be even more efficacious as mice receiving all three therapies showed a statistically significant increase in survival (Figure 2.6B). Of note, these therapies appear to confer additive

survival benefits, suggesting that each therapy likely targets a distinct mechanism of tolerance (Figure 2.6B).

Taken together, these data demonstrate that short-term, reversible RANKL blockade of mTEC development can be used to create a therapeutic window that allows tumor self-antigen specific T cells to escape thymic deletion. Furthermore, central tolerance blockade can be utilized in combination with therapies which target peripheral tolerance as a means to further enhance anti-tumor immunity.

<u>Concluding Remarks</u>

In conclusion, our findings provide strong evidence that mTECs can be selectively and therapeutically targeted by RANKL blockade in adult mice and that anti-RANKL can be utilized as an approach to enhance anti-tumor responses. To date, previous efforts on the therapeutic manipulation of TECs have shown global effects that involve both cTECs and mTECs and disrupt thymocyte development [62]. The selectivity for mTECs with anti-RANKL thus provides evidence that central tolerance can be transiently suppressed in adult hosts while maintaining T cell generation. Although autoimmunity is a dangerous potential consequence of this approach, the treatment may also be an attractive new method to help break tolerance for cancer immunotherapy. Importantly, we find that the medullary epithelial compartment of the thymus recovers after withdrawal of anti-RANKL antibody, and thus, only a transient window of central tolerance suppression occurs. This window may be an

attractive feature of this approach, especially if coupled with methods that preferentially expand tumor specific T cells over pathogenic autoreactive T cells. Currently, there has been intense interest and progress in manipulating peripheral tolerance for immunotherapy [92, 100]. Given our results, it will also be of interest to determine if a combination of methods that target both central and peripheral tolerance could further enhance anti-tumor immune responses. Finally, it is important to note that our results also have implications for patients in the clinical setting receiving denosumab, a humanized monoclonal antibody that blocks RANKL that is widely used in the treatment of osteoporosis in adults [103]. Further study will be needed in such patients regarding their susceptibility to autoimmunity and for other potential defects in central tolerance.

Materials and Methods

Mice

C57BL/6, NOD, *B6.RAG1$^{-/-}$ Tyrp1^{B-w} TRP-1 TCR* transgenic, and *B6.OPG$^{-/-}$* mice were purchased from The Jackson Laboratories. Mice were treated intraperitoneally with 100μg of anti-RANKL (IK22/5) or isotype control (2A3) (BioXCell) antibody 3 times per week as stated in the text. *B6.OT-II*, *B6.RIP-mOVA*, *B6.IRBP$^{-/-}$*, and *NOD.Aire$^{GW/+}$* mice were described previously [12, 13, 96]. Mice were treated at 3-5 weeks of age and harvested at timepoints indicated in the text. All mice were housed in the animal facilities at UCSF or UNC, Chapel Hill according to guidelines of the Institutional Animal Care and Use Committee.

Quantitative PCR

RNA was extracted from sorted mTECs using the Qiagen RNeasy Micro Plus kit and cDNA was synthesized with the Invitrogen Superscript III kit. Applied Biosystems Taqman gene expression assays were used for all targets.

Histology and Immunofluorescence

Hematoxylin and eosin (H&E) staining was performed as described previously [96]. For immunofluorescence, thymi were harvested and embedded in O.C.T. media (Tissue-Tek). 8µm frozen thymic sections were fixed in 100% acetone, blocked and stained for keratin-5, keratin-8 (Abcam) or Aire (eBiosciences). Secondary antibodies were purchased from Invitrogen. Thymic sections were visualized using a Zeiss Apotome widefield microscope. For tumor immunostaining, tumors were harvested and fixed in 10% formalin as previously described [88]. Fixed tumors were embedded in paraffin and sectioned for staining with anti-CD3 antibody and counterstained with DAPI. Tumor sections were visualized using an Olympus BX60 fluorescent microscope and analyzed using ImageJ software.

Flow Cytometry

TECs were isolated as previously described [104]. Briefly, thymi were minced and digested with DNase I and Liberase TM (Roche) before gradient centrifugation with Percoll PLUS (GE Healthcare). Enriched stromal cells were

stained with the indicated surface marker antibodies (BioLegend). For lymphocyte staining, all surface marker antibodies were obtained from BioLegend. For intracellular staining, cells were stained using the Foxp3 Staining Buffer Set and stained with anti-Foxp3 or anti-Aire (eBiosciences). All data were collected using a BD LSR II flow cytometer and analyzed with either FloJo software (TreeStar)or FACS Diva (BD Biosciences). Cell sorting was performed using a BD FACS Aria III cell sorter.

IRBP P2 peptide Immunization and Tetramer Analysis

Mice were immunized with 100 μg of P2 peptide (IRBP, amino acids 271-290) emulsified in complete freund's adjuvant as described previously [15]. Tetramer analysis was performed on pooled lymph nodes and spleen from treated mice 10 days after immunization. P2-I-A[b] tetramer was generated by the NIH Tetramer Core Facility, and tetramer staining was performed as described previously [15, 105]. After tetramer enrichment, cells were stained with antibodies for flow cytometry, and counting beads (Invitrogen) were used to enumerate tetramer^{+} cells.

B16 Melanoma Tumor Challenge

B6.RAG1^{-/-}TRP-1 TCR transgenic mice were injected subcutaneously in the left flank with 1.0 x 10^{5} B16 melanoma cells. For adoptive transfer studies, spleens from donor mice were pooled and CD25-depleted prior to transfer into *B6.RAG1^{-/-}* hosts. Recipient mice were inoculated with 7.5 x 10^{4} B16 melanoma

cells 7 days post-transfer. For tumor studies in C57BL/6 mice, male mice were treated with anti-RANKL or isotype control antibodies and then injected subcutaneously in the left flank with 1.0×10^5 B16 melanoma cells. For studies combining anti-RANKL treatment with peripheral tolerance blockade, mice were inoculated with 5.0×10^4 B16 melanoma cells. GVAX and anti-CTLA4 were administered in accordance with previously described protocols [101]. Tumor growth was monitored by taking measurements of length (L) and width (W), and tumor volume was calculated as $LW^2/2$. For generation of survival curves, death was defined as tumor size greater than 1000 mm^3.

Statistical Analysis

Statistical analysis was performed using Prism 6.0 (Graphpad). Mann-Whitney Rank sum testing was performed on tetramer analysis and H&E infiltrate scores. Student's *t*-test was performed for TEC and lymphocyte analyses. Log rank test was performed for Kaplan-Meier survival curves. * denotes $p \leq 0.05$, ** denotes $p \leq 0.01$ and *** denotes $p \leq 0.001$.

Figure 2.1. Selective depletion of mTECs with anti-RANKL blockade

(A) Absolute numbers of mTECs and cTECs in mice harvested after two weeks of treatment with isotype (gray) or anti-RANKL (αRANKL, blue) antibody. Thymi were analyzed by flow cytometry and mTECs were defined as CD45$^-$, EpCAM$^+$, MHC II$^+$, Ly51$^-$ events and cTECs were defined as CD45$^-$, EpCAM$^+$, MHC II$^+$, Ly51$^+$ events. (B) Representative flow cytometry plots of mTECs in (A) showing relative composition of mTEC subsets. Values represent mean ±SEM. Bar graphs (right) of total cell numbers of each mTEC subset depicted by mean ±SEM. (C) Top panels show immunostaining for keratin-8 (green) and keratin-5 (red) on thymic sections from isotype or anti-RANKL treated mice. Bottom panels show immunostaining for keratin-5 (red) and Aire (green). Scale bars depict either 500μm (top) or 50μm (bottom). (D) Gene expression analysis on mTECs sorted from wildtype mice treated with either isotype (gray) or anti-RANKL (blue) antibody. Results standardized to Cyclophilin A and normalized to isotype-treated mice with bars depicting mean ±SD. (E) Representative flow cytometry plots of thymocytes from wildtype mice treated for 2 weeks with isotype or anti-RANKL antibody. Values depict mean ±SD. Total thymocyte numbers (right) are indicated with each circle depicting an individual animal and bars showing the mean. (F) Flow cytometric analysis of Foxp3 staining in CD4 SP thymocytes from (E). Plots (right) show percentage and number of thymic CD4$^+$ Foxp3$^+$ cells. Data shown is representative of two to four independent experiments containing three or more individual mice within each group.

Figure 2.1
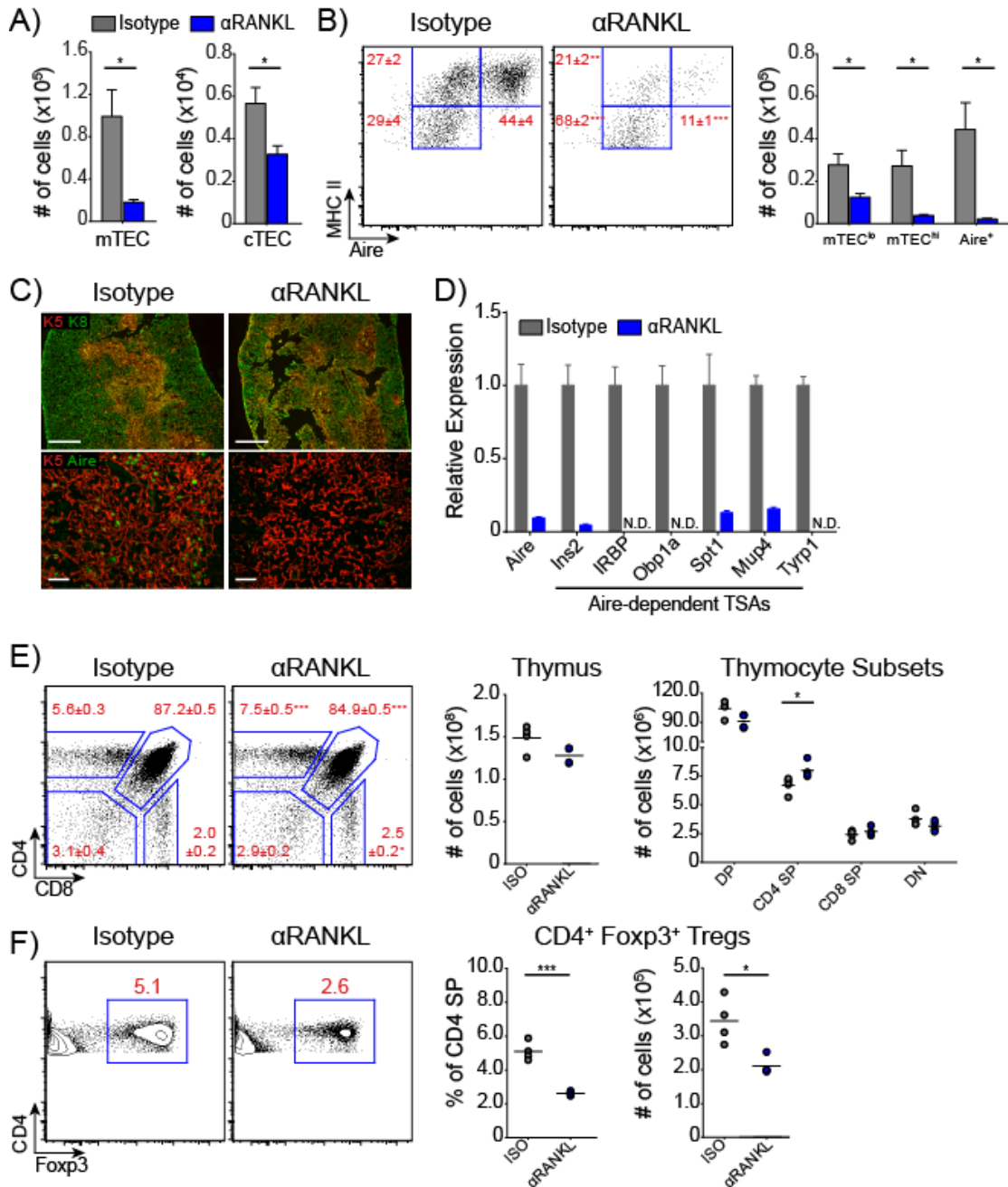
Figure 2.2. Increased Aire+ mTECs in OPG$^{-/-}$ mice

(A) Quantitative PCR analysis of Aire and OPG gene expression in MHC II^{lo} and MHC II^{hi} mTECs sorted from wildtype B6 mice. Results standardized to Cyclophilin A and normalized to MHC II^{lo}. **(B)** Absolute numbers of mTECs and cTECs in OPG$^{+/+}$ (black bars) and OPG$^{-/-}$ (red bars) mice. Thymi were analyzed by flow cytometry and mTECs were defined as CD45$^-$, EpCAM$^+$, MHC II$^+$, Ly51$^-$ events and cTECs were defined as CD45$^-$, EpCAM$^+$, MHC II$^+$, Ly51$^+$ events. **(C)** Representative flow cytometry plots of mTECs in (B) showing relative composition of indicated mTEC subsets. Values depict mean ±SEM. Bar graphs (right) depict total cell numbers of each mTEC subset and indicate mean ±SEM. **(D)** Immunostaining for keratin-8 (green) and keratin-5 (red) on frozen thymic sections from OPG$^{+/+}$ and OPG$^{-/-}$ mice. Data is representative of at least three independent experiments with at least three mice per group.

Figure 2.2
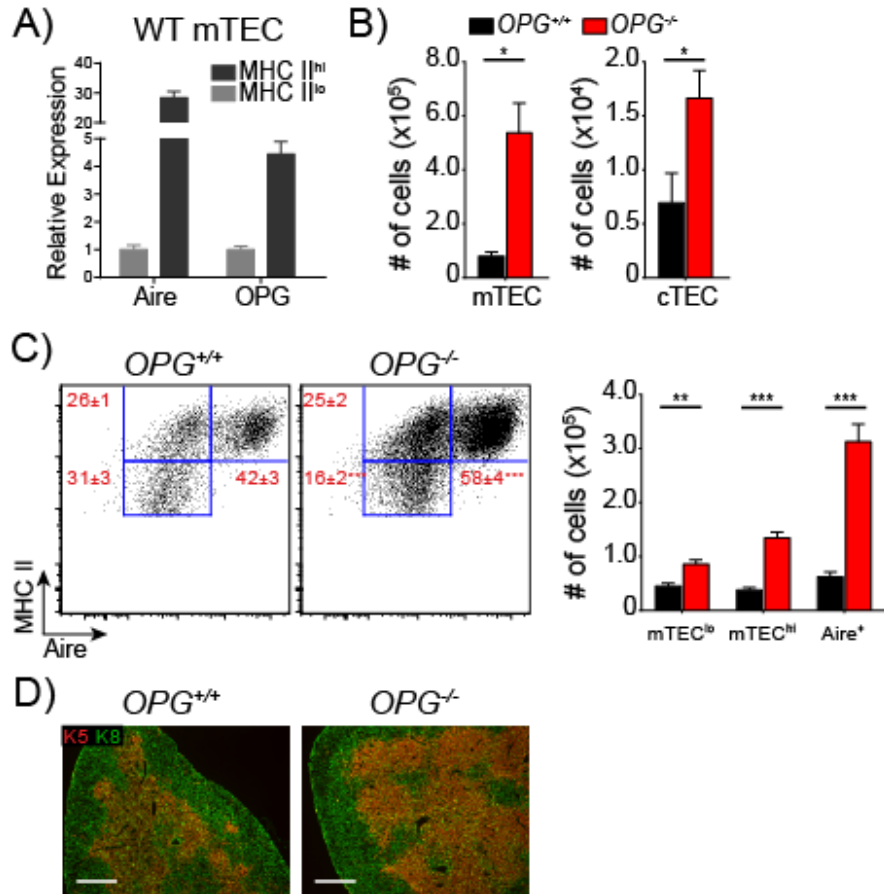
Figure 2.3. Regeneration of mTECs after anti-RANKL withdrawal

(A) Experimental layout for analysis of mTEC recovery after anti-RANKL withdrawal. Wildtype mice were treated for 1 week with isotype or anti-RANKL (black arrows) and harvested at indicated time points (red arrows). Graph (bottom) depicts relative composition of mTEC^{lo} mTEC^{hi} and Aire^{+} mTECs at each time point in anti-RANKL treated mice. Values represent mean ±SEM. (B) Representative flow cytometry plot of mTECs from each of the indicated time points from (A). Values represent percent of Aire^{+} mTECs. (C) Immunostaining for keratin-8 (green) and keratin-5 (red) on thymic sections from isotype or anti-RANKL-treated mice harvested at 10 weeks. Scale bars depict 500μm. Data shown is representative of at least two independent experiments with three to five mice per group.

Figure 2.3
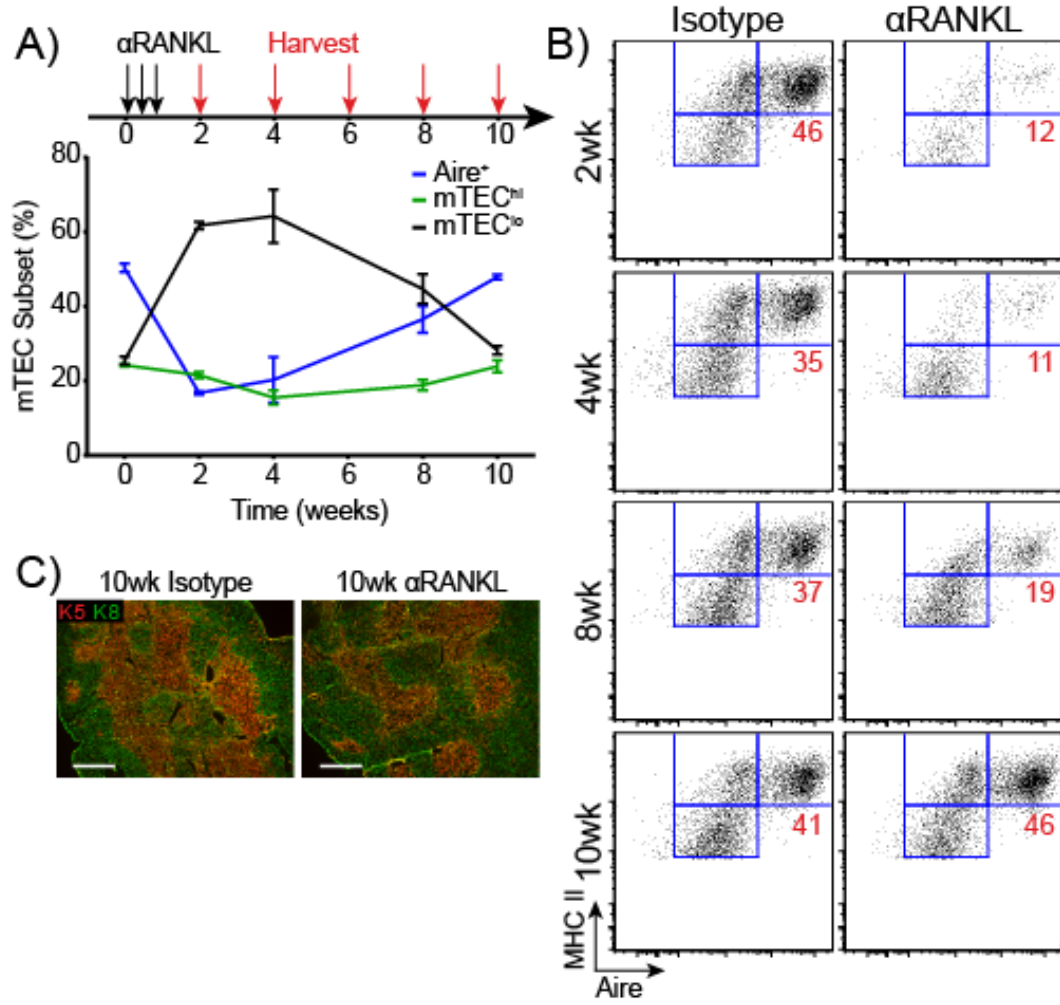
Figure 2.4. Anti-RANKL mediated mTEC ablation leads to altered negative selection

(A) Representative flow cytometry plots showing thymocytes from mice harvested after two weeks of indicated treatment. Percentages of CD4 SP (top) and OT-II clonotype-specific (bottom) T cells are shown. Values represent mean ±SD. **(B)** Quantification of OT-II clonotype-specific CD4 SP cells from (A). Graph shows mean ±SEM. **(C)** Representative histograms for Foxp3 staining in CD4 SP events from (A). **(D)** Wildtype mice were treated with isotype or anti-RANKL antibody for three weeks, immunized with P2 peptide, and then harvested 10 days later for tetramer analysis. Representative flow cytometry plots of CD4$^+$ T cells are shown for each condition. Values indicate absolute numbers of CD44$^+$ P2-I-A^b-specific T cells. *IRBP$^{-/-}$* mice were included as positive controls. Each dot on the graph represents an individual mouse, bars show mean, and the dotted line represents the limit of detection. Data shown is representative of two to three independent experiments.

Figure 2.4

A)

	Isotype		αRANKL	
OT-II:	WT	RIP-mOVA	WT	RIP-mOVA

18.4 ± 4.8   3.0 ± 1.0   16.6 ± 2.4   16.3 ± 1.1

CD4 / CD8

92.0 ± 2.1   52.6 ± 12.3   90.6 ± 1.7   90.8 ± 1.5

Vα2 / Vβ5

B)

OT-II+ cells (x10^6)

OT-II: WT / OVA+ (Isotype)   WT / OVA+ (αRANKL)

C) CD4 SP

% of Max

ISO OVA-
ISO OVA+
αRANKL OVA-
αRANKL OVA+

Foxp3

D)

Isotype   αRANKL   IRBP-/-

CD44 / P2-I-A^b Tetramer

3   594   1141

P2-I-A^b+ T cells

ISO   αRANKL   IRBP-/-

*
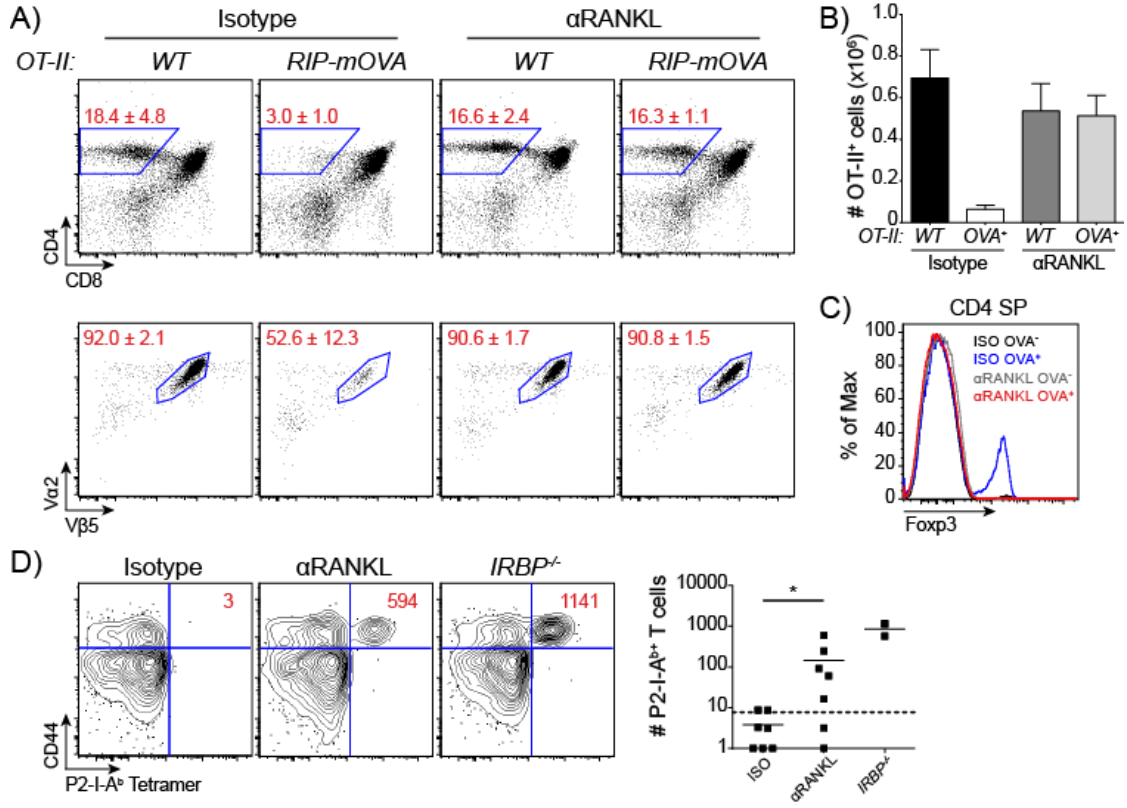
Figure 2.5. RANKL blockade increases anti-melanoma immune response

(A-B) *RAG1^{-/-} x TRP-1* TCR Tg mice were treated with isotype or anti-RANKL antibody for 2 weeks. Thymus (A) and spleen (B) were harvested for analysis, and representative flow cytometry plots show percent of CD4$^+$ (top) and CD4-gated Vβ14$^+$ (bottom) T cells. Values represent mean ±SEM. **(C)** Survival curves of *RAG1^{-/-} x TRP-1* TCR Tg mice inoculated with B16 melanoma following treatment with isotype or anti-RANKL antibody, n=7-8 mice for each group. **(D)** Representative immunostaining for CD3 (pink) with DAPI counterstain (purple) on tumor sections from isotype or anti-RANKL treated mice in (C). Scale bars depict 50µm. Average densities of CD3+ cells per tumor area are quantified on the right. Four sections were evaluated for each treatment group and 6 imaging fields were randomly scored from each section. Graphs depict mean ±SEM. **(E)** Survival curves of *RAG1^{-/-}* recipients inoculated with B16 melanoma following adoptive transfer of splenocytes from either anti-RANKL (blue) or isotype (gray) treated *RAG1^{-/-} x TRP-1* TCR Tg mice, n=10 mice for each group. All data shown is representative of at least two independent experiments.

Figure 2.5

A) Thymus

Isotype | αRANKL
0.9 ± 0.1 | 7.0 ± 2.8

CD4 / CD8

48.7 ± 2.5 | 88.0 ± 4.4

CD4 / Vβ14

B) Spleen

Isotype | αRANKL
0.4 ± 0.1 | 1.5 ± 0.6

CD4 / CD8

40.4 ± 1.5 | 83.0 ± 2.9

CD4 / Vβ14

C) % Survival vs Days after tumor inoculation

Isotype
αRANKL
*p<0.05

D) CD3 DAPI

Isotype | αRANKL

CD3+ T cells per tumor area (mm²)

ISO / αRANKL
*

E) % Survival vs Days after tumor inoculation

Isotype -> RAG-/-
αRANKL -> RAG-/-
**p<0.01
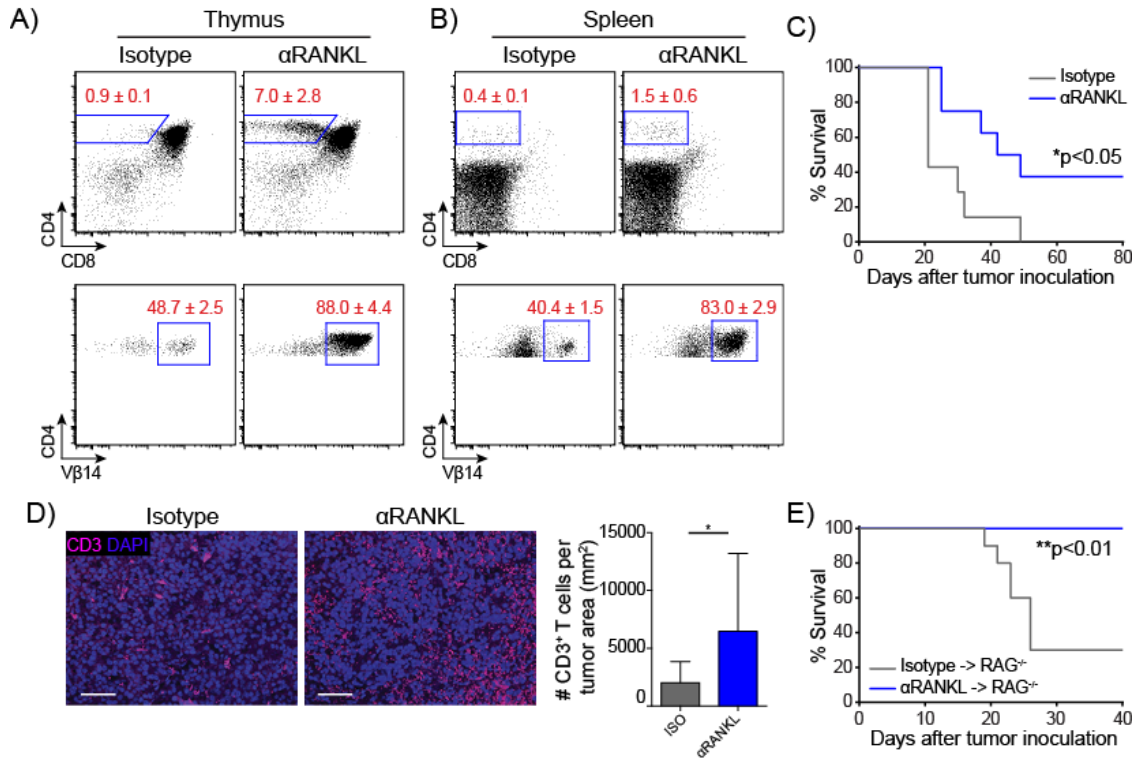
Figure 2.6. Combination therapies to suppress both central and peripheral tolerance enhance anti-tumor immunity

(A) Survival curves of B6 wildtype mice treated with anti-RANKL or control antibodies for two weeks and then inoculated with B16 tumors 2 weeks after treatment, n=7 mice per group. **(B)** Survival curves of B6 wildtype mice treated with anti-RANKL or control antibodies for two weeks and then inoculated with B16 tumors 1 week after treatment, n=9-10 mice per group. GVAX and anti-CTLA4 were administered on days 3, 6 and 10 following tumor inoculation.

Figure 2.6
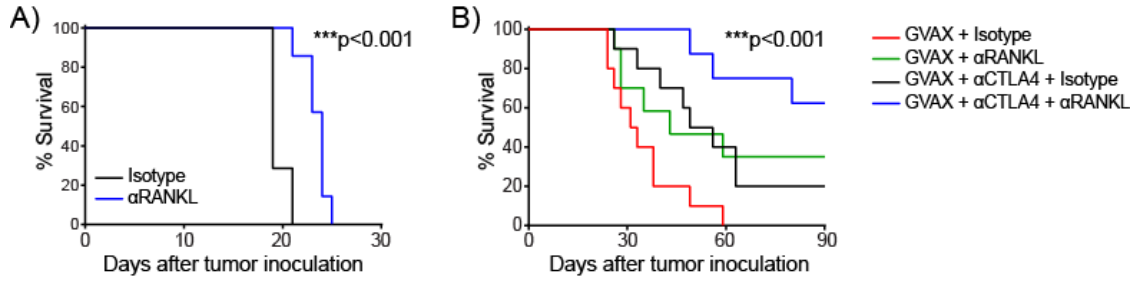
Figure S2.1. Increased thymic Tregs in OPG$^{-/-}$ mice

(A) Total thymocytes (left) and frequency (middle) and absolute numbers (right) of thymocyte subsets are indicated with each circle depicting an individual animal and bars showing the mean. **(B)** Flow cytometric analysis of Foxp3 staining in CD4 SP thymocytes from (A). Plots (right) show percentage and number of thymic CD4$^+$ Foxp3$^+$ cells. Data shown is representative of two to three independent experiments containing three or more individual mice per group.

Figure S2.1

A)

Thymus

Thymocyte Subsets

B)

CD4⁺ Foxp3⁺ Tregs
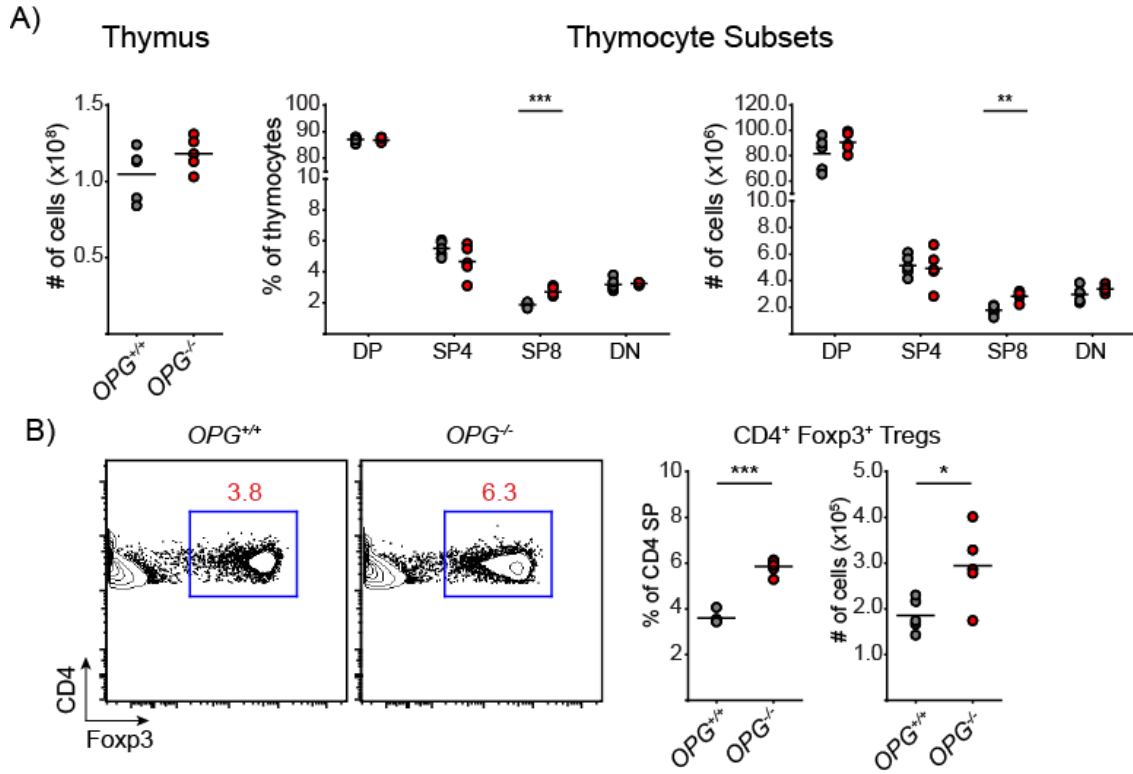
Figure S2.2. Negative selection resumes normally after withdrawal of anti-RANKL

(A) Mice of the indicated genotypes were treated for two weeks with anti-RANKL and then allowed to recover for 14 weeks. Representative flow cytometry plots showing thymocytes from mice harvested at the end of the 14-week recovery period. Percentages of CD4 SP (top) and OT-II clonotype-specific (bottom) T cells are shown. Values represent mean ±SD. **(B)** Quantification of OT-II clonotype-specific CD4 SP cells from (A). Graph shows mean ±SEM.

Figure S2.2
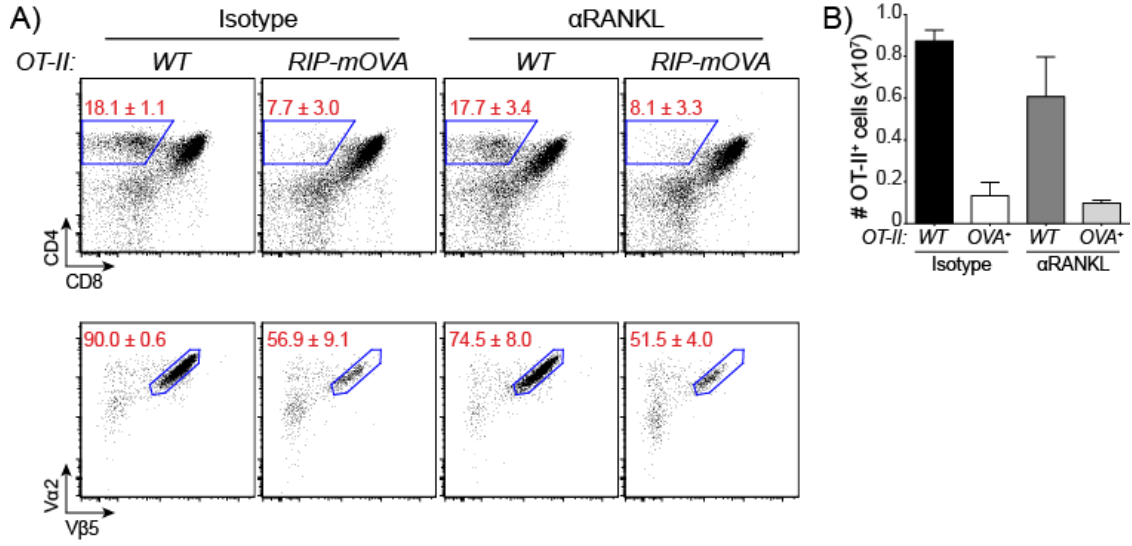
Figure S2.3. RANKL blockade causes increased T cell activation in NOD mice

(A) NOD wildtype (top) and *NOD.Aire*[GW/+] (bottom) mice were treated at weaning for two weeks with anti-RANKL and then harvested after 9 weeks of recovery. Shown are representative flow cytometry plots of $CD4^+$ splenocytes. Values shown on plots indicate the percent of T cells showing an activated-memory ($CD44^{hi}$ $CD62L^{lo}$) phenotype. **(B)** Total splenocyte cellularity of mice harvested in (A). **(C)** Quantification of $CD4^+$ and $CD8^+$ T cells displaying an activated-memory from (A). Shown are the percent and absolute numbers of $CD4^+$ and $CD8^+$ T cells with each circle depicting an individual animal and bars showing the mean. **(D)** Plots depict the infiltrate scores of lacrimal and salivary glands of mice harvested in (A), values depict mean ±SEM.

Figure S2.3
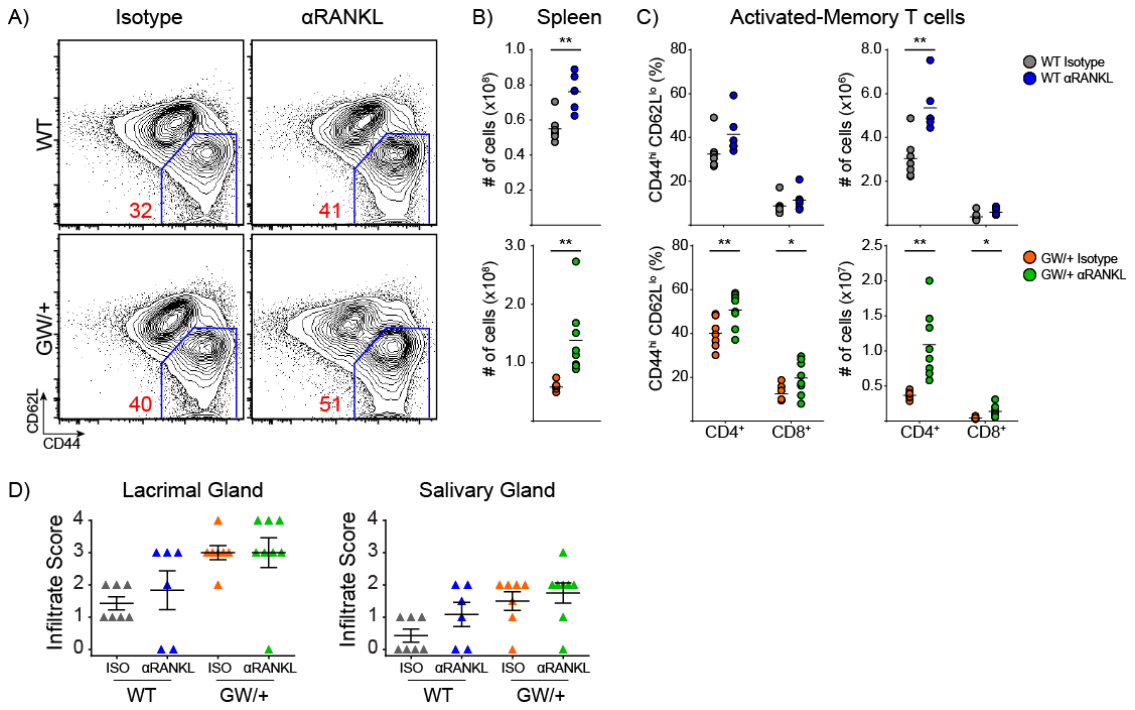
Figure S2.4. Anti-RANKL treatment of TRP-1 mice causes autoimmune vitiligo

(A) *RAG1$^{-/-}$ x TRP-1* TCR Tg mice were treated with anti-RANKL or control antibody for two weeks and then harvested several weeks later. RNA was prepared from pieces of ear tissue and qPCR analysis was conducted for Tyrosinase and Tyrp1. Results standardized to β2m and normalized to B6 wildtype mice with bars depicting mean ±SD. **(B)** *RAG1$^{-/-}$* mice were given an adoptive transfer of splenocytes from either isotype of anti-RANKL treated *RAG1$^{-/-}$ x TRP-1* TCR Tg mice. The flanks of these mice were shaved to stimulate new hair growth to determine whether the mice showed clinical signs of autoimmune vitilito. The two mice on the left were given splenocytes from isotype-treated mice, and the two mice on the right were given splenocytes from anti-RANKL treated mice. **(C)** Images of mice in (B) several weeks after adoptive transfer.

Figure S2.4

A)

B)

C)
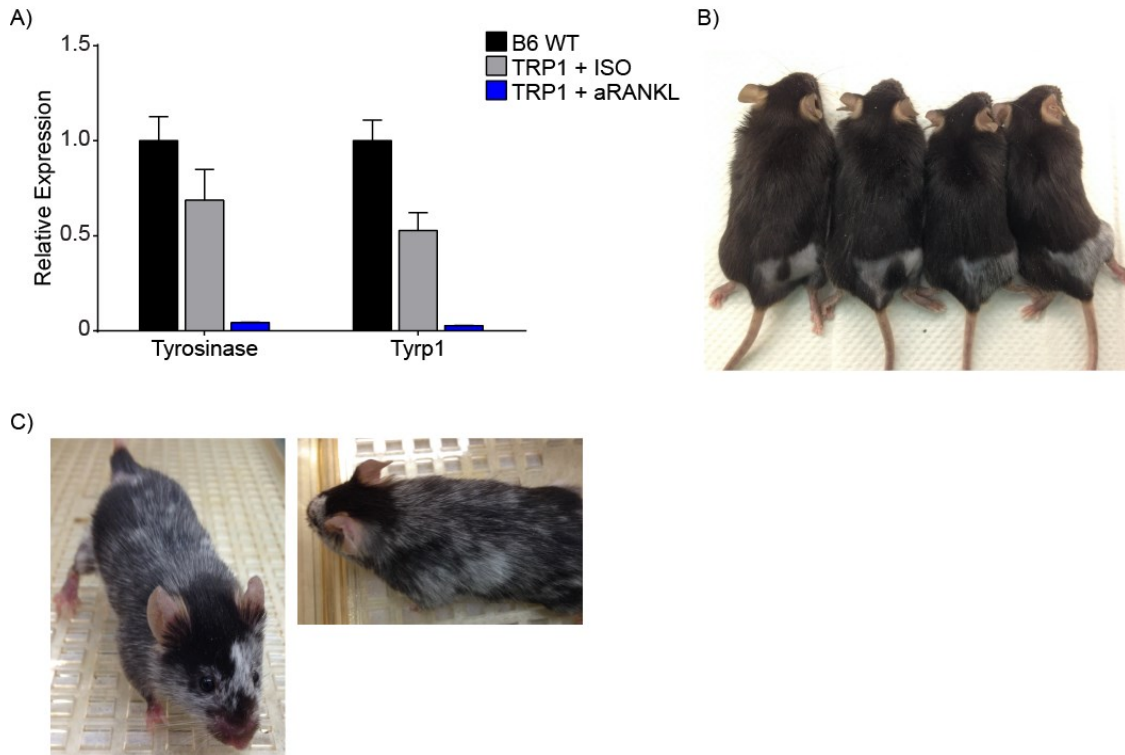
Chapter 3: Canonical microRNAs in Thymic Epithelial Cells Promote Central Tolerance

Abstract

Medullary thymic epithelial cells (mTECs) facilitate the deletion of developing self-reactive T cells by displaying a diverse repertoire of tissue-specific antigens (TSAs), a process which largely depends on the expression of the autoimmune regulator (Aire) gene. Mature microRNAs (miRNA) that regulate gene expression post-transcriptionally are generated in a multi-step process. The microprocessor complex including DGCR8 cleaves canonical miRNAs, but alternative DGCR8-independent miRNA biogenesis pathways exist as well. In order to study the role of canonical miRNAs in TECs we ablated *Dgcr8* using a *FoxN1-Cre* transgene. We report that DGCR8-deficient TECs are unable to maintain proper thymic architecture and exhibit a dramatic loss of thymic cellularity. Importantly, DGCR8-deficient TECs develop a severe loss of Aire$^+$ mTECs. Using a novel immunization approach to amplify and detect self-reactive T cells within a polyclonal T-cell receptor (TCR) repertoire, we demonstrate a link between the loss of *Aire* expression in DGCR8-deficient TECs and the breakdown of negative selection in the thymus. Thus, DGCR8 and canonical miRNAs are important in TECs for supporting central tolerance.

Introduction

Thymic epithelial cells (TECs) support T-cell development in two distinct stages. Cortical thymic epithelial cells (cTECs) facilitate the positive selection of thymocytes that have undergone T-cell receptor (TCR) rearrangements capable of recognizing self-MHC [1]. Positively selected thymocytes undergo negative selection by medullary thymic epithelial cells (mTECs) to eliminate self-reactive T cells [85]. To prevent autoimmunity, mTECs display a diverse repertoire of tissue-specific antigens (TSAs) whose expression is otherwise restricted to peripheral tissues [18, 32, 91]. Developing thymocytes bearing a TCR recognizing the TSAs undergo apoptosis to purge the developing T-cell pool of self-reactive T cells [13-15]. TSA expression in mTECs is largely dependent on autoimmune regulator (Aire), which is expressed in a subset of mature mTECs expressing high levels of MHC II and the co-stimulatory molecule CD80 [34, 35, 91]. Both patients and mice with mutations in *AIRE* develop multi-organ autoimmunity which underscores the importance of TSA expression for the elimination of self-reactive T cells in maintaining tolerance [26, 27, 32].

MicroRNAs (miRNAs) are ~22 nucleotide long noncoding RNAs that mediate sequence-dependent post-transcriptional gene repression [79, 80]. The primary miRNA transcripts of canonical miRNAs are processed by a complex formed by DROSHA and DGCR8 to generate ~60-80nt hairpin precursor miRNAs. After export to the cytoplasm, these hairpins are further processed by the RNase III enzyme Dicer to produce mature miRNAs.

However, Dicer does not exclusively process miRNA precursors but rather includes a variety of small RNAs such as endogenous siRNAs, endogenous shRNAs, mirtrons, and Alu RNAs [106-108]. By ablating key genes required for miRNA biogenesis we and others have previously demonstrated the importance of miRNAs in various lymphocyte populations [109-113]. Similarly, Dicer is important for TEC biology [82-84]. However, since Dicer is not restricted to processing miRNAs it remains unclear whether TEC development and function are truly dependent on the canonical miRNA pathway [106-108].

To further define the role of canonical miRNAs in TECs, we generated mice with TEC-specific deletion of *Dgcr8*, a component of the miRNA-specific microprocessor complex [107, 114]. Here we find that DGCR8 is critical for maintaining the proper expression of *Aire* and the overall architecture of the thymic medulla. Furthermore, we demonstrate a breakdown in thymic negative selection in these animals by detecting pathogenic autoreactive T-cell clones in the periphery that are normally deleted in the thymus. Thus, proper thymic architecture and central tolerance depend on canonical miRNAs expressed in TECs.

Results and Discussion

Thymic architecture and TEC composition depend on miRNAs

To study the role of canonical miRNAs in TEC function we first analyzed *Dgcr8* expression in mTECs and cTECs from C57BL/6J wildtype mice and found no significant differences in expression (data not shown). We then

utilized *FoxN1-Cre* knock-in mice, which express Cre recombinase in all TECs without disrupting FoxN1 function, to conditionally inactivate *Dgcr8* in TECs (*Dgcr8*$^{\Delta TEC}$) [114, 115]. We used qPCR analysis to verify that the deletion of *Dgcr8* in *Dgcr8*$^{\Delta TEC}$ mice was comparable between mTECs and cTECs (data not shown). At 2 weeks of age *Dgcr8*$^{\Delta TEC}$ mice exhibited evidence of disrupted thymic architecture with a loss of the distinct keratin-8 (K8) and keratin-5 (K5) staining patterns as compared with the characteristic separation between cortex and medulla in littermate control mice (Figure 3.1A). The TECs in *Dgcr8*$^{\Delta TEC}$ mice appeared to be thinned out and many expressed both keratin markers (K5^{+}K8^{+}), a feature characteristic of immature TECs [116]. Though Aire^{+} cells were detectable at 2 weeks by immunofluorescent staining, they appeared to be reduced in number. By 6 weeks of age the *Dgcr8*$^{\Delta TEC}$ thymi had further deteriorated and developed large patches lacking K5/K8 staining (Figure 3.1A). Aire^{+} cells were further depleted and nearly all remaining TECs were K5^{+}K8^{+}. Hematoxylin and eosin (H&E) staining revealed confluent cellularity, demonstrating that the absence of K5/K8 staining did not represent a general absence of cells (e.g. a liquid filled cyst) but rather a specific loss of TEC or TEC identity (Figure 3.1A).

To quantify and further characterize these changes in thymic architecture we performed flow cytometry on TECs. As expected from the histologic analysis, overall TEC cellularity was significantly reduced in 2-week old *Dgcr8*$^{\Delta TEC}$ mice and further decreased by 6 weeks of age (Figure 3.1B, S3.1A). Although *Dgcr8*$^{\Delta TEC}$ mice showed increased frequencies and absolute

56

numbers of cTECs at 2 weeks of age, cTEC numbers were comparable to those of littermate controls by 6 weeks. In contrast, mTEC cellularity was reduced by nearly 80% in 2-week old $Dgcr8^{\Delta TEC}$ mice and progressed to a 95% loss by 6 weeks (Figure 3.1B). Within the mTEC compartment in 2-week old mice, the relative frequency of Aire$^+$ cells was reduced while the immature mTEC^{lo} (MHC II^{low} Aire$^-$) and the more mature mTEC^{hi} (MHC II^{hi} Aire$^-$) cell subsets were relatively enriched (Figure 3.1C) [34, 35]. In contrast, absolute cell numbers were reduced across all mTEC subsets at both 2-week and 6-week time points (Figure 3.1D). However, the loss was most prominent in the Aire$^+$ cells. Thus, proliferating immature mTEC precursors could be partially compensating for the loss of the most mature mTECs. Supporting this notion, increased frequencies of the relatively enriched mTEC^{lo} and mTEC^{hi} cell subsets expressed the proliferation marker Ki67 (Figure 3.1D). By 6 weeks of age, both mTEC^{hi} and Aire$^+$ cells were relatively depleted in $Dgcr8^{\Delta TEC}$ mice while the mTEC^{lo} subset was enriched. Similar to the 2-week time point, a larger proportion of mTEC^{lo} cells expressed the proliferation marker Ki67 (Figure 3.1D). Thus, increased proliferation rates of mTEC precursor cells partially compensated for the loss of the more differentiated mTECs.

To investigate whether the loss of Aire$^+$ mTEC resulted from the TEC-intrinsic loss of $Dgcr8$ expression in mTEC or was an indirect consequence of disturbed TEC-thymocyte crosstalk we analyzed neonatal mice. While overall thymocyte cellularity was comparable between $Dgcr8^{\Delta TEC}$ and control mice 2 days postnatally, $Dgcr8^{\Delta TEC}$ mice exhibited a significant loss of both mTEC and

cTEC cellularity (Figure 3.2 A-E). The mTEC loss was specific to the mature mTEC^{hi} and Aire^{+} subsets which is indicative of an initial TEC-intrinsic maturation defect in the thymi of *Dgcr8$^{\Delta TEC}$* mice. Additional impaired TEC-thymocyte crosstalk may occur at later timepoints.

Together, these findings demonstrate that DGCR8-dependent canonical miRNAs are essential for TEC cellularity and mTEC maturation, particularly the accumulation and maintenance of *Aire*-expressing mTECs. This suggests that the histologically apparent mTEC voids in 6 week old mice represent a true absence of mTECs. In addition, the altered relative TEC composition suggests a superimposed differentiation defect in which the mature mTEC^{hi} and Aire^{+} mTEC subsets are diminished while the immature mTEC^{lo} cells accumulate and exhibit increased proliferation. These findings are consistent with the increased presence of K5^{+}K8^{+} cells in *Dgcr8$^{\Delta TEC}$* thymic sections suggesting that the loss of the most differentiated mTEC may trigger a proliferative response in immature TECs to compensate for the overall loss of TEC cellularity.

miRNAs are required for the maintenance of thymocyte cellularity

The profoundly altered thymic architecture and TEC cellularity suggested that thymocyte development could be affected by TEC-specific miRNA-deficiency. Thymi from 6-8 week old *Dgcr8$^{\Delta TEC}$* mice showed a significant reduction of over 60% in thymic cellularity (Figure 3.3A). In contrast, the relative frequencies of CD4^{-}CD8^{-} double negative (DN), CD4^{+}CD8^{+} double positive

(DP), CD4$^+$ single positive (SP), CD8$^+$ SP thymocytes and CD4$^+$Foxp3$^+$ Treg cells were not affected in *Dgcr8*$^{\Delta TEC}$ mice. As a consequence, absolute numbers of all thymocyte developmental stages were proportionally reduced. These results suggest that although *Dgcr8*$^{\Delta TEC}$ mice have a severely disrupted thymic architecture and significant reduction in TECs, the remaining TECs are sufficient to support T-cell development. This finding is reminiscent of Smad4-deficient TEC that lead to substantial thymic hypoplasia but intact relative thymocyte development [117]. Thus, the thymus appears to have a remarkable ability to maintain thymocyte development despite severely impaired TEC numbers and composition. Next we analyzed whether the reduction of thymic T-cell numbers resulted in peripheral T-cell lymphopenia. In contrast to the thymic cellularity, total splenic cellularity was not different between *Dgcr8*$^{\Delta TEC}$ and control mice, and CD4$^+$ and CD8$^+$ T-cell numbers were only modestly reduced (Figure 3.3B). Thus, homeostatic proliferation in the periphery most likely compensated for the reduced thymic cellularity. However, despite the relatively normal thymocyte development and the presence of substantial numbers of T cells in lymph nodes and spleen, we could not exclude that the thymocytes developing in a *Dgcr8*$^{\Delta TEC}$ microenvironment were functionally impaired or had a skewed TCR repertoire due to defective thymocyte selection. Indeed, mice with *Dicer*-deficient TECs develop collagen-induced arthritis with increased incidence but decreased severity suggesting both an altered T-cell repertoire and possibly impaired T-cell function [82]. Thus, *Dicer*-deficient TEC

are not able to support numerically and functionally normal thymocyte development.

miRNA deficiency in TECs causes a breakdown in central tolerance

Given the complex consequences on T cells developing in *Dicer*-deficient TEC [82] and the prominent and progressive loss of Aire[+] mTECs we sought to determine whether *Dgcr8*[ΔTEC] mice had a defect in central tolerance. *Dgcr8*[ΔTEC] mice did not develop spontaneous autoimmunity as evidenced by immune infiltrates in various organs or the presence of autoantibodies when compared with littermate controls, even when aged out beyond 45 weeks (data not shown). These findings are consistent with previous work which found that *Aire* expression during the perinatal period is sufficient to induce central tolerance [97]. In addition, similar results have been reported for mice with *Dicer*-deficient TECs [84]. In these studies, depletion of T cells at 2 weeks of age to allow the seeding of potentially autoreactive T cells developing in a *Dicer*-deficient TEC microenvironment led to multiorgan autoimmune disease after 30 weeks [84]. Thus, the presence of some Aire[+] TEC during the perinatal period, peripheral *Aire* expression, and other peripheral tolerance mechanisms likely cooperated to prevent the development of spontaneous autoimmunity in *Dgcr8*[ΔTEC] mice [91, 118].

We hypothesized that although *Aire* expression is partially maintained in young *Dgcr8*[ΔTEC] mice, self-reactive T cells could have escaped thymic deletion due to the disturbance of thymic architecture and the progressive loss of Aire[+] mTECs,

but be kept in check by peripheral tolerance mechanisms. We aimed at testing this hypothesis in the polyclonal T-cell repertoire employing a novel approach to expand and detect Aire-dependent autoreactive T cells. In previous work we determined that IRBP-specific T cells are normally deleted efficiently in the thymus of *Aire*-sufficient hosts and that such cells escape deletion in Aire-deficient thymi and provoke autoimmune uveitis [13]. Utilizing a previously described tetramer enrichment protocol, we developed methods to detect T cells with this specificity in the polyclonal repertoire of Aire-deficient hosts [15, 105]. Thus, we hypothesized that escaped self-reactive IRBP-specific CD4$^+$ T cells could be detected in *Dgcr8*$^{\Delta TEC}$ mice given the loss of proper Aire-expression in these mice. To expand T cells for detection, we immunized *Dgcr8*$^{\Delta TEC}$ and control mice with a MHC II binding IRBP peptide epitope (P2) and 10 days later pooled lymph nodes and spleen to enumerate CD4$^+$ P2-I-A^b reactive T cells. Consistent with the loss of Aire$^+$ mTECs, immunized *Dgcr8*$^{\Delta TEC}$ mice showed a significant expansion of P2-specific CD4$^+$ T cells when compared with littermate controls (Figure 3.4A, S3.1B). Importantly, this expansion was also associated with a breakdown in immune tolerance with the generation of IRBP-specific autoantibodies and autoimmune uveitis in immunized *Dgcr8*$^{\Delta TEC}$ mice when compared with control mice (Figure 3.4B-C).

Concluding Remarks

In summary, we show here that *Dgcr8* expression in TECs is critical for the maintenance of proper corticomedullary thymic architecture and that

canonical miRNAs are unequivocally required to support both TEC and thymocyte cellularity. miRNAs are critical for TEC differentiation and composition and for the development and maintenance of Aire$^+$ mTECs. Using a novel immunization approach to expand and detect autoreactive T cells in a polyclonal TCR repertoire, we demonstrate that TECs rely on miRNAs to prevent a breakdown in central tolerance. Furthermore, we show that immunization with self-antigen followed by tetramer-mediated detection of expanded self-reactive T-cell clones can be used as an effective and rapid tool to screen for central tolerance defects in animal models. Thus, such an approach may be useful to screen for hidden central tolerance defects in large scale mutagenesis projects.

Materials and Methods

Mice

FoxN1-Cre knock-in mice were kindly provided by N. Manley [115]. Floxed *Dgcr8* mice were kindly provided by R. Blelloch [114]. IRBP$^{-/-}$ mice were described previously [13]. Throughout this study *Dgcr8*$^{\Delta TEC}$ represents *B6.FoxN1-Cre$^+$Dgcr8$^{fl/fl}$* mice and littermate controls are both *B6.FoxN1-Cre$^+$ Dgcr8$^{fl/+}$* mice and all *B6.FoxN1-Cre$^-$* mice. Mice were housed and bred under specific-pathogen free conditions at the University of California, San Francisco (UCSF) Animal Barrier Facility. Animal experiments were approved by the Institutional Animal Care and Use Committee (IACUC) at UCSF.

Histology and Immunofluorescence

Thymi were harvested and embedded in Tissue-Tek Optimal Cutting Temperature (OCT) media. 8 µm frozen thymic sections were fixed in 100% acetone and blocked in 10% goat serum before incubation with primary antibodies. Primary antibodies were purchased from either Abcam (keratin-5, keratin-8) or eBioscience (Aire) and all secondary antibodies were purchased from Invitrogen. Immunofluorescence slides were visualized using a Zeiss Apotome widefield microscope. For eye disease scoring, eyes were processed by formalin fixation and H&E staining as previously described [13, 15]. Sections were blindly scored for severity of infiltration and tissue destruction. H&E slides were imaged using a Zeiss AxioImager brightfield microscope.

Flow Cytometry

Thymic stromal cells were isolated as previously described [104]. Briefly, thymi were minced with razor blades and digested with DNase I and Liberase TM (Roche) before gradient centrifugation with Percoll PLUS (GE Healthcare). Enriched stromal cells were blocked with the Fc-receptor blocking antibody 2.4G2 and stained with the indicated surface marker antibodies (BioLegend). For intracellular staining with anti-Aire-A647 (eBiosciences) and anti-Ki67-PE (BD Biosciences), cells were stained using the Foxp3 Staining Buffer Set (eBiosciences). For staining of lymphocytes, all surface marker antibodies were obtained from BioLegend except anti-Foxp3-APC which was obtained from eBiosciences. Flow cytometry was performed using a LSR II flow cytometer

(BD Biosciences), and raw data were analyzed using FACS Diva (BD Biosciences) and Flow Jo (Tree Star).

Immunization

As described previously, 7-8 week old mice were immunized subcutaneously with 100 µg of P2 peptide emulsified in 100 µL of CFA [15]. For induction of autoimmune uveitis, mice were given an i.p. injection of 400 ng pertussis toxin at the time of immunization. Mice were harvested 10 days following immunization for tetramer analysis and 21 days following immunization for uveitis analysis.

Tetramer Analysis

P2-I-A^b tetramer (Interphotoreceptor retinol binding protein 3, amino acids 294-306) was generated by the NIH Tetramer Core Facility, and tetramer staining was performed according to previously described protocols [15, 105]. Briefly, mice were harvested 10 days following immunization and lymphocytes were pooled from lymph nodes and spleen. Cells were stained with tetramer for 1 hour at room temperature and enriched for tetramer$^+$ cells using anti-APC microbeads and MACS columns (Miltenyi Biotech). Positively-selected cells were stained with antibodies for flow cytometry, and counting beads (Invitrogen) were used to enumerate tetramer$^+$ cells.

Generation of ^{35}S-Radiolabeled IRBP and Autoantibody Assay

The autoantibody assay was described previously [14]. Briefly, full-length cDNA for mouse IRBP (Thermo Scientific, #MMM1013) was used for in vitro transcription and translation and labeling with ^{35}S-methionine using the TNT system kit (Promega). The ^{35}S-IRBP was immunoprecipitated with serum samples in 96-well PVDF filtration plates (Millipore). Serum samples were analyzed in triplicate with 20,000 counts per minute (cpm) of ^{35}S-IRBP per well. Radioactivity of immunoprecipitated material was evaluated with a liquid scintillation counter (1450 MicroBeta TriLux, Perkin Elmer). Serum samples from Aire$^{+/+}$ and Aire$^{-/-}$ mice were used as negative and positive standards, respectively (data not shown). The IRBP autoantibody index for each serum sample was found by the following calculation: ([cpm in unknown sample – cpm in negative standard] ÷ [cpm in positive standard – cpm in the negative standard] x 100).

Statistical Analysis

Statistical analysis was performed using Prism 6.0 (Graphpad). Mann-Whitney testing was performed for tetramer analysis, autoantibody indices, and histological analyses. Student's *t*-test was performed for TEC and lymphocyte analyses. * denotes $p \leq 0.05$, ** denotes $p \leq 0.01$ and *** denotes $p \leq 0.001$.

Acknowledgements

Figure 3.1. Thymic architecture and TEC composition depend on miRNAs

(A) Frozen thymic sections from $Dgcr8^{\Delta TEC}$ and littermate control mice were assessed for expression of keratin-5 (K5, red), keratin-8 (K8, green), and Aire (green) by immunofluorescent staining at indicated timepoints. Scale bars = 200 μm (K5 K8) and 50 μm (K5 Aire). The bottom panel shows H&E staining of indicated genotypes at the 6-week time point, scale bars = 500 μm. Data shown are representative images from 2-3 independent experiments. **(B)** Enumeration of total mTEC and cTEC cellularity by flow cytometry. cTECs were defined as CD45$^-$, EpCAM$^+$, Ly51$^+$, MHC II$^+$ events. mTECs were defined as CD45$^-$, EpCAM$^+$, Ly51$^-$, MHC II$^+$ events. **(C)** Subset composition was assessed by flow cytometry of mTECs as defined in **(B)**. **(D)** Quantification of total TEC cellularity and assessment of the proliferation marker Ki67 for the mTEC subsets shown in **(C)**. mTEC subsets were defined as mTEC^{lo} (MHC II^{low}, Aire$^-$), mTEC^{hi} (MHC II^{hi}, Aire$^-$), and Aire$^+$ (MHC II^{hi}, Aire$^+$). White bars in **(B)** and **(D)** indicate $Dgcr8^{\Delta TEC}$ mice, black bars indicate littermate controls. Data shown in **(B-D)** are shown as mean ±SEM of 3-10 samples and are representative of at least two independent experiments. * denotes p≤0.05, ** denotes p≤0.01 and *** denotes p≤0.001, Student's t-test.

Figure 3.1
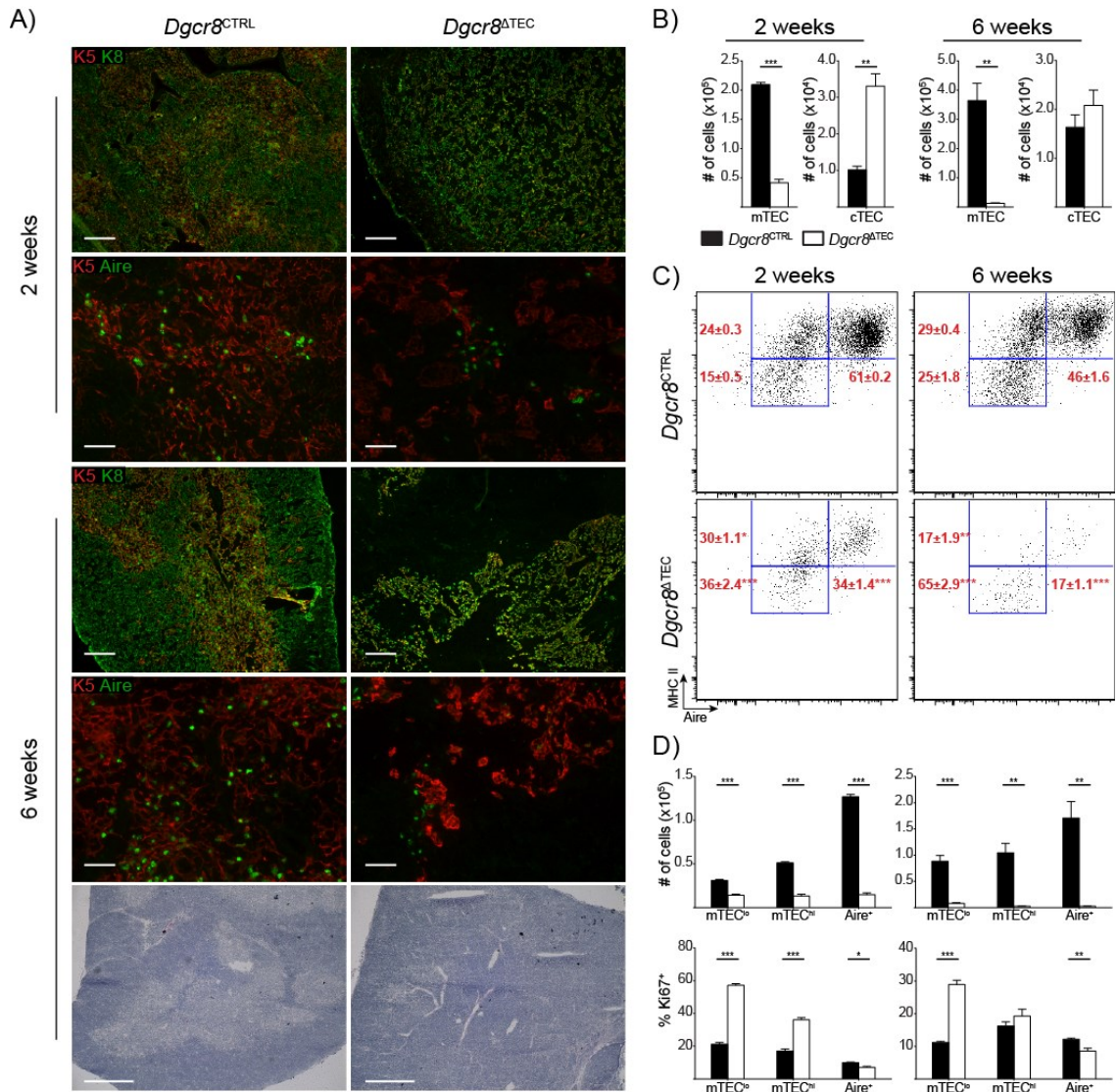
Figure 3.2. Loss of DGCR8 causes a TEC-intrinsic mTEC maturation defect

(A) Frozen thymic sections from $Dgcr8^{\Delta TEC}$ and littermate control mice were assessed for expression of keratin-5 (K5, red), keratin-8 (K8, green), and Aire (green) by immunofluorescent staining at indicated timepoints. Scale bars = 200 µm (K5 K8) and 50 µm (K5 Aire). Data shown are representative images from 2 independent experiments. (B) Enumeration of total mTEC and cTEC cellularity by flow cytometry. cTECs were defined as $CD45^-$, $EpCAM^+$, $Ly51^+$, MHC II^+ events. mTECs were defined as $CD45^-$, $EpCAM^+$, $Ly51^-$, MHC II^+ events. (C) Subset composition was assessed by flow cytometry of mTECs as defined in (B). (D) Quantification of total TEC cellularity and assessment of the proliferation marker Ki67 for the mTEC subsets shown in (C). mTEC subsets were defined as $mTEC^{lo}$ (MHC II^{low}, $Aire^-$), $mTEC^{hi}$ (MHC II^{hi}, $Aire^-$), and $Aire^+$ (MHC II^{hi}, $Aire^+$). (E) Total thymic cellularity from p2 neonatal mice was enumerated by flow cytometry: $CD4^-CD8^-$ double negative (DN), $CD4^+CD8^+$ double positive (DP), $CD4^+$ single positive (SP), and $CD8^+$ SP thymocytes. White bars in (B), (D) and (E) indicate $Dgcr8^{\Delta TEC}$ mice, black bars indicate littermate controls. Data shown in (B-E) are mean ±SEM of 4-9 samples and are representative of two independent experiments. * denotes p≤0.05, ** denotes p≤0.01 and *** denotes p≤0.001, Student's t-test.

Figure 3.2

A) *Dgcr8*CTRL   *Dgcr8*ΔTEC

p2 Thymi

K5 K8

K5 Aire

B) p2 TECs

# of cells (x10⁴)

mTEC

# of cells (x10⁴)

cTEC

■ *Dgcr8*CTRL   □ *Dgcr8*ΔTEC

C) *Dgcr8*CTRL   *Dgcr8*ΔTEC

MHC II

Aire

25±2.9   9±0.7***
46±1.5   29±1.8   73±2.6**   18±2.1**

D)

# of cells (x10⁴)

mTEClo   mTEChi   Aire⁺

% Ki67⁺

mTEClo   mTEChi   Aire⁺

E) p2 Thymocytes

# of cells (x10⁷)

■ *Dgcr8*CTRL   □ *Dgcr8*ΔTEC

# of cells (x10⁶)

DP   CD4 SP   CD8 SP   DN

% of thymocytes

DP   CD4 SP   CD8 SP   DN
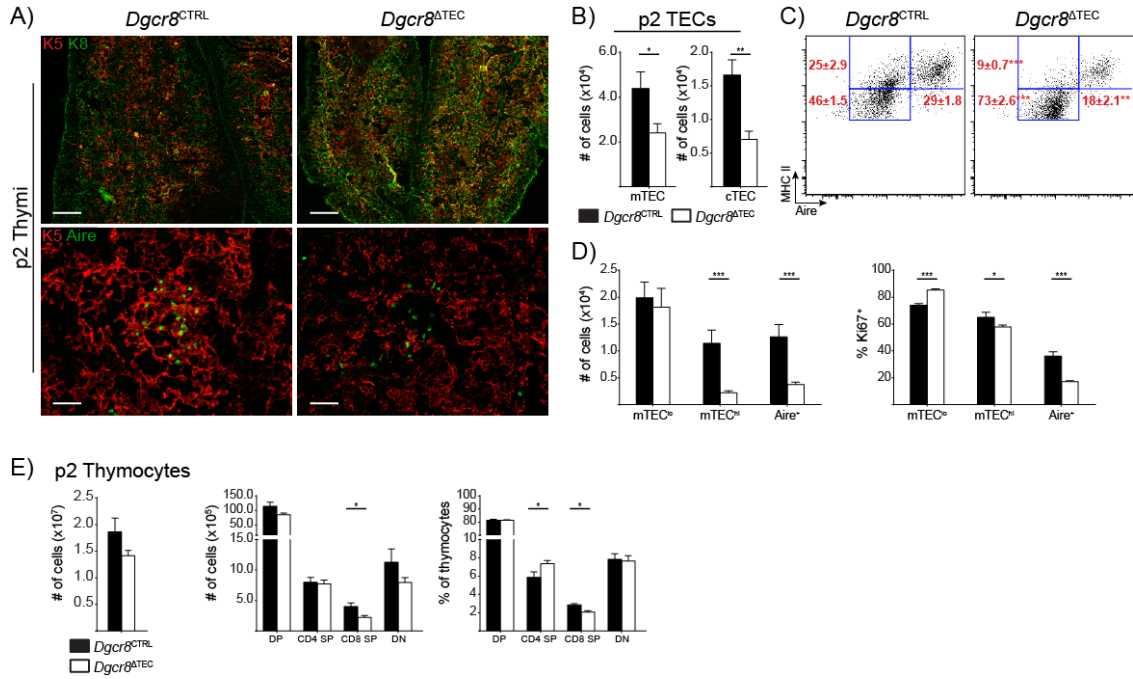
Figure 3.3. miRNAs are required for the maintenance of thymocyte cellularity

(A) Total thymic cellularity from 6-week old mice was assessed by flow cytometry. Plots show thymocyte subsets: $CD4^-CD8^-$ double negative (DN), $CD4^+CD8^+$ double positive (DP), $CD4^+$ single positive (SP), $CD8^+$ SP thymocytes and $CD4^+Foxp3^+$ Treg cells. Relative frequencies are shown as a proportion of all thymocytes with the exception of Treg cells, which are shown as a proportion of $CD4^+$ SP thymocytes. Total thymocyte data are shown as mean ±SEM of 9-13 samples pooled from four independent experiments. Thymocyte subset data is shown as mean ± SEM of 7-8 samples pooled from at least two independent experiments. (B) Total splenic cellularity from 6-8 week old mice. Indicated lymphocyte subsets are shown as a proportion of all splenocytes with the exception of Treg cells, which are shown as a proportion of $CD4^+$ T cells. All splenocyte data are shown as mean ± SEM of 7-11 samples pooled from four independent experiments. White bars in (A) and (B) indicate $Dgcr8^{\Delta TEC}$ mice, black bars indicate littermate controls. * denotes $p \leq 0.05$, ** denotes $p \leq 0.01$ and *** denotes $p \leq 0.001$, Student's *t*-test.

Figure 3.3

Figure 3.4. miRNA deficiency in TECs causes a breakdown in central tolerance

(A) Mice were immunized with P2 peptide and then harvested 10 days later by flow cytometry following a tetramer pulldown assay. Plots are pre-gated on DAPI⁻, NK1.1⁻, CD11b⁻, CD11c⁻, F4/80⁻, B220⁻, CD3⁺ events. Absolute numbers of P2-specific cells are inset within the flow cytometry plots. Tetramer data are pooled from 4-5 samples in three independent experiments. *IRBP*⁻/⁻ mice were included as a positive control for immunization and tetramer pulldown. **(B)** The IRBP-specific immune response was assessed by an IRBP autoantibody assay in mice immunized with P2 peptide and harvested 21 days later. **(C)** Eyes harvested from mice in **(B)** were H&E stained and scored for infiltrates. Scale bars = 200 µm. Data in **(B)** and **(C)** is shown as mean ± SEM of 7-8 samples pooled from two independent experiments. * denotes p≤0.05, and ** denotes p≤0.01, Mann-Whitney test.

Figure 3.4

A)

B) IRBP Autoantibodies

C)
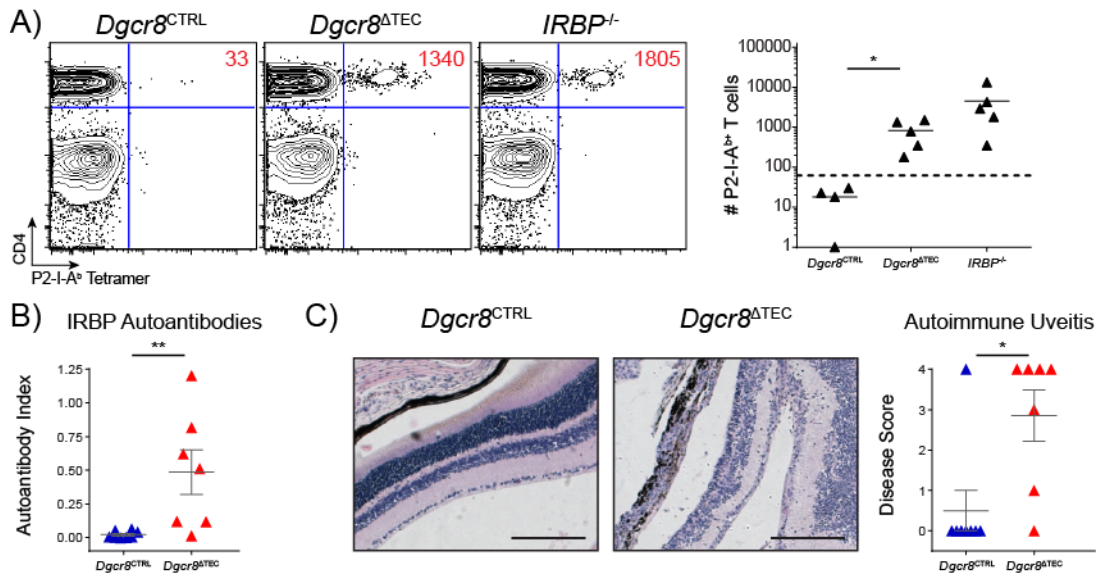
Figure S3.1. Flow cytometry gating strategies for thymic epithelial cells and tetramer pulldown assays

(A) Gating strategy for cTECs and mTECs including all parent gates. cTECs were defined as CD45$^-$, EpCAM$^+$, Ly51$^+$, MHC II$^+$ events. mTECs were defined as CD45$^-$, EpCAM$^+$, Ly51$^-$, MHC II$^+$ events. **(B)** Gating strategy for IRBP P2-tetramer analysis including all parent gates. Tetramer plots are pre-gated on FSC/SSC, DAPI$^-$, NK1.1$^-$, CD11b$^-$, CD11c$^-$, F4/80$^-$, B220$^-$, CD3$^+$ events.

Figure S3.1

A) TEC Gating:
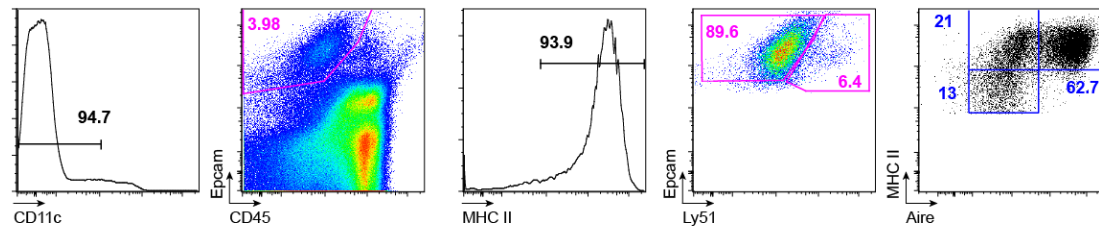
B) Tetramer Gating:
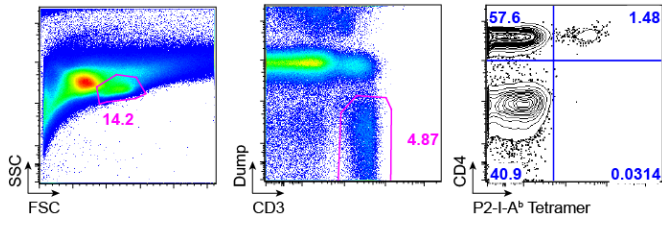
Chapter 4: miR-205 is Highly Expressed in Medullary Thymic Epithelial Cells but its Role in the Postnatal Thymus Remains Unclear

Abstract

Thymic epithelial cells (TECs) play a major role in supporting T cell development in the thymus. Cortical thymic epithelial cells (cTECs) facilitate positive selection of developing thymocytes whereas medullary thymic epithelial cells (mTECs) facilitate the deletion of self-reactive thymocytes in order to prevent autoimmunity. The mTEC compartment is highly dynamic with continuous maturation and turnover, but the genetic regulation of these processes remains poorly understood. MicroRNAs (miRNAs) have been identified as important regulators of gene expression, and recent work has shown that miRNA-deficient TECs are unable to maintain proper thymic function. However, the individual miRNAs responsible for these phenotypes and their mechanisms of action remain unknown. Here, we characterize miR-205 as being highly expressed in mTECs during both thymic ontogeny and in the postnatal thymus. Genetic ablation of miR-205 in TECs, however, was unable to reveal the role of miR-205 in TEC function during homeostatic conditions. Immunization-based approaches did not suggest any defects in central or peripheral tolerance, and miR-205 deficient TECs showed comparable recovery from thymic stress conditions as compared to littermate

controls. Thus, despite its high levels of expression in mTECs, the role of miR-205 in the postnatal thymus remains unclear.

Introduction

Thymic epithelial cells (TECs) are critical mediators of T cell development in the thymus. Cortical thymic epithelial cells (cTECs) facilitate positive selection in the cortex as thymocytes rearrange and assemble T cell receptors (TCRs) capable of recognizing self-MHC [1]. Positively selected thymocytes migrate to the medulla to undergo negative selection by medullary thymic epithelial cells (mTECs) [1, 2]. To prevent autoimmunity, mTECs eliminate self-reactive thymocytes from the developing T cell pool by displaying a repertoire of tissue-specific antigens (TSAs) whose expression is normally limited to peripheral tissues [13, 18, 119, 120]. This ectopic expression of TSAs is largely dependent on autoimmune regulator (Aire), which is expressed in a mature subset of mTECs [11, 32, 36]. Patients and mice with defects in *AIRE* develop multi-organ autoimmune disease, which emphasizes the importance of TSA expression in mTECs as a means to promote central T cell tolerance [26-28, 32].

Several groups have recently shown that mTECs and cTECs represent a highly dynamic population with continuous cycling and turnover in the postnatal thymus [34, 37, 62, 68, 69, 73, 75]. However, the precise regulation of these processes and their impact on thymic function remain largely unknown. While thymocytes represent one of the best genetically characterized cell types,

genetic programs in TECs are understood poorly [121]. Thus, further work is necessary to identify genes and signaling pathways necessary for maintaining homeostasis within the TEC compartments.

MicroRNAs (miRNAs) are ~22 nucleotide noncoding RNAs that mediate post-transcriptional repression of genes in a sequence-dependent manner [78, 79]. Primary miRNA transcripts are processed by the DROSHA /DGCR8 complex to generate ~60-80nt hairpin precursor miRNAs [80]. These hairpins are further processed in the cytoplasm by Dicer to produce mature miRNAs. Mature miRNAs contain a "seed sequence" at nucleotide positions 2-8, and this seed sequence mediates repression through complementary base-pairing within the 3'-untranslated region (UTR) of target mRNAs. Each miRNA can target hundreds of mRNAs, and each mRNA can in turn be regulated by many miRNAs [79, 80]. Thus, miRNAs represent key regulators of gene networks and can be exploited to discover novel pathways.

Recent work by our group and others has shown that miRNA-deficiency in TECs causes a severe disruption of thymic function which leads to the breakdown of central tolerance [81-84]. However, the individual miRNAs responsible for these phenotypes and their precise mechanisms of action remain largely unknown. Identifying the specific miRNAs which are important for TEC biology will allow us to investigate novel networks of genes that are important for establishing and maintaining central tolerance. Understanding these novel pathways will provide new insight into the regulation of the thymic

microenvironment and will contribute to the discovery of therapeutic targets to modulate thymocyte development and central tolerance.

Here, we identify miR-205 as being highly expressed in mTECs and we characterize its expression during thymic ontogeny and in the postnatal thymus. To characterize its role in mTECs, we utilized a conditional knockout allele to ablate miR-205 in TEC lineages. Mice lacking miR-205 in TECs showed normal T cell development and failed to show evidence of autoimmunity or defects in central tolerance. Despite the high levels of miR-205 expression in mTECs, we were unable to detect a phenotype in miR-205 deficient TECs under both homeostatic and thymic stress conditions. Thus, the role of miR-205 in the postnatal thymus and its functional relevance in mTEC biology remains unknown.

Results and Discussion

miR-205 is expressed in medullary thymic epithelial cells

In order to identify miRNAs differentially expressed in medullary thymic epithelial cells (mTECs), we FACS-purified thymic cell subsets from adult mice. We sorted mTECs, cortical thymic epithelial cells (cTECs), and CD45^{+} cells as three distinct populations and prepared RNA for microarray analysis (Figure S4.1A). The CD45^{+} thymocytes were included as a reference population so we could identify TEC-specific miRNAs. These microarray data revealed a distinct miRNA signature for each cell type while also demonstrating a high degree of reproducibility amongst the replicate samples (Figure 4.1A). Based on these

analyses, we chose to focus our studies on miR-205 because of its high signal intensity in mTECs and its differential expression in mTECs when compared to CD45$^+$ cells (Figure 4.1B). We performed qPCR analysis on sorted thymic subsets to validate our microarray data, and miR-205 expression was confirmed to be highest in mTECs and showed intermediate expression in cTECs (Figure 4.1C).

To characterize the temporal and spatial expression pattern of miR-205 we utilized a conditional knockout allele in which a lacZ reporter and loxP sites were targeted into the miR-205 locus (*miR-205*^{lacZ}) (Figure S4.2A) [122]. While this conditional allele can be used to ablate miR-205 in a tissue-specific manner, its promoter-less lacZ reporter can also be used to monitor the transcriptional activity of the endogenous miR-205 promoter. We performed whole-mount X-gal staining of *miR-205*^{lacZ} embryos and observed strong lacZ activity in the thymus as early as e14.5 and quite prominently by18.5 (Figure 4.2A-C). X-gal staining of tissue sections from e18.5 *miR-205*^{lacZ} embryos showed positive lacZ activity within a scattered subset of cells within the developing thymus (Figure 4.2C). The limited number of cells showing positive lacZ activity appeared to support the notion that miR-205 is expressed in the stromal compartment of the thymus rather than thymocytes. Transcriptional activity is not always a true readout of a mature miRNA expression [123], so we performed *in situ* hybridization for miR-205 in wildtype mice to both validate these lacZ findings and to characterize miR-205 expression in the adult thymus. Our *in situ* hybridization data revealed a staining pattern that is consistent with

expression throughout the thymic medulla and suggested that mTECs which express miR-205 do not show any distinct anatomical localization with respect to the cortex or the corticomedullary junction (Figure 4.2D).

Since we interested in characterizing the role of miR-205 in mTEC function, we further analyzed its expression within the mTEC compartment. As mTECs undergo maturation, they upregulate MHC II and Aire such that they begin their development as mTEC^{lo} (MHC II^{lo} Aire$^-$) cells and transition through the mTEC^{hi} (MHC II^{hi}, Aire$^-$) stage and eventually become Aire$^+$ (MHC II^{hi}, Aire$^+$) cells [34-36]. We therefore used an Aire-GFP (*Adig*) reporter allele to purify both immature Aire$^-$ and mature Aire$^+$ mTEC subsets from *Aire$^{+/+}$* mice and performed qPCR analysis for miR-205 [104]. Our results indicate that miR-205 is highly expressed in both mTEC subsets and that it appears to be enriched in the immature Aire$^-$ mTECs (Figure 4.2E). Interestingly, when we used the *Adig* reporter to purify GFP$^+$ and GFP$^-$ mTECs from *Aire$^{-/-}$* mice, we found that although miR-205 was still highly expressed in both mTEC subsets, its expression was more comparable between the two subsets (Figure 4.2F). Recent work has suggested that Aire is required in mTECs in order for them to complete their differential program, so our results support the notion that miR-205 expression is slightly enriched in immature mTECs [38, 124, 125]. Taken together, our results suggest that miR-205 is highly expressed in mTECs during both thymic ontogeny and in the postnatal thymus.

TEC-specific ablation of miR-205

To study the role of miR-205 in TEC function we crossed *miR-205*[lacZ] mice to a Rosa26-FLP strain to excise the lacZ and neomycin cassettes (Figure S4.2A). We next utilized *FoxN1-Cre* knock-in mice, which express Cre recombinase in all TECs without disrupting FoxN1 function [115], to conditionally inactivate miR-205 in TECs (*miR-205*[ΔTEC]) (Figure S4.2A). By purifying mTECs from both *miR-205*[CTRL] and *miR-205*[ΔTEC] mice we were able to confirm both the proper expression of miR-205 in *miR-205*[CTRL] mice as well as its efficient ablation in *miR-205*[ΔTEC] (Figure 4.3A). In parallel, we performed *in situ* hybridization on thymi from these mice to demonstrate uniform ablation in *miR-205*[ΔTEC] mice (Figure 4.3B).

miR-205 deficiency in TECs does not perturb thymic function under homeostasis

Previous work has shown that miR-205 can target *ZEB2* and thereby play a role in regulating the epithelial-to-mesenchymal transition (EMT) [126-128]. EMT is an important physiologic process during embryonic development and wound repair [129], but its role in TEC biology remains unknown. *ZEB1* and *ZEB2* are transcription factors which drive EMT progression by downregulating "epithelial" genes such as E-cadherin, claudins and occludins while upregulating "mesenchymal" genes such as N-cadherin, vimentin and fibronectin [129, 130]. The contribution of these "epithelial" genes to antigen processing and presentation in mTECs has not been studied. While one recent report suggests that Aire+ mTECs are derived from a unique claudin-3,4[+]

lineage of mTECs [131], the implications of this finding are not clear and warrant further investigation. Therefore, as a regulator of EMT progression, miR-205 appears to promote the "epithelial" phenotype and thus we hypothesized that miR-205 deficiency might lead to abnormal thymic architecture or altered mTEC differentiation.

To understand the physiologic role of miR-205 in TECs during homeostasis, we first analyzed untreated adult *miR-205*^CTRL and *miR-205*^ΔTEC mice. Immunostaining of thymi revealed similar patterns of keratin-5 (K5) and keratin-8 (K8) staining, which indicated that the overall corticomedullary architecture of the thymus was preserved in *miR-205*^ΔTEC mice (Figure 4.4A). Staining for Aire was also comparable between the two genotypes, which suggested that mTEC maturation was not impaired in the absence of miR-205 in TECs (Figure 4.4A). Staining for Aire and claudin-3 was also comparable between the two genotypes, which suggested that mTEC maturation was not impaired in the absence of miR-205 in TECs (Figure 4.4A).

To further characterize these thymi we performed flow cytometry on TECs. Consistent with the histology, we did not observe any significant differences in mTEC and cTEC cellularity (Figure 4.4B). We used MHC II and Aire to further characterize the mTEC compartment and found the immature mTEC^lo (MHC II^lo Aire^-), intermediate mTEC^hi (MHC II^hi, Aire^-) and mature Aire^+ (MHC II^hi, Aire^+) mTEC subsets to be comparable in both proportion and cell number between *miR-205*^CTRL and *miR-205*^ΔTEC mice (Figure 4.4C-D). Furthermore, there were no differences in the proportion of mTECs which

expressed the proliferation marker Ki67 (Figure 4.4D). Taken together, these results indicate that miR-205 deficient thymi showed no changes in the development, maintenance, or maturation of TECs.

Next, we characterized the impact of miR-205 deficiency on thymocyte selection. We did not observe any significant changes in total thymic cellularity between $miR\text{-}205^{CTRL}$ and $miR\text{-}205^{\Delta TEC}$ mice (Figure 4.4E). Similarly, when analyzing thymocyte subsets between the two groups, we did not observe any significant differences in the relative frequencies or absolute numbers of $CD4^-$ $CD8^-$ double negative (DN), $CD4^+CD8^+$ double positive (DP), $CD4^+$ single positive (SP), $CD8^+$ SP thymocytes and $CD4^+Foxp3^+$ Treg cells (Figure 4.4E). Overall, thymocyte selection appeared unchanged, suggesting that miR-205 deficient TECs are sufficient to support T cell development.

Central and peripheral tolerance is maintained with miR-205 deficiency in TECs

We next sought to determine whether miR-205 deficiency in the thymus led to any changes in peripheral lymphocytes. We analyzed splenocytes from adult mice but did not detect any significant changes in the total number of splenocytes between $miR\text{-}205^{CTRL}$ and $miR\text{-}205^{\Delta TEC}$ mice (Figure 4.5A). The relative frequency and absolute number of $CD19^+$ cells, $CD4^+$ T cells and $CD8^+$ T cells was also comparable between the two genotypes (Figure 4.5A). Further analysis of T cell subsets showed no difference in Treg cells (CD25+ Foxp3+) and in T cells with an activated-memory ($CD44^{hi}$ $CD62L^{lo}$) phenotype (Figure

4.5A). Together, these results suggest that peripheral T cell homeostasis is maintained in *miR-205*$^{\Delta TEC}$ mice.

To look for evidence of spontaneous autoimmunity, we performed hematoxylin and eosin (H&E) staining on various organs from aged mice but were unable observe any differences in immune infiltrates between *miR-205*$^{\Delta TEC}$ mice and littermate controls (data not shown). Despite the absence of any overt disease in *miR-205*$^{\Delta TEC}$ mice, we sought to determine whether these mice had a defect in central tolerance. Specifically, we hypothesized that self-reactive T cells could escape thymic deletion due to potential defects in antigen processing or presentation but remain in check due to peripheral tolerance. To test this hypothesis in the polyclonal T cell repertoire, we utilized an immunization-based approach to expand and detect Aire-dependent autoreactive T cells in the periphery of *miR-205*$^{\Delta TEC}$ mice. We have previously shown that T cells specific for the self-antigen IRBP are efficiently deleted in the thymus of *Aire*-sufficient hosts, and that these cells can escape thymic deletion and provoke autoimmune uveitis in *Aire*-deficient mice or in mice harboring defects in negative selection [13, 81]. Previously, we have shown that these autoreactive CD4$^+$ IRBP-specific cells can be detected in the periphery of *Aire*$^{-/-}$ mice through the use of a peptide-class II tetramer, P2-I-A^b [15, 81]. To determine whether these cells could escape thymic deletion in *miR-205*$^{\Delta TEC}$ mice, we immunized mice with an MHC II binding IRBP (P2) epitope to expand cells for detection in the periphery. Ten days following immunization, we pooled lymph nodes and spleen to enumerate total numbers of CD4$^+$ P2-I-A^b-specific T

cells by flow cytometry. Consistent with the absence of any overt TEC phenotype or spontaneous autoimmunity, we did not detect any differences in the expansion of IRBP-specific T cells in either 8-week old or 5-month old *miR-205*$^{\Delta TEC}$ mice when compared to controls (Figure 4.5B). We concluded from these experiments that under homeostatic conditions, *miR-205*$^{\Delta TEC}$ mice do not exhibit overt defects in central T cell tolerance and lack evidence suggesting a breakdown in peripheral tolerance.

Thymic stress conditions do not reveal a role for miR-205 in TECs

Several groups have reported difficulty in characterizing the phenotypes of miRNA knockout mice when analyzing mice under homeostatic conditions [132-134]. This difficulty is likely due to the role of many miRNAs acting as fine tuners of gene expression rather than molecular switches. Furthermore, it has been proposed that the regulatory role of miRNAs is to buffer changes in gene expression during critical periods of physiological stress [135, 136]. Therefore, we employed the use of two different thymic stress models in an attempt to reveal a TEC phenotype in *miR-205*$^{\Delta TEC}$ mice.

The thymus is a highly dynamic organ with the capacity to undergo significant changes in response to pathologic stress. Many groups have demonstrated that the thymus can undergo involution in response to various insults including hormones, infection, irradiation and inflammatory cytokines [60-65], and recent work using TEC ablation models has now shown that both cTECs and mTECs have a remarkable ability to recover from thymic injury [37,

62, 69]. Given the reports describing miR-205 as a regulator of cell cycle and proliferation [137-140], we hypothesized that TECs from $miR\text{-}205^{\Delta TEC}$ mice would be impaired in their ability to recover from thymic damage. One group recently took advantage of this approach to demonstrate that miR-29a deficiency lowers the threshold for the thymus to undergo involution in response to systemic administration of polyinosinic-polycytidylic acid (poly(I:C)) [82]. In accordance with these studies we administered systemic poly(I:C) to $miR\text{-}205^{\Delta TEC}$ mice and littermate controls. While we observed a substantial degree of thymic involution, we failed to uncover any difference in dose-response between the two groups (Figure 4.6A). We focused our analysis on the 12-day recovery timepoint following administration of the high-dose poly(I:C). Although total thymic cellularity had returned to baseline at this time, the mTEC compartment was still undergoing recovery as indicated by the lower cellularity in the mTEC^{hi} subset (Figure 4.6B-D). However, we again failed to see any difference between $miR\text{-}205^{\Delta TEC}$ mice and controls which suggested that miR-205 does not play a role in TECS during recovery from poly(I:C)-induced thymic involution.

To confirm these findings in an independent thymic stress model, we chose to administer sub-lethal total body irradiation (SL-TBI) to $miR\text{-}205^{CTRL}$ and $miR\text{-}205^{\Delta TEC}$ mice. Irradiation of the thymus causes thymic involution by promoting both thymocyte apoptosis as well as direct damage to the TEC compartment [61, 70, 71]. This was an important consideration in choosing this model because many models of thymic stress are driven by the depletion of

developing thymocytes [60, 62, 66, 67], and the impact on the TEC compartment is likely secondary to the withdrawal of cross-talk interactions between developing thymocytes and the stromal compartment [62, 141]. After exposing mice to SL-TBI we harvested their thymi for analysis at both 15-days and 30-days of recovery. However, we failed to observe any differences between the two genotypes at either the 15-day timepoint when total thymic cellularity was depleted, or at the 30-day timepoint when total cellularity had returned to baseline levels (Figure 4.7A). Interestingly, while total mTEC cellularity was comparable between *miR-205*^{CTRL} and *miR-205*$^{\Delta TEC}$ mice at 15-day and 30-day timepoints, the cTECs showed slightly lower numbers in the *miR-205*$^{\Delta TEC}$ mice at the 30-day timepoint (Figure 4.7B). Subset analysis of the mTEC compartment failed to reveal significant changes in frequency or total cell number between the two groups (Figure 4.7C-D). Interestingly, we did observe an increased proportion of Aire$^+$ cells in *miR-205*$^{\Delta TEC}$ mice which expressed Ki67 (Figure 4.7D). However, given that the overall mTEC subset frequencies and total cell numbers were comparable between the two groups at both recovery timepoints, it remains unclear whether this change in Ki67 expression bears any significance on the overall ability of miR-205 deficient TECs to recover from SL-TBI mediated injury. Our results from these stress models indicate that miR-205 is not required in TECs to recover from either poly(I:C) or SL-TBI mediated thymic insult. Taken together with the lack of phenotype under homeostatic conditions, the role of miR-205 in the postnatal thymus remains unclear.

There are many possible explanations for our inability to detect a phenotype in *miR-205*[ΔTEC] mice and hence uncover the role of miR-205 in mTECs. miR-205 is expressed in many epithelial tissues including the skin and stomach and is best characterized as an epithelial miRNA [142-144]. Interestingly, it is often co-expressed with several other epithelial miRNAs such as miR-203 and the miR-200 family [126, 127, 144]. While miR-205 does not have any known miRNA family members with conserved seed sequences, it remains possible that several of its co-expressed epithelial miRNAs could functionally compensate for it in the context of miR-205 deficiency. For example, although miR-205 has been implicated as a regulator of EMT through its ability to target *ZEB2*, the same studies showed an even greater functional relationship between members of the miR-200 family and EMT progression [126, 127].

It also remains possible that the function of miR-205 in TECs is to regulate early developmental steps during thymic ontogeny, and hence our studies in the postnatal thymus were not sufficient to interrogate this role. A recently published study characterized miR-205 transcription throughout embryonic development by performing X-gal staining on *miR-205*[lacZ] embryos [142]. Of note, the authors were able to detect lacZ activity in the pharyngeal pouches at e11.5 and e12.5 [142]. This observation is of note because the earliest expression of FoxN1 correlates with these timepoints during thymic development [145, 146]. If the critical role of miR-205 was limited to this early period of development, it remains possible that the timing of *FoxN1-Cre*

90

expression was not sufficient to ablate miR-205 during this critical period. Alternatively, *miR-205*$^{\Delta TEC}$ mice could have recovered from any transient defects during thymic development such that the postnatal thymus is phenotypically normal. However, in the event that miR-205 is only required during thymic development, it remains unclear why mTECs maintain such a high level of miR-205 expression in adult mice.

<u>Concluding Remarks</u>

In summary, we performed miRNA profiling of thymic stromal cells and identified miR-205 as a candidate miRNA with preferential expression in mTECs. We show here that miR-205 is highly expressed in mTEC populations during both embryonic development and in the postnatal thymus. To characterize the role of miR-205 in mTECs, we utilized a miR-205 conditional allele in combination with *FoxN1-Cre* to target the ablation of miR-205 to TEC lineages. We were unable to detect a phenotype in miR-205 deficient TECs in adult mice, and both thymocyte development and peripheral lymphocyte homeostasis appeared comparable between *miR-205*$^{\Delta TEC}$ mice and controls. Immunization with an Aire-dependent self-antigen failed to reveal a breakdown in central tolerance, and *miR-205*$^{\Delta TEC}$ mice did not show any other signs of overt autoimmunity. Finally, thymic stress models were unable to suggest a role for miR-205 in TECs as *miR-205*$^{\Delta TEC}$ mice showed similar recovery to littermate controls following either poly(I:C) or SL-TBI mediated thymic involution. Thus, the role of miR-205 in the postnatal thymus remains unclear.

Materials and Methods

Mice

FoxN1-Cre knock-in mice were kindly provided by N. Manley [115]. Targeted *miR-205* (*miR-205*^{lacZ}) mice have been described previously [122]. To generate conditional knockout mice *miR-205*$^{lacZ/+}$ mice were crossed to a Rosa-FLP allele to excise the lacZ and neomycin cassettes. After confirming the deletion of these two elements, we out-crossed the Rosa-FLP allele and then backcrossed *miR-205*$^{fl/+}$ mice to the B6 background for 3 generations. At this point *miR-205*$^{fl/+}$ mice were crossed with *B6.FoxN1-Cre* mice for experimental analysis. Throughout this study *miR-205*$^{\Delta TEC}$ represents *FoxN1-Cre*$^+$ *miR-205*$^{fl/fl}$ mice and littermate controls are *FoxN1-Cre*$^+$ *miR-205*$^{fl/+}$ mice and all *FoxN1-Cre*$^-$ mice. *IRBP*$^{-/-}$, Aire-GFP (*Adig)*, and *Aire*$^{-/-}$ mice have been described previously [13, 32, 104]. Mice were housed and bred under specific-pathogen free conditions at the University of California, San Francisco (UCSF) Animal Barrier Facility. Animal experiments were approved by the Institutional Animal Care and Use Committee (IACUC) at UCSF.

Thymic Stress Models

For poly(I:C)-induced thymic involution, High Molecular Weight poly(I:C) (Invivogen) was reconstituted in sterile saline according to the manufacturer's instructions. Mice were treated intraperitoneally on day (-3) and day 0 and then harvested at the indicated recovery timepoints. For sub-lethal total body irradiation (SL-TBI) experiments, mice were exposed to a single 550 cGy dose

of radiation on day 0 and allowed to recover without hematopoietic rescue until they were analyzed at the designated timepoints.

Flow Cytometry

Thymic stromal cells were isolated as described previously [104, 147]. Briefly, thymi were minced with razor blades and digested with DNase I and Liberase TM (Roche) before gradient centrifugation with Percoll PLUS (GE Healthcare). Enriched stromal cells were first incubated with the Fc-receptor blocking antibody 2.4G2 and then stained with the indicated surface marker antibodies (BioLegend). For lymphocyte staining, all surface marker antibodies were obtained from BioLegend. For intracellular staining, cells were processed using the Foxp3 Staining Buffer Set and stained with anti-Foxp3-APC (eBiosciences), anti-Ki67-PE (BD Biosciences), or anti-Aire-A647 (eBiosciences). All data were collected using a BD LSR II flow cytometer and analyzed with either FloJo software (TreeStar) or FACS Diva (BD Biosciences). Cell sorting for microarray and qPCR analyses was performed using a BD FACS Aria III cell sorter.

RNA Isolation

Total RNA was extracted from FACS-sorted samples using TRIzol (Invitrogen) according to the manufacturer's instructions.

Quantitative PCR

RNA was extracted as described above. As described previously [148], reverse

transcriptase reactions were performed using the Applied Biosystems TaqMan MicroRNA RT kit and quantitative PCR reactions were performed using the Applied Biosystems TaqMan miRNA assay system. All reactions were normalized to sno202.

Microarray Analysis

Thymic subsets were FACS-purified from 4-week old NOD wildtype mice. Thymi from 10-12 female mice were pooled together for stromal cell isolation, and RNA was extracted as described above. Sample preparation, labeling, and array hybridizations were performed according to standard protocols from the UCSF Shared Microarray Core Facilities and Agilent Technologies (http://www.arrays.ucsf.edu and http://www.agilent.com). Total RNA quality was assessed using a Pico Chip on an Agilent 2100 Bioanalyzer (Agilent Technologies, Palo Alto, CA). RNA was labeled with Cy3-CTP using the miRCURY LNA microRNA power labeling kit (Exiqon, Inc, Woburn, MA), according to manufacturer's protocol. Labeled RNA was hybridized to Agilent custom UCSF miRNA v3.5 multi-species 8x15K Ink-jet arrays (Agilent). Hybridizations were performed for 16 hrs, according to the manufacturers protocol (Agilent). Arrays were scanned using the Agilent microarray scanner (Agilent) and raw signal intensities were extracted with Feature Extraction v10.1 software (Agilent).

X-gal Staining

For staining of embryos, *miR-205*[lacZ] embryos were harvested and fixed with 4% paraformaldehyde and 0.2% glutaraldehyde as described previously [122, 142]. For larger e18.5 embryos, internal organs were dissected out for additional fixation and permeabilized in 0.02% NP40, 0.01% sodium deoxycholate, and 2mM PBS for one hour prior to staining. Overnight X-gal staining was performed at room temperature and embryos were then fixed in 2% paraformaldehyde and stored in 70% ethanol.

In Situ Hybridization

In situ hybridization was performed on frozen thymic sections. At harvest, thymi were fixed for 2 hours in 4% paraformaldehyde and equilibrated for 7 hours in 30% sucrose. We used double DIG labeled LNA probes against either miR-205 or a scramble control (Exiqon). We followed the manufacturer's instructions and hybridized the probes overnight at 57ºC with the following modifications: Post-hybridization stringency washes: 2x SSC for 60' at 57ºC, 1x SSC for 10' at RT, 0.5x SSC for 10' at RT, 0.1x SSC for 45' at 57ºC. Tissues were then blocked with 1% goat serum in 0.1% PBS-Tween-20 (PBST) for 2 hours before overnight incubation with a 1:5000 dilution of anti-DIG-AP antibody (Roche) at 4ºC. Following antibody incubation and overnight washes in PBST, alkaline phosphatase activity was detected using an NBT/BCIP solution (Roche). Slides were visualized using either a Zeiss Apotome or a Zeiss AxioImager brightfield microscope.

Histology and Immunofluorescence

Thymi were harvested and embedded in Optimal Cutting Temperature (OCT) media (Tissue-Tek). 8µm frozen thymic sections were fixed in 100% acetone, blocked in 10% goat serum, and then stained for keratin-5 (Abcam), keratin-8 (Abcam), claudin-3 (Invitrogen), or Aire (eBiosciences). Secondary antibodies were purchased from Invitrogen. Immunofluorescent staining was visualized using a Zeiss Apotome widefield microscope.

Immunization and Tetramer Analysis

Mice were immunized with 100 µg of IRBP P2 peptide (amino acids 271-290) emulsified in Complete Freund's Adjuvant (CFA) as described previously [15]. Tetramer analysis was performed on pooled lymph nodes and spleen harvested from treated mice 10 days after immunization. P2-I-A^b tetramer (Interphotoreceptor retinol binding protein 3, amino acids 294-306) was generated by the NIH Tetramer Core Facility, and tetramer staining was performed as described previously [15, 105]. Briefly, cells were stained with tetramer for 1 hour at room temperature before enrichment for tetramer^{+} cells using anti-APC microbeads and MACS columns (Miltenyi Biotech). Positively-selected cells were stained with antibodies for flow cytometry, and counting beads (Invitrogen) were used to enumerate the absolute number of tetramer^{+} cells.

Statistical Analysis

Statistical analysis was performed using Prism 6.0 (Graphpad). Mann-Whitney testing was performed for tetramer analysis. Student's *t*-test was performed for TEC and lymphocyte analyses. * denotes p≤0.05, ** denotes p≤0.01 and *** denotes p≤0.001.

Figure 4.1. miRNA profiling in TECs identifies miR-205 as highly expressed in mTECs

(A) Thymic subsets were purified from 4-5 week old *NOD* wildtype mice for miRNA profiling by microarray analysis. The heatmap depicts the union of differentially expressed miRNAs from any comparison (FDR <0.05) with an absolute log2 fold change >1 relative to the signal intensity of CD45$^+$ cells. **(B)** Plot depicts average log2 fold change (FC) between mTEC vs CD45$^+$ cells on the *y*-axis and average log2 signal intensity across all samples on the *x*-axis. Red dots indicate genes that are differentially expressed in mTECs vs CD45$^+$ cells with an FDR <0.05. **(C)** Thymic stromal subsets were FACS-purified from 4-6 week old *B6* wildtype mice to confirm the expression of miR-205 in mTECs by qPCR analysis. All reactions were standardized to sno202 and then normalized to CD45$^+$ cells with error bars depicting mean ±SD.
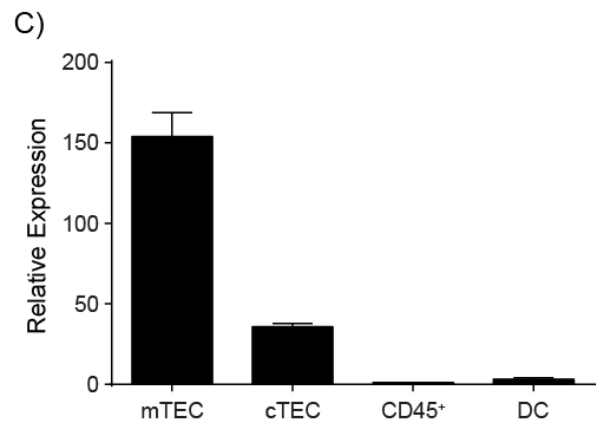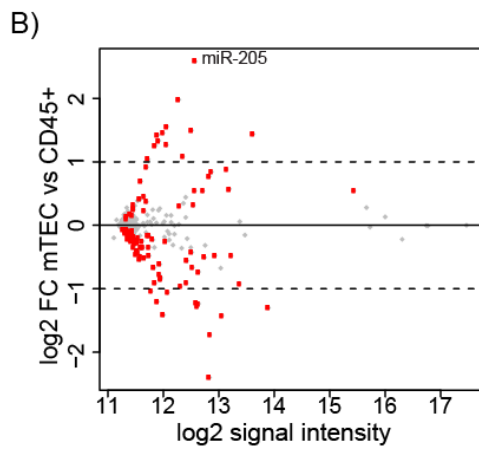
Figure 4.1
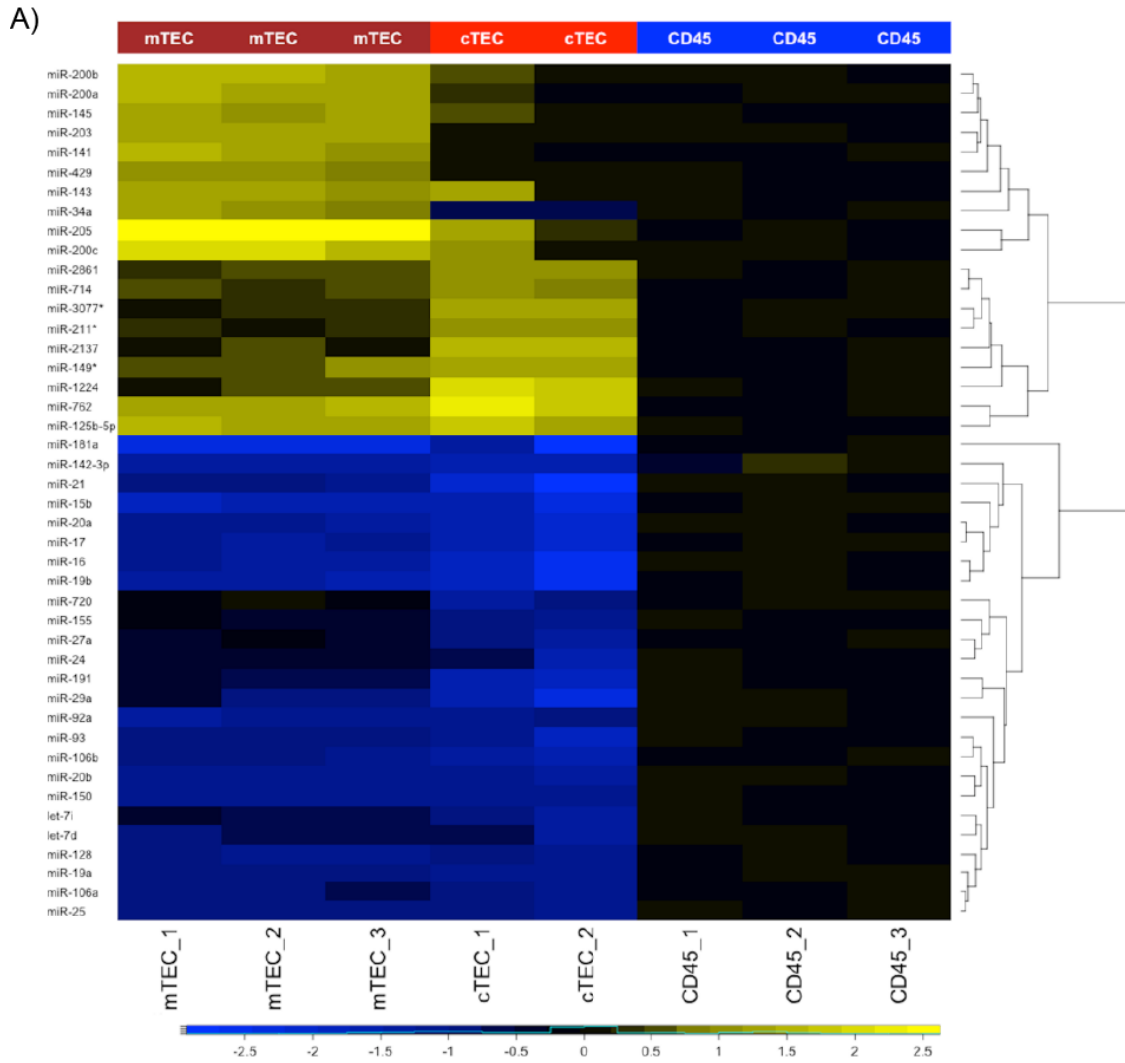
Figure 4.2. miR-205 is expressed during thymic ontogeny and maintained in the adult thymus

(A) X-gal staining was performed on e14.5 *miR-205*[lacZ] embryos to identify patterns of miR-205 transcription. The diagram on the left indicates the orientation of the tissues that were sectioned for analysis. **(B)** Whole-mount X-gal staining was performed on a dissected e18.5 *miR-205*[lacZ] embryo (left) and positive lacZ reporter activity was observed in the thymus (arrow). A dissected and stained *miR-210*[lacZ] embryo (right) is shown as a negative control for lacZ activity in the thymus. **(C)** Thymic sections from an e18.5 *miR-205*[lacZ] embryo were cut and then stained with X-gal. Arrows indicate positive lacZ reporter activity in a subset of cells in the thymus. **(D)** *in situ* hybridization for miR-205 was performed on frozen thymic sections from 6-8 week old B6 wildtype mice. Serial sections were hybridized using either a miR-205 probe or a scramble probe. Image pairs from two samples are shown. Scale bars = 200 μm. **(E-F)** Sorted thymic subsets from either *Aire*^{+/+} **(E)** or *Aire*^{-/-} **(F)** mice were analyzed by qPCR for miR-205 expression. Both genotypes carried the Aire-GFP (*Adig*) allele to facilitate the sorting of Aire^{+}/GFP^{+} and Aire^{-}/GFP^{-} mTEC subsets. Reactions were standardized to sno202 and then normalized to CD45^{+} cells with error bars depicting mean ±SD.

Figure 4.2

A)

E14.5

10x   40x

B)

miR-205   miR-210

C)

10x   40x

D)

miR-205 probe   scramble probe

sample A

sample B

E)

Relative Expression

Aire⁻ mTEC   Aire⁺ mTEC   cTEC   CD45⁺   DC

F)

Relative Expression

GFP⁻ mTEC   GFP⁺ mTEC   cTEC   CD45⁺   DC
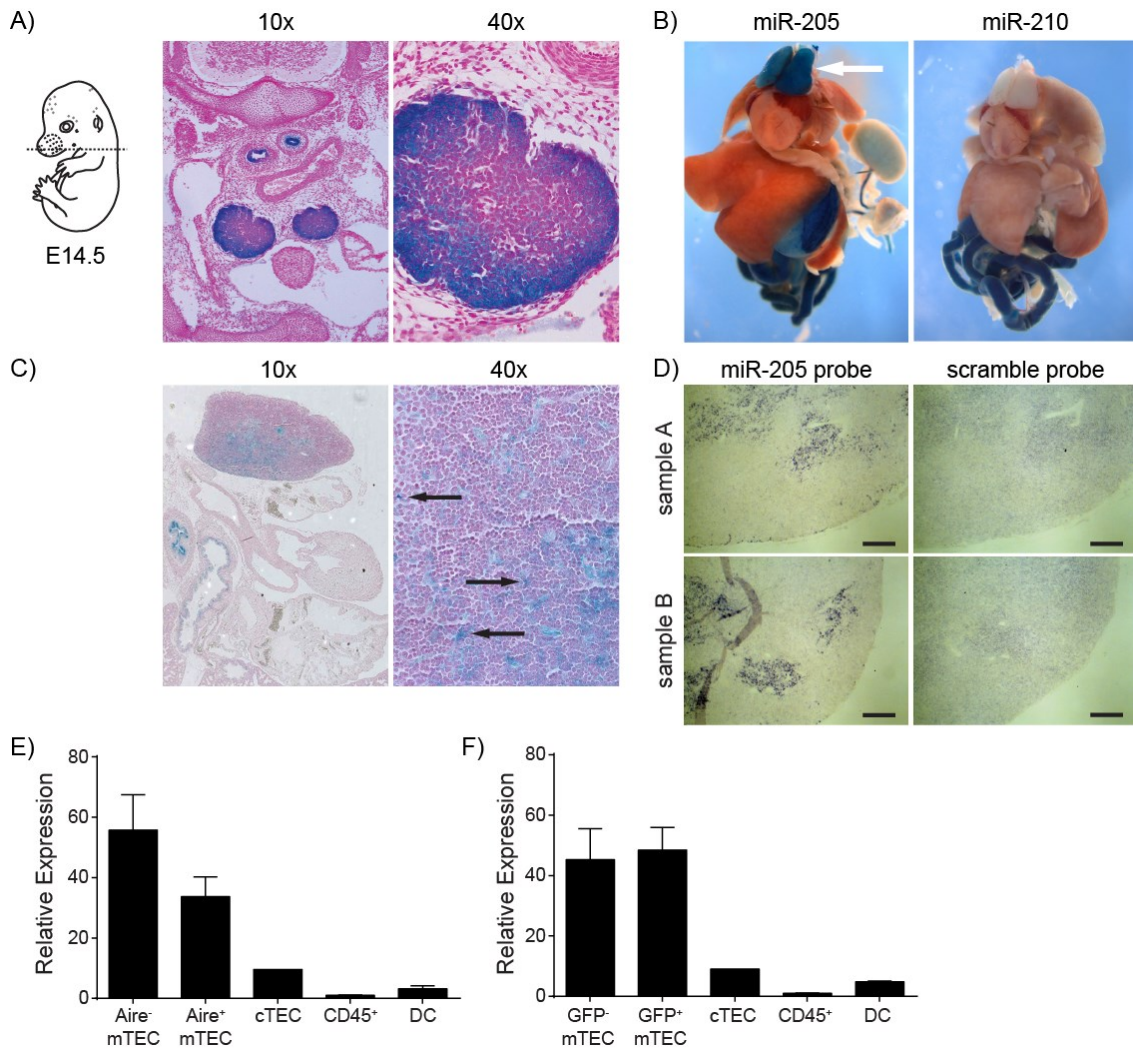
Figure 4.3. Validation of miR-205 ablation in TECs

(A) mTECs from 4-6 week old *miR-205*^CTRL and *miR-205*^ΔTEC mice were sorted to analyze miR-205 expression by qPCR. Reactions were normalized to sno202 and normalized to CD45$^+$ cells. Values depict mean ±SD. Data is representative of two independent experiments. **(B)** *in situ* hybridizations were performed using a miR-205 probe on frozen thymic sections from 4-6 week old *miR-205*^CTRL and *miR-205*^ΔTEC mice to confirm the uniform deletion of miR-205 in mTECs. Scale bars = 200 μm (top), and 100 μm (bottom).

Figure 4.3

A)

B)
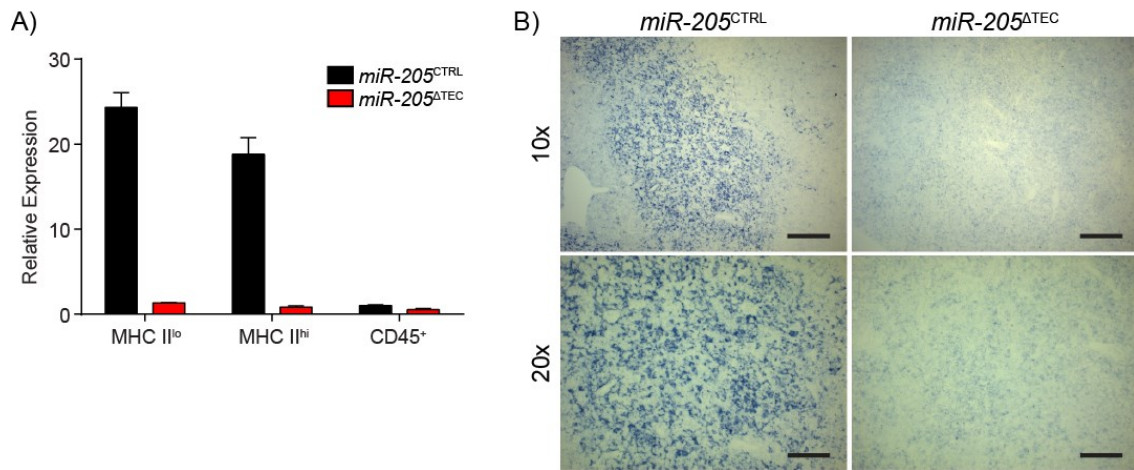
Figure 4.4. miR-205 deficient thymi appear phenotypically normal under homeostatic conditions

(A) Frozen thymic sections from 6-week old *miR-205*$^{\Delta TEC}$ and littermate control mice were assessed for expression of keratin-5 (K5, red), keratin-8 (K8, green), claudin-3 (Cld-3, red), and Aire (green). Top = K5 and K8, scale bars = 200 µm. Middle = K8 and Cld-3, scale bars = 200 µm. Bottom = K5 and Aire, scale bars = 50 µm. **(B)** Enumeration of total mTEC and cTEC cellularity in 5-month old mice by flow cytometry. cTECs were defined as CD45$^-$, EpCAM$^+$, Ly51$^+$, MHC II$^+$ events. mTECs were defined as CD45$^-$, EpCAM$^+$, Ly51$^-$, MHC II$^+$ events. **(C)** Subset composition was assessed by flow cytometry of mTECs as defined in **(B)**. **(D)** Quantification of total TEC cellularity and assessment of the proliferation marker Ki67 for the mTEC subsets shown in **(C)**. mTEC subsets were defined as mTEC^{lo} (MHC II^{low}, Aire$^-$), mTEC^{hi} (MHC II^{hi}, Aire$^-$), and Aire$^+$ (MHC II^{hi}, Aire$^+$). Data in **(B-D)** are shown as mean ±SEM of 8 samples per group and representative of at least two independent experiments. **(E)** Total thymic cellularity from 4-month old mice was assessed by flow cytometry. Plots show thymocyte subsets: CD4$^-$CD8$^-$ double negative (DN), CD4$^+$CD8$^+$ double positive (DP), CD4$^+$ single positive (SP), and CD8$^+$ SP thymocytes. Relative frequencies are shown as a proportion of all thymocytes with the exception of Treg cells, which are shown as a proportion of CD4$^+$ SP thymocytes. Data are shown as mean ±SEM of 3 samples and are representative of at least 3 independent experiments. White bars in **(B-E)** indicate *miR-205*$^{\Delta TEC}$ mice, black bars indicate littermate controls.

Figure 4.4
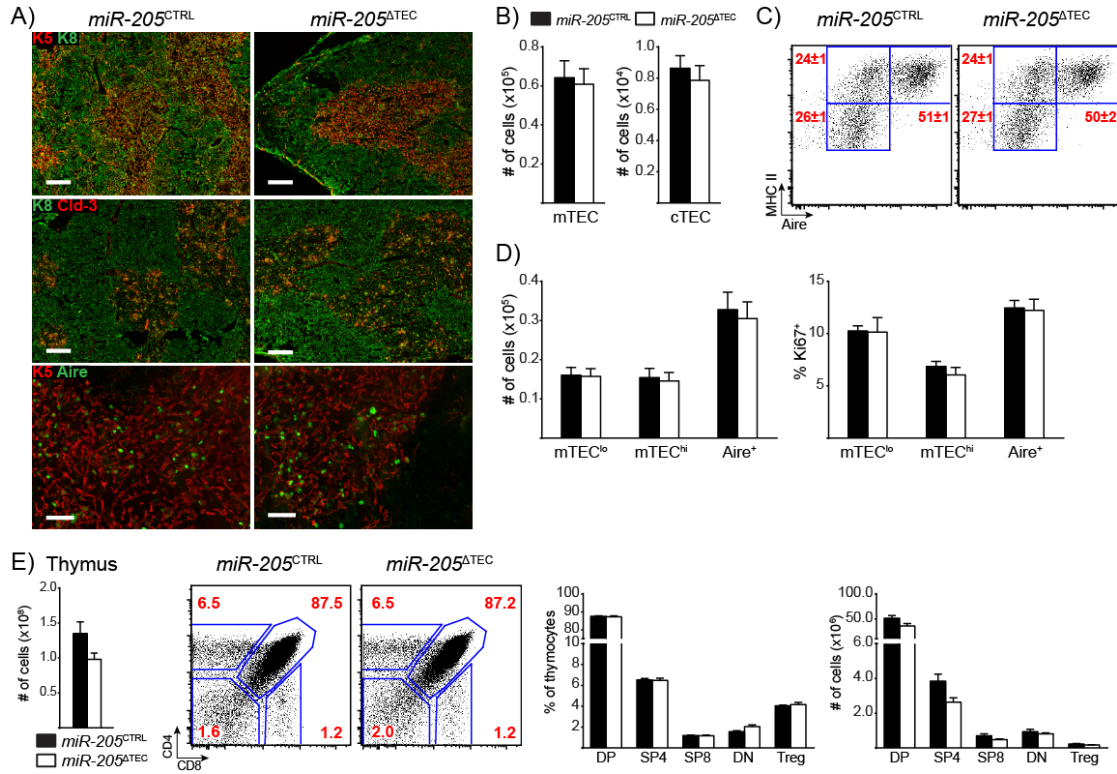
Figure 4.5. Central and peripheral tolerance is maintained in miR-205-deficient mice

(A) Total splenic cellularity from 4-month old mice. Indicated lymphocyte subsets are shown as a proportion of all splenocytes with the exception of Treg cells (CD4$^+$ CD25$^+$ Foxp3$^+$) and activated-memory phenotype T cells (CD44^{hi} CD62L^{lo}), which are shown as a proportion of their respective T cell populations. Splenocyte data are shown as mean ± SEM of 3 samples per group, and are representative of at least 3 independent experiments. White bars indicate *miR-205*$^{\Delta TEC}$ mice, black bars indicate littermate controls. **(B)** Mice were immunized with P2 peptide and then harvested 10 days later and analyzed by flow cytometry following a tetramer pulldown assay. Plots are pre-gated on DAPI$^-$, NK1.1$^-$, CD11b$^-$, CD11c$^-$, F4/80$^-$, B220$^-$, CD3$^+$ events. Absolute numbers of P2-specific cells are inset within the flow cytometry plots and plotted below. Tetramer data are pooled from 8-10 samples per group from two independent experiments. *IRBP*$^{-/-}$ mice were included as a positive control for immunization and tetramer pulldown

Figure 4.5
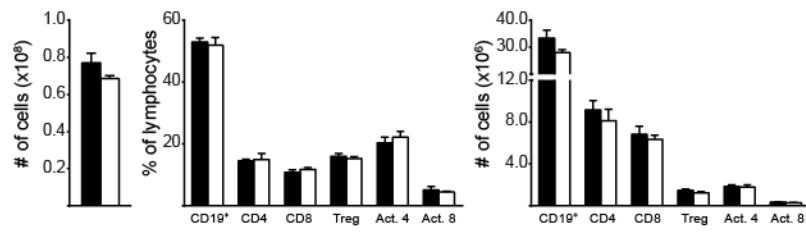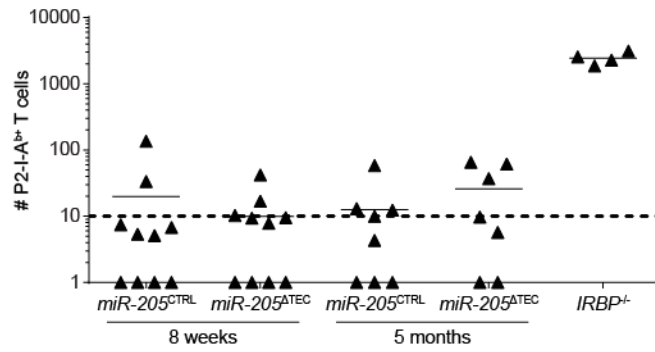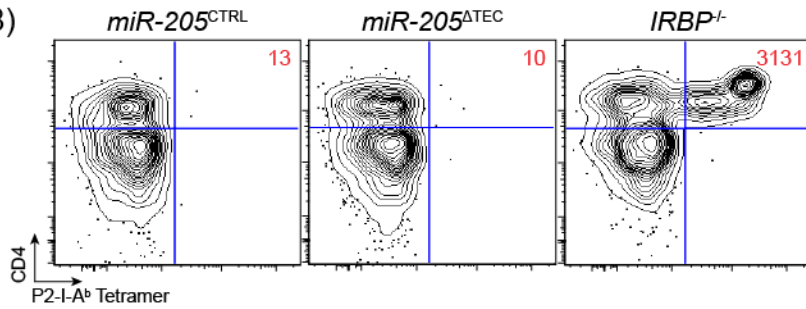
Figure 4.6. miR-205 deficient TECs show comparable sensitivity and recovery potential in response to poly(I:C) mediated thymic involution

(A) 4-week old mice were treated with varying doses of poly(I:C) at day (-3) and day (0) before being harvested at day 4 of their recovery for enumeration of total thymic cellularity. **(B)** Mice were treated with 250µg of poly(I:C) as conducted in **(A)** and then harvested at 12 days of recovery to enumerate total thymic cellularity. **(C)** Enumeration of total mTEC and cTEC cellularity in 4-week old mice shown in **(B)**. cTECs were defined as CD45$^-$, EpCAM$^+$, Ly51$^+$, MHC II$^+$ events. mTECs were defined as CD45$^-$, EpCAM$^+$, Ly51$^-$, MHC II$^+$ events. **(D)** Subset composition was assessed by flow cytometry of mTECs as defined in **(C)**. Quantification of total TEC cellularity and assessment of the proliferation marker Ki67 for the mTEC subsets shown on the left. Data in **(B-D)** are shown as mean ±SEM of 7 samples per group and are representative of at least two independent experiments. Gray bars in **(B-E)** indicate untreated *miR-205*^{CTRL} mice, gray bars indicate poly(I:C) treated *miR-205*^{CTRL} mice, and red bars indicate poly(I:C) treated*miR-205*$^{\Delta TEC}$ mice.

Figure 4.6
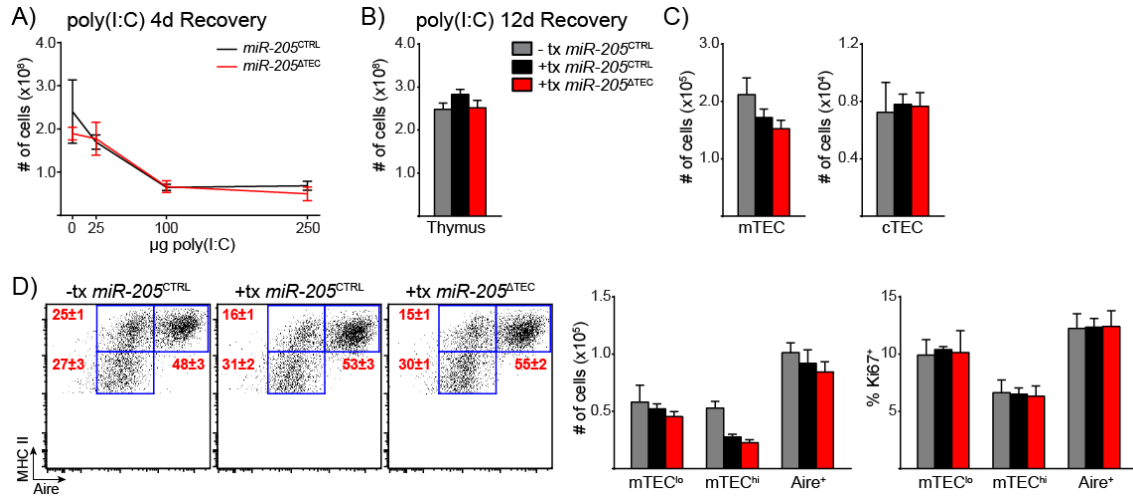
Figure 4.7. Radiation-induced thymic stress does not reveal a role for miR-205 in TECs

(A) 6-week old mice were exposed to sub-lethal total body irradiation and then harvested at either 15 or 30 days recovery to enumerate total thymic cellularity. **(B)** Enumeration of total mTEC and cTEC cellularity from mice shown in **(A)**. cTECs were defined as $CD45^-$, $EpCAM^+$, $Ly51^+$, MHC II^+ events. mTECs were defined as $CD45^-$, $EpCAM^+$, $Ly51^-$, MHC II^+ events. **(C)** Subset composition was assessed by flow cytometry of mTECs as defined in **(B)**. **(D)** Quantification of total TEC cellularity and assessment of the proliferation marker Ki67 for the mTEC subsets shown in **(C)**. Data in **(B-D)** are shown as mean ±SEM of 10 samples per group pooled from two independent experiments. For data in **(B)** and **(D)** blue bars indicate untreated *miR-205*^{CTRL} mice, gray and black bars indicate treated *miR-205*^{CTRL} mice, red and orange bars indicate treated *miR-205*$^{\Delta TEC}$ mice. * denotes p≤0.05, Student's *t*-test.

Figure 4.7
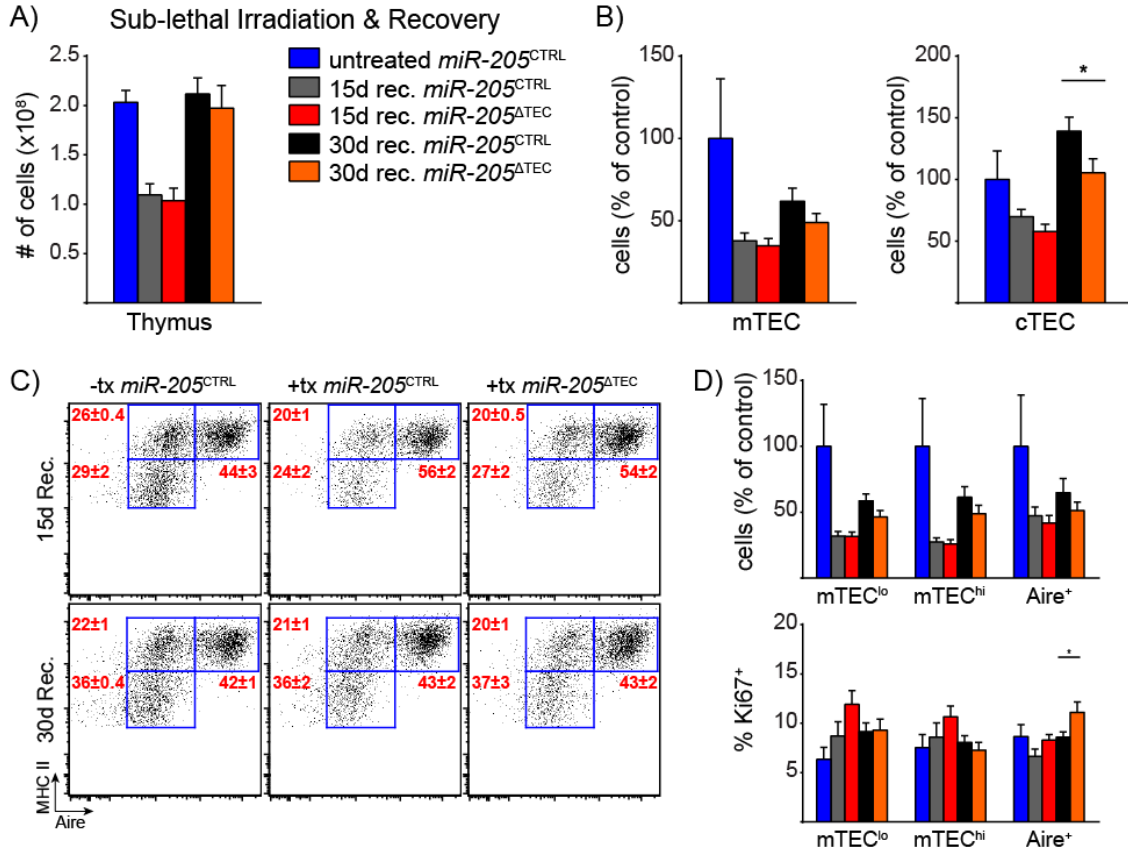
Figure S4.1. Gating strategy for FACS-purification of thymic subsets for microarray analysis

(A) Thymic subsets were purified from 4-5 week old *NOD* wildtype mice for miRNA profiling by microarray analysis. cTECs were defined as CD45$^-$, EpCAM$^+$, MHC II$^+$, Ly51$^+$ events. mTECs were defined as CD45$^-$, EpCAM$^+$, MHC II$^+$, Ly51$^-$ events. CD45+ cells were defined as EpCAM$^-$, CD45$^+$ events.

Figure S4.1

A) TEC Gating:
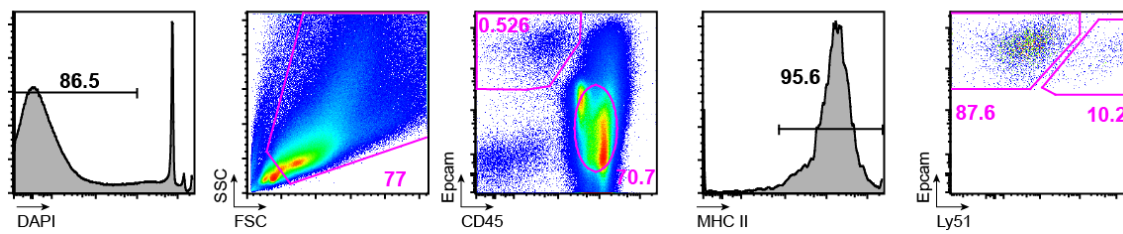
Figure S4.2. Overview of miR-205 conditional knockout targeting construct

(A) The endogenous *miR-205* locus was targeted with a construct containing both a promoter-less lacZ reporter as well as a neomycin cassette. To generate conditional knockout mice, targeted mice were crossed to Rosa26-FLP mice (*miR-205*^fl/fl^), and then bred to *FoxN1-Cre* mice to ablate miR-205 in TECs (*miR-205*^ΔTEC^).

Figure S4.2

A)
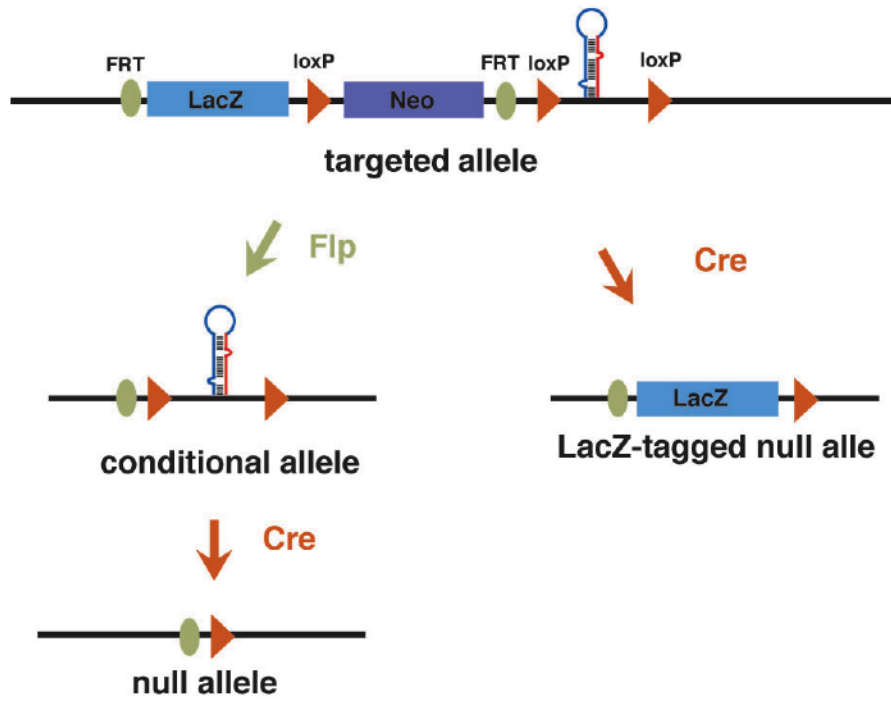
Chapter 5: Discussion and Concluding Remarks

T cell development takes place in a two-step process that is critically dependent on thymic epithelial cell (TEC) function [1, 5]. Early T cell progenitors first undergo positive selection in the cortex, a process by which they rearrange functional TCRs and select for clones which recognize self-MHC molecules on cortical thymic epithelial cells (cTECs) [1, 5]. Positively selected thymocytes then migrate to the medulla where they encounter medullary thymic epithelial cells (mTECs) and dendritic cells in order to go through negative selection [2]. To prevent autoimmunity, mTECs display a diverse repertoire of tissue-restricted antigens (TSAs), whose expression is normally limited to peripheral tissues, in order to purge the T cell repertoire of self-reactive thymocytes [7-10]. As a result of direct antigen presentation by mTECs or indirect presentation by dendritic cells [7-10], self-reactive thymocytes undergo deletion or are recruited into the regulatory T cell lineage [11-19]. This process of negative selection is necessary to prevent autoimmunity, as demonstrated by mouse models with defects in the thymic medulla [20-25]. The ectopic expression of TSAs in the thymus is largely dependent on autoimmune regulator (Aire), which is expressed in a mature subset of mTECs [11, 32, 34-36]. The importance of this process is underscored by the development of multi-organ autoimmunity in both patients and mice with defective *AIRE* expression [26, 27, 31, 32, 96].

While central tolerance protects against the development of autoimmunity, this process also reposes a challenge for generating a robust tumor-specific immune response [16, 85]. Since many tumor antigens are expressed as TSAs in thymus, high-affinity effector T cells capable of recognizing tumor self-antigens may be purged from the developing T cell repertoire [86-89]. Thus, the development of methods that selectively and transiently deplete *Aire*-expressing mTECs may be an attractive method to enhance tumor-specific immune responses. Prior work has implicated RANK-RANKL cytokine crosstalk between thymocytes and mTECs as critical for the mTEC development [47, 48, 52-54]. However, it remains unclear whether these pathways are required for TEC maintenance in the adult thymus and whether *in vivo* RANKL blockade can be applied therapeutically to target the mTEC compartment.

Within the thymus, mTECs represent a dynamic population with continuous cycling and turnover [34, 68]. Models of TEC ablation and recovery have also shown that mTECs have robust proliferative potential and can quickly regenerate in response to thymic injury [37, 62, 69]. However, the precise regulation of these processes and their impact on thymic function remain largely unknown. Thus, further work is necessary to identify novel genes and signaling pathways necessary for maintaining mTEC homeostasis.

RANKL blockade transiently depletes mTECs to suppress central tolerance

In Chapter 2, we performed a series of experiments to show that *in vivo* RANKL blockade could deplete mature mTECs and be utilized to enhance anti-tumor immunity. We began by testing the hypothesis that *in vivo* anti-RANKL antibody would disrupt thymocyte-mTEC cytokine crosstalk and lead to a depletion of mature mTECs. This loss of mature, Aire+ mTECs was evident both by flow cytometry and histology, but more importantly, it was reflected at the functional level whereby Aire-dependent TSA transcripts were correspondingly absent. Consistent with a defect in negative selection, we observed an increase in the overall number of CD4 SP thymocytes. Interestingly, we also observed a reduction in thymic Tregs. This observation is consistent with previous reports suggesting that Treg induction depends on the ability of Tregs to encounter their cognate antigens [16, 19, 37]. Using TCR transgenic models of negative selection, we showed that RANKL blockade could rescue self-reactive cells from thymic deletion. Furthermore, we extended these findings to the polyclonal repertoire by using a previously described immunization-based approach to amplify and detect T cells that are normally deleted in an Aire-dependent manner [15].

An important observation with RANKL blockade was that the positive selection of thymocytes was maintained even in the absence of mature mTECs. This finding was critical to the use of anti-RANKL as a therapeutic agent because in order to rescue self-reactive T cells from thymic deletion, the cortex

must be capable of supporting ongoing positive selection. The selectivity of anti-RANKL's ability to target mature mTECs separates this approach from earlier models of TEC manipulation. Previous work has utilized agents such as corticosteroids and inflammatory cytokines to disrupt TEC development [60, 62, 64]. Although these therapies inhibit TEC function, they fail to show specificity in targeting mTEC development as they often rely on thymocyte depletion to indirectly affect TECs.

Lastly, the ability of mTECs to recover after withdrawal of anti-RANKL is consistent with the robust regenerative potential of mTECs and cTECs in the adult thymus [37, 62, 69]. Interestingly, we observed enrichment of the immature mTEC^{lo} population prior to the initiation of mTEC recovery. This observation is consistent with recent reports which describe a putative slow-cycling TEC progenitor cell which resides in this phenotypic MHC II^{lo} TEC population [73, 75]. The recovery of mTECs and recommencement of thymic negative selection after this repopulation are important considerations for the use of anti-RANKL as a therapeutic agent because they highlight the transient nature of this targeted therapy. Together, these findings demonstrate the efficiency of *in vivo* RANKL blockade in achieving transient suppression of tolerance induction in the thymus.

Manipulation of central tolerance can enhance anti-tumor immunity

After demonstrating the transient suppression of Aire^{+} mTECs with *in vivo* RANKL blockade in Chapter 2, we went on to show that manipulating

central tolerance could be used therapeutically to enhance the immune response to cancer. We took advantage of a TCR transgenic model in which T cells recognizing the melanoma antigen TRP-1 undergo thymic deletion in an Aire-dependent manner [88, 98]. We treated these mice with anti-RANKL and showed that TRP-1 cells could be rescued from thymic deletion (Figure 5.1A). We went on to challenge these mice with tumors to demonstrate that this thymic rescue of tumor self-antigen specific T cells could result in increased survival in response to melanoma. Indeed, mice treated with anti-RANKL showed a statistically significant increase in survival and also showed evidence of increased T cell infiltrates within their tumors. Interestingly, TRP-1 mice treated with anti-RANKL also showed evidence of autoimmune depigmentation, or vitiligo, which further supports to notion that melanocyte antigen-specific T cells had escaped thymic deletion in these mice.

We next extended these findings to the polyclonal repertoire and challenged wildtype mice with tumors after treating them with anti-RANKL. Similar to our findings in the TRP-1 TCR transgenic model, mice treated with anti-RANKL showed a statistically significant increase in survival. We next hypothesized that using combination therapy to target both central and peripheral tolerance could lead to even greater benefits in survival. To test this hypothesis, we combined anti-RANKL treatment with GVAX (vaccination with irradiated, GM-CSF secreting B16 tumor cells) and anti-CTLA [101, 102]. We observed a striking increase in the overall survival when mice received these combination therapies. Interestingly, the additive nature of the survival benefit

attained from GVAX and anti-CTLA4 suggests that these two therapies act in the periphery through independent mechanisms and also reinforces our hypothesis that anti-RANKL mediates its effect by targeting central tolerance (Figure 5.1B). Although autoimmunity is a dangerous potential consequence of this approach, these treatments may also be an attractive new method to help break tolerance for cancer immunotherapy.

MicroRNAs in TECs are critical for supporting central tolerance

In Chapter 3 of this work, we explored the role of canonical miRNAs in supporting central tolerance. We utilized a floxed *Dgcr8* conditional allele in combination with a *FoxN1-Cre* knock-in allele to generate TECs deficient for canonical miRNAs. We harvested thymi from mice with DGCR8-deficient TECs and observed a dramatic loss of thymic cellularity which mapped to both the TEC and thymocyte compartments. Interestingly, the phenotype in these mice worsened with age as they gradually lost the ability to maintain Aire$^+$ mTECs and showed evidence of disorganized thymic architecture. Although these mice did not develop spontaneous autoimmunity, we hypothesized that continued T cell output from miRNA-deficient thymi would allow for the escape of self-reactive T cells. Using an immunization-based approach, we were able to expand and detect IRBP-specific T cells in the periphery of these mice and show that these cells could provoke autoimmune uveitis. The absence of spontaneous disease in mice with clear defects in negative selection suggests that intact peripheral tolerance mechanisms may be sufficient to keep escaped

self-reactive T cells in check. Indeed, these observations are consistent with an earlier report that describes a critical perinatal window of Aire expression that is necessary to protect against spontaneous autoimmunity [97]. Indeed, the lack of spontaneous autoimmunity in both DGCR8-deficient TECs as well as anti-RANKL treated mice is consistent with these earlier findings. Both of the models we present here represent a model of acquired Aire-deficiency relative to this critical perinatal window. It is therefore likely that each of these models depicts a scenario in which self-reactive T cells are capable of escaping into the periphery but may require additional stimulation in the periphery to overcome tolerance.

Lastly, in Chapter 4 we profiled miRNA expression in TECs with the hope of identifying a specific miRNA responsible for part of the phenotypes observed in our DGCR8-deficient TEC model. We performed microarray analysis to identify miRNAs expressed differentially in mTECs relative to thymocytes and chose to focus our studies on miR-205. We characterized the expression pattern of miR-205 and observed high expression levels throughout embryonic development and onwards in the post-natal thymus. Its expression was preferential for mTECs relative to cTECs, and it appeared slightly enriched in immature mTECs. We utilized a *miR-205* conditional allele to target its ablation in TECs to characterize the role of miR-205 in TEC biology, but we were unable to detect a phenotype under homeostatic conditions. Several groups studying miRNA knockouts have reported similar negative findings under homeostatic conditions [132], so we utilized thymic stress models

including poly(I:C) administration and sub-lethal irradiation to yield clues as to the potential role of miR-205. Despite these models of thymic involution and recovery, we were unable to observe any differences in miR-205 deficient TECs and control mice. Therefore, although miR-205 is highly expressed in mTECs, its role in the post-natal thymus remains unclear.

Concluding Remarks

Therapeutic manipulation of thymic function yields significant promise in improving outcomes in human disease. We have shown in this work the proof of principle experiments that highlight the potential benefit of transiently suppressing central tolerance as a means to enhance the anti-tumor immune response. Given the current interest in targeting peripheral tolerance mechanisms in cancer immunotherapy [92, 100], it remains to be seen whether the suppression of central tolerance could be used to complement such existing therapies. Indeed, we provide evidence that anti-RANKL, GVAX and anti-CTLA4 show an additive survival benefit in a melanoma tumor model. Furthermore, while we used anti-RANKL to disrupt thymocyte-mTEC interactions and suppress central tolerance, one can easily imagine a scenario in which agonist signaling through the TNFSF signaling pathway might enhance mTEC function. In agreement with this hypothesis, we observed an increase in Aire[+] mTECs and thymic Tregs in OPG-deficient mice that lack negative feedback for RANK signaling. Furthermore, it remains to be seen whether such agonist TNFSF signaling could be used in combination with known agents such

as KGF and IL-22 which have both shown to be useful in driving TEC proliferation [61, 70, 71]. Lastly, further work is needed to identify novel genes and pathway that are critical for TEC biology. For example, although it is now clear that miRNAs are required in TECs to maintain proper thymic function, [81-84], the identities of the specific miRNAs that mediate these effects and the pathways they regulate remain unclear.

Figure 5.1. Manipulation of central tolerance by RANKL blockade

(A) Schematic showing the impact of anti-RANKL on central T cell tolerance in the thymus. RANKL blockade depletes the Aire[+] mTEC population along with its expression of tissue-specific antigens. As a result, antigen-specific T cells, including those specific for tumor antigens, are able to escape thymic deletion. The rescue of these tumor self-antigen specific T cells results in an enhanced anti-tumor immune response and increased survival in response to tumor challenge. Model slide is adapted from work by Zhu, M. *et al.* [88] (B) Cancer immunotherapy is currently focused on breaking peripheral tolerance as a means to enhance anti-tumor immunity. There is a great deal of interest in developing combination therapies to further enhance the efficacy of these treatments. Along these lines, we propose a combination therapy which targets both central and peripheral tolerance as a means to promote anti-tumor immunity.

Figure 5.1

A)

B)
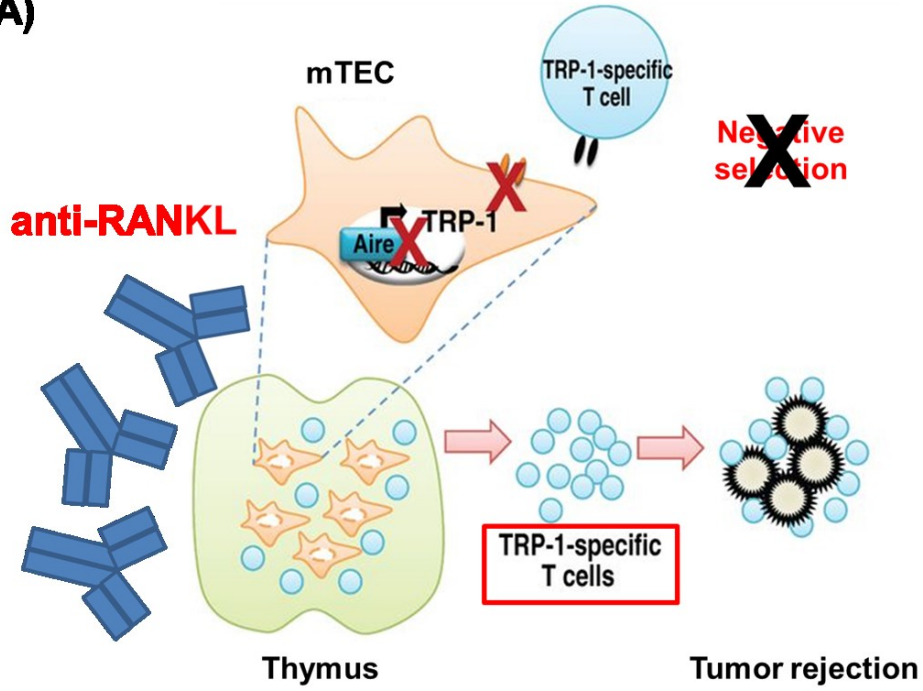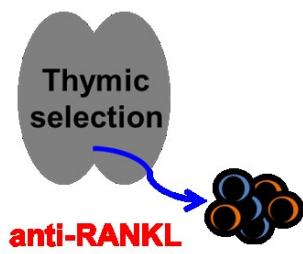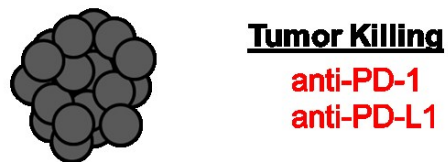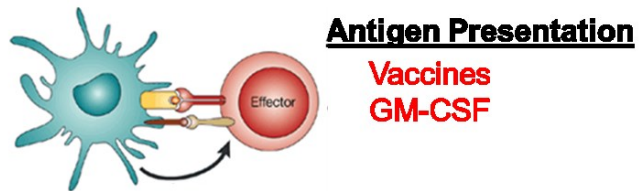
Appendix: Selected Protocols

Thymic Stromal Cell Isolation

Reagents and Materials

DMEM (High Glucose)

DNase I (Roche, 10104159001)

Liberase TM (Roche, 5401127001)

Percoll PLUS (Sigma)

Glass Pasteur Pipettes (Fisher Brand, 9'' pipettes, 13-678-8B)

Transfer pipettes

70um Cell Strainers

DNase 1: reconstitute with 1mL water to yield 100mg/mL

Liberase TM: reconstitute one 50mg bottle with 10mL water, gently shake while on ice for ~10-15' and then freeze down either 288uL or 576uL aliquots

Digestion Media:

DMEM (High Glucose)	15 mL	30 mL	60 mL
2% HI FBS	300 uL	600 uL	1.2 mL
100 ug/mL DNase I	15 uL	30 uL	60 uL
Liberase TM	288 uL	576 uL	864uL

Percoll Densities:

1.124

Percoll Stock	9 mL	27 mL	36 mL	45 mL
10x PBS	1 mL	3 mL	4 mL	5 mL

1.115

1.124 Percoll	9.274 mL	18.548 mL	27.822 mL	37.096 mL
1x PBS	0.726 mL	1.452 mL	2.178 mL	2.904 mL

1.065

1.124 Percoll	5.24 mL	10.48 mL	15.72 mL	20.96 mL
1x PBS	4.76 mL	9.52 mL	14.28 mL	19.04 mL

Tissue Isolation and Digestion

1. Harvest thymi into separate small Petri dishes with 5 mL digestion media. If harvesting many thymi, keep everything on ice until ready to proceed, otherwise RT is fine.
2. Mince thymi with new, clean razor blades. Wipe down between samples and replace every 2-4 samples when you notice dulling.
3. Transfer minced organs and media to labeled 15 mL conical tubes using glass Pasteur pipettes. Use 2-3 mL digestion media to rinse remaining tissue from Petri dishes and then add to the conical tubes.
4. Place 15ml conicals containing minced thymi into a 37°C water bath.
5. Mix with medium-speed pipettor every 6 min for a total of 36 min
6. Spin down cells at 1300 rpm for 5 min at 4°C.
7. Resuspend thoroughly in 5 mL cold AutoMACS buffer (1x PBS, 0.5% BSA, 2mM EDTA) with transfer pipettes to stop digestion, leave on ice for 10' minutes.
8. Spin down cells at 1300 rpm for 5 min at 4°C.

Percoll Gradients

9. Resuspend cells in 4 mL dense (1.115) Percoll and transfer through a 70 uM cell-strainer into new, FBS-coated tubes.
10. Create a Percoll gradient by gently layering 2 mL of light (1.065) Percoll onto the heavy fraction, followed by 2 mL of 1x PBS.
11. Spin the tubes for 30 minutes at 2700 rpm, 4°C, with the break set to 0 and the acceleration set to 5 (half of max on our setting)
12. During the spin, the stromal cells will settle at the boundary between the light Percoll and 1x PBS, while the lymphocytes will be between the light and heavy Percoll fractions. See Below.

13. Once the gradients finish spinning, remove them as gently as possible and aspirate the desired cells using a transfer pipette. The **stromal fraction** will be a visible layer of cells between **the PBS and the light (1.065) Percoll layers,** and the **thymocyte fraction** will be a visible layer of cells between the **light and heavy Percoll layers.**
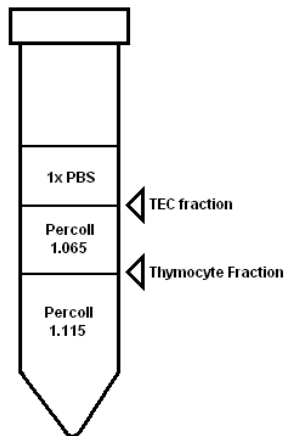
14. Use transfer pipettes to collect the "stromal" TEC fraction into a new 15mL conical tube containing 8mL FACS buffer.
15. Assuming a collection volume of ~2mL, mix each of the new tubes containing ~10mL of sample and take a 100ul aliquot for cell counting on the ViCell
    a. Use 100ul sample + 900ul PBS, use "default" cell type
    b. Over time we've found that ~half of the cells are lost in the next wash, so factor this in when back-calculating cell numbers
    c. We have found that if you perform an extra wash and count the same sample before/after the 2nd wash, the "after" count will be roughly half of the "before" count.
    d. When sorting, you need fairly large quantities of antibody so it's worth the effort to perform the 2nd wash and use that count so as not to waste antibody reagents
16. Spin down collected samples and resuspend in 3.5mL FACS buffer
17. Use transfer pipette to filter into a filter-top FACS tube
18. Spin down, then resuspend pellet in 100uL 2.4G2 blocking buffer and incubate on ice for 10 min

     a. When you have finished calculating cell counts, adjust volume of any samples as needed

Antibody Staining

2.4G2 blocking buffer (1:50 dilution of 1mg/ml stock in FACS buffer)

FoxP3 Transcription Factor staining kit (eBioscience)

Aire-e660 (eBioscience)

Ki67-PE (BD Biosciences)

1. Generally, resuspend 10^7 cells in 100uL 2.4G2 and quickly vortex.
2. Incubate on ice for 10 min. Prepare antibody mix. Unless specified, each antibody is diluted 1:100 in FACS buffer such that the final concentrations will be 1:200 when added to the samples.
3. Add 100uL antibody mix per sample and quickly vortex. Incubate covered on ice for 30-45 min.
     a. If preparing compensation tubes and staining dense fraction thymocytes, keep in mind that the CD8 epitope is cleaved off by most Collagenase D based enzymes such as Liberase.
4. At the end of the incubation, top off tubes with chilled FACS buffer and spin down to conduct the first wash.
5. After decanting supernatant, resuspend in 500uL of diluted Fix Reagent.
6. Incubate covered on ice for 30 min.
7. Wash twice with 2.5mL diluted Perm Buffer. Be sure to increase centrifuge to 1400 rpm since fixed cells are much smaller.
8. Make 1:100 dilution of intracellular antibodies in Perm Buffer. Both Aire and Ki67 work well in these conditions.
9. After the 2nd Perm Buffer wash, resuspend each sample in 100uL intracellular antibody mix. These antibodies represent a 1:100 final concentration.
10. Incubate covered on ice for 30-45 min.
11. Wash twice with 2.5mL diluted Perm Buffer.

12. Wash once with FACS buffer.
13. Resuspend in 200-300uL FACS buffer and filter into a mini FACS tube.

Modifications for TEC Sorting / Enhanced TEC Recovery

1. This modified protocol has proven to yield slightly more than 2x the number of mTECs that one can normally obtain when following the standard protocol

2. When harvesting different genotypes for two independent sorts on the same day, consider off-setting the harvest times. If you harvest both together, one sample will essentially be dying off in the ice bucket while the other is running on the sorter.

3. Digestion buffer and Percoll gradients are the same.
4. However, this time you will harvest thymi into DMEM with 2% FBS.
5. Pool together 5-6 thymi per dish and mince until ~1-2mm chunks remain.
6. Transfer minced thymi into one 15 mL conical per dish.
7. Vortex vigorously for 10-15" and allow large chunks to settle.
   a. You can also give this a quick pulse spin in the centrifuge such that only the larger stuff settles.
   b. Some people repeat this step to get rid of even more thymocytes.
8. Carefully transfer all of the supernatant into a new 15mL conical. The supernatant contains the released thymocytes and can be discarded.
9. Add 3-4mL digestion buffer to the remaining chunks of minced thymi. Resuspend with glass Pasteur pipette and incubate in 37°C water bath for a total of 12 min
   a. Mix aggressively at 4 min and 10 min, and allow the undigested chunks to settle before the 12 min mark (or do the quick spin to force down the remaining undigested tissue)
   b. After 12 min collect all of the supernatant and transfer into a 15mL conical on ice. Mix in modified AutoMACS buffer (adjust to 5mM EDTA) in a 1:1 ratio to quench the digestion.

10. Add 3-4mL new digestion media to the remaining chunks of undigested tissue, repeat this entire process two more times (total 3 rounds of digestion, 36 mins)

11. Pool together all of the "collected" fractions and spin down. Resuspend in regular AutoMACS and follow the regular stromal prep protocol.

12. When harvesting the percoll gradients, pool light fraction cells into one 15mL conical. Top off with FACS buffer to fill the tube. Filter everything into a new 15mL tube and spin down. Do not take an aliquot to count yet.

13. Resuspend pellet in 10mL FACS buffer and filter into a new 15mL conical.

14. Take an aliquot for cell counting. Then spin down the tubes while the counts are going.
    a. These counts should be accurate because they are being done after the 2nd wash step. No need to adjust the counts.

15. Proceed with antibody staining, except wash twice at the end of the surface antibody staining.

16. Sort cells using 100um nozzle. Sample gating strategy is shown below.
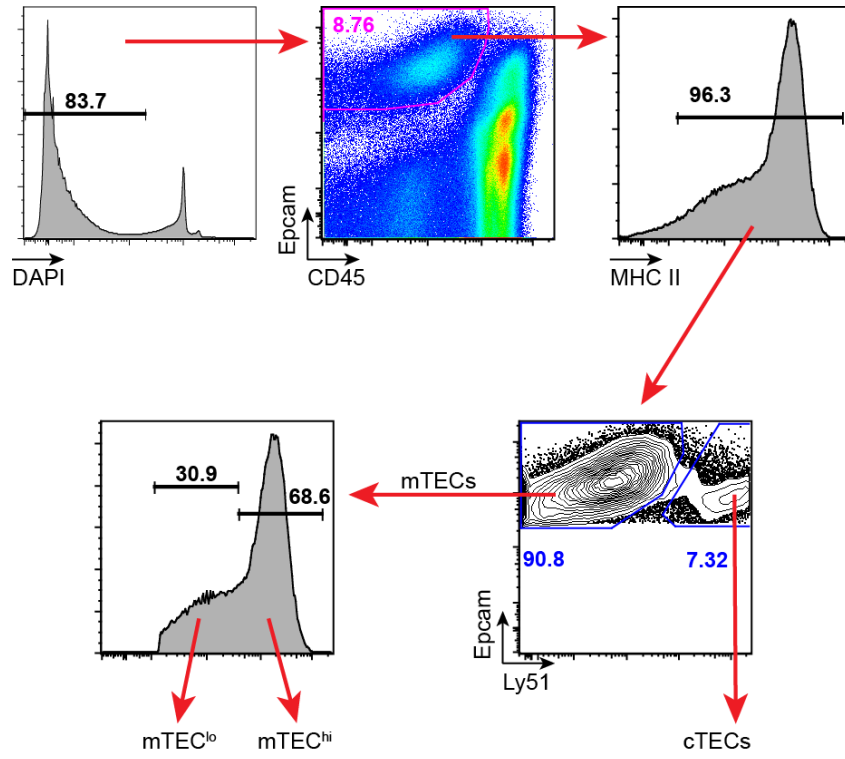
RNA Preparation: qPCR Analysis / Total RNA /

Microarray / RNAseq

Pelleting and Cell Lysis

1. Collect cells in a 1:1 mix of DMEM:FBS
2. For low cell numbers it is better to sort into 1.5mL Eppendorf tubes to minimize loss of cells while pelleting. When using the 100µm nozzle on the BD Aria3u, expect to recover cells in ~100µl of sheath fluid per 30k cells. This may change over time so be sure to check your collection tube every ~100k cells or so.
3. Spin down sorted cells in the large swing bucket centrifuge for 10 min, ~2000rpm
4. Pellet will be at the bottom of the tube rather than along the side. Aspirate most of the media using a P1000 and leave about 50µl media
5. Spin down for ~10-20sec in benchtop centrifuge at 8000g
6. Pellet will now be at side of tube. Aspirate remaining media with P200 or P20
7. Flick the pellet to disrupt the clump of cells and proceed with the protocol below which is most appropriate for your downstream application

RNA Prep using Qiagen RNeasy Plus Micro Kit

Note: This RNA prep method works best for 1-500,000 cells and is successful when its RNA is used to make cDNA for qPCR Analysis. It has **_not_** been very good for microarray/RNAseq. We get strange Nanodrop readings and many of our samples to fail the array core's QC analysis. It works beautifully, however, when used to produce RNA for downstream cDNA synthesis and qPCR analysis.

Reagents Not Supplied in Kit

14.3 M β-Mercaptoethanol (commercial β-ME usually at 14.3M)

70% Ethanol (RNase-Free)

80% Ethanol (RNase-Free)

QiaShredder Columns (Qiagen)

1. Prepare **Lysis Buffer** during this step, need 350µl per sample:
    a. Add **10µl β-Mercaptoethanol** per **1ml Buffer RLT Plus**
2. Flick the pellet to break up clump of cells and add **350 µl Lysis Buffer**
3. Pipette to mix, then transfer lysate into QiaShredder Column and spin for 1' at max speed to homogenize the sample
    a. Homogenized lysates can be stored at -80ºC for several months. Before use, recommended to completely thaw in 37ºC bath for a couple minutes or just at room temperature
4. **Make sure benchtop centrifuge is at RT (don't drop below 20ºC)**
5. Transfer lysate to **gDNA Eliminator** spin column, spin 30" @ >8000g
6. Discard column, save flowthrough. Add **350µl 70% Ethanol** and mix by pipetting
7. Transfer to **RNeasy MinElute** spin column. Spin 15sec @ >8000g
8. Discard flowthrough. Add **700µl Buffer RW1**. Spin 15sec @ >8000g
9. Discard flowthrough. Add **500µl Buffer RPE**. Spin 15sec @ >8000g
10. Discard flowthrough. Add **500µl 80% Ethanol**. Spin 2min @ >8000g

11. Transfer spin column to new 2ml collection tube. Leave lid open, spin 5min @ full speed
    a. Orient open lids carefully to prevent breakage. Leave space between samples.
12. Transfer spin column to new 1.5ml collection tube (Epi). Add **13µl water** to center of membrane. Close lid, spin 1min @ full speed. Yields ~11µl
    a. **Some options:**
    b. Re-eluting with the flow-through can increase yield, as can using pre-heated water for the original elution
    c. If proceeding for SuperScript RT reaction and planning on performing a double reaction, consider eluting with 17ul water to yield ~16ul for the RT Rxn

cDNA Synthesis for qPCR Analysis

SuperScript III First-Strand Synthesis kit (Invitrogen, 18080)

Notes: each 1x reaction has an upper limit for RNA input. We're assuming here that sorted cells (TECs in particular) will not give you enough RNA to saturate the upper limit of RNA input.

Generally following the manufacturer's protocol, with the following modifications:
1. Set up a double-sized reaction such that everything is scaled up 2x
2. This allows you to use all of your eluted RNA from the Qiagen method:
    a. Step 1 = 16ul RNA + 2ul dNTP mix + 2ul Oligo(DT)$_{20}$
3. Set up reactions in a PCR strip to ensure adequate temperature cycling, change the caps each time you need to open the tubes to add reagents
4. Final yield should be 40ul reaction + 2ul RNase H =42ul cDNA for use in qPCR analyses. Depending on the cellularity that went into the RNA prep, may need to dilute out the cDNA before use.

Preparing Total RNA using TRIzol Reagent

Adapted from Invitrogen's protocol and Lukas Jeker

Reagents Needed

TRIzol (Invitrogen)

Chloroform

Isopropanol

70% Ethanol (RNase-Free)

Glycoblue Glycogen (Ambion)

1. Flick the pellet to break up clump of cells and add 500ul TRIzol
2. Mix with pipette and then vortex for ~30" to lyse/homogenize
   a. Proceed ahead or freeze in -80
3. **Cool down centrifuge to 4°C before starting!**
4. Thaw samples, vortex 15"
5. 10' room temp (RT)
6. Samples in 500µl Trizol: add 0.1ml chloroform
7. Shake 15" → set up in sandwich between 2 epi racks and shake vigorously
8. 3'RT
9. 15' @ 4°C 12'000g
   o Label new tubes in this step
10. Transfer 260µl aqueous phase to new eppendorf tube
    o aspirate with a pipette tip _very slowly_ and gradually tilt the epi while aspirating in order to maintain the interface
    o can try to follow up with a smaller pipette tip very carefully
    o the key is to release the pipette in one smooth motion to avoid any drawback through the interface
11. Add 1ul GlycoBlue Glycogen, vortex
12. Add 260µl isopropanol, vortex 1-2"
13. Precipitate @ -20°C 1h

14. Spin 10' @ 4°C 12'000g
    o Label new tubes in this step
15. Remove sup (without touching the pellet)
16. Wash once with 500ul of fresh 75% Ethanol, transfer to new 0.5ml tube (will facilitate resuspension in low volumes)
17. Vortex
18. Spin 5' @4°C 7500 g, aspirate 450µl
19. Spin 5' @4°C 7500 g
20. Aspirate any remaining ethanol with p200 and p20 tips
21. Lay out paper towels on the bench and lay the tubes on their side to air dry
    a. Be careful not to over-dry as the pellets will not go into solution
22. dissolve in 10µl H2O
23. Incubate 10' at 55°C
24. Return to ice, quick spin, freeze in -80

Preparing RNA for Microarray/RNAseq

Quick - RNA Miniprep (Zymo Research, R1054S)

Notes: We used this kit for RNAseq analysis in Fall 2013 and it gave very good results with respect to the RNA's QC and also in terms of the quality of data that came out the other end. We followed the manufacturer's protocol with the following details:

1. Use 300ul Lysis Buffer, pipette to mix and vortex
2. Use Spin-Away Filters for lysate clearance and gDNA removal
3. Do not perform on-column DNase I treatment!
4. Elute in 30ul of pre-heated water

IRBP Peptide Immunization and Tetramer Pulldown for FACS Analysis

Protocol adapted from Ruth Taniguchi by Imran Khan and Maria Mouchess

Peptide/CFA for Immunization

1. Thaw peptide stock, dilute 1:10 in PBS
2. CFA = IFA + lyophilized H37Ra resuspended to 4mg/ml
   a. Will not dissolve, but get into suspension before using
3. Mix diluted peptide in 1:1 ratio with CFA
4. Final should be 100ug of peptide in 100ul CFA mix, generally a good idea to make some extra emulsion because of loss in loading syringe(s)
   a. Sample dilution for immunizing 5 mice (make 1ml for "10 mice"):
   b. 50ul reconstituted peptide + 450ul PBS + 500ul CFA = 1ml
5. Mix together in 50ml conical
6. Sonicate 10-15" on max intensity, spin 30" full speed in tabletop centrifuge
   a. Repeat 2-3 times as needed, the emulsion should be one homogenous mixture without any liquid phase separation
7. Load about 200ul into 1ml syringe, then invert the syringe in an empty 50ml conical and spin 30" full speed in tabletop centrifuge
   a. Cut a piece of bacterial culture tube to sit inside the 50ml conical
   b. The butt of the syringe should be suspended in the conical as shown below. With centrifugation the bubbles to rise to the top so you can easily expel them and continue filling the syringe
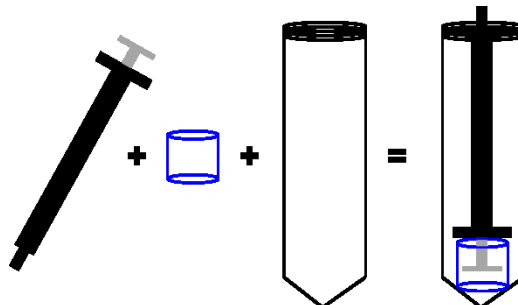
8. Once the bubbles are cleared, eject the newly formed fraction of air and finish loading the syringe
9. Load 25g needle on syringe and expel the air within the deadspace
10. Inject 50ul emulsion subcutaneously in each side of the chest wall
   a. Inject slowly and wait a few seconds before withdrawing needle
   b. **Optional:** anesthetize mice with 50-70ul Ketamine/Xylaxine. This is to help ensure a smooth immunization, not for surgical analgesia
11. Analyze mice 8-10 days later for tetramer analysis (we typically go for 10 days) or 21 days later for uveitis induction

Day of Harvest

1. Set up one small 6cm petri dish with **70um cell strainer** for each mouse, fill with 5ml DMEM
   a. Harvest both LN/SPL into filter, store on ice until finished harvesting all mice (unless specified, everything is on ice from here)
   b. Mash LN/SPL through filter using 3ml syringe plunger, transfer to 15mL conical, wash with additional 5mL media
   c. Spin down all tubes (5' @ 1350rpm), aspirate as much of supernatant as possible

2. Resuspend pelleted cells in 200ul **Tetramer Block** using P1000, pipette as best you can to resuspend and get rid of the clumps
   a. Vortex a few times and get rid of all clumpy stuff hanging on to the edge of the tube
   b. Use a P1000 set at ~250ul to draw up cells, click pipette until you get the final volume and write down the volume on the tube
   c. Add 1:100 dilution of tetramer (stock at 1mg/ml) to each sample (i.e. 2.5ul for 250ul)

d. Vortex all samples and store in dark at Room Temp for 1 hour, vortex every 15-20 minutes

3. Top off tubes with FACS buffer and spin, aspirate Supernatant
   a. Resuspend in 200ul FACS buffer and remove any clumps
   b. Vortex **anti-APC microbeads** prior to use
   c. Add 50ul anti-APC microbeads, vortex
   d. Incubate for 30 minutes on the cold room rocker, cover with foil to keep dark
   e. During incubation get the **MACS columns** ready by placing a cell strainer on each column and washing with 3ml FACS buffer (discard flowthrough)

4. Top off tubes with FACS buffer and spin, pour off supernatant
   a. Resuspend in 3ml FACS buffer (keep tube) and apply to columns through the filter. Discard flowthrough
   b. Once columns are loaded and sample is no longer flowing through, wash each sample tube with 6ml FACS buffer and apply to column
   c. Apply 3ml for a final wash directly to the filter on the columns
   d. Label new 15ml conical for collection tubes
   e. Remove columns from the magnet and place on new collection tubes, elute "positive fraction" from columns with 5ml FACS buffer using plunger

5. Label up tubes and label vicell cups for cell counting
   a. Counting tubes: 100ul of "positive fraction" + 100ul FACS buffer
   b. Vicell cups: 200ul positive fraction + 800ul PBS/FACS buffer (1:5 dilution)
   c. Spin down positive fraction for **antibody staining**

d. Label new FACS tubes for cell staining, aliquot 10.5ul antibody mix to each tube

6. Aspirate supernatant, be careful to leave extra ~25ul or so near the bottom
   a. Resuspend in 100ul 2.4G2 block, transfer 100ul to staining tubes
   b. Collect all remaining cells for comp. controls
   c. Stain on ice for 30-60' (CD3 staining seems to work better with 45'+ staining)

7. Wash cells for FACS analysis
   a. Resuspend samples in ~300ul and filter into mini tubes for FACS
   b. Set up FSC and SSC such that you can see both counting beads and your lymphocyte population in the same plot, this will be important for the FloJo analysis in order to backcalculate the total cell number. **SSC will need to be on log scale** so you can see both beads and lymphocytes together!
      i. See sample gating below
   c. Add DAPI and collect all events in sample tube
   d. For counting tubes, add 25ul **counting beads** just prior to FACS analysis (be sure to note the lot number and **concentration for counting beads**)
   e. Collect counting samples until you have ~5-8,000 beads

Calculating absolute number of total tetramer+ cells

1. Load both positive fraction files and bead event files into Flojo under different groups
2. After gating lymphocytes for the positive fraction and completing the full analysis, drag the lymphocyte gate and apply to your "bead sample" group
3. Open up the FSC v SSC plot for bead samples and you should now see the lymphocyte gate on there
4. Draw a gate around the bead events and apply to all samples
5. Create two different statistics tables and export the following information to generate the final statistics:

   Bead samples
   % beads
   % lymphocytes

   Positive fraction samples
   % singlets
   % T cells
   % CD4+
   % CD4+ CD44^{hi} Tetramer+
   % CD8+
   % CD8+ CD44^{hi} Tetramer+

6. Absolute # of events collected for a given sample: assuming 100ul out of 5ml positive fraction was used for count tubes (1:50 dilution), and that 25ul of beads were used with a lot concentration of 2.6×10^4 beads/25ul

   Absolute # lymphocytes = 2.6×10^4 x (%lymphocytes / %beads) x (50)

   Total Tet+ = (*Absolute # lymphocytes*) x (%singlets) x (%Tcells) x (%CD4+) x (CD4+ %Tet+)

7. To generate the "limit of detection" statistic (LOD), repeat the above calculations to generate the total number of CD8+ tetramer+ events
   a. For an MHC II tetramer there shouldn't be any, so this accounts for the "stickiness" of the tetramer/background noise
   b. LOD = mean + 3 x St. Dev of the CD8+ tet+ events in all samples

c. This will likely change between experiments and tetramer batches so keep this in mind when plotting multiple data sets together

Sample Gating:

Bead Sample:

beads and lymphocytes:

9.61

3.51

SSC-A / FSC-A

% beads
% lymphocytes

Positive Fraction Sample:

lymphocytes:

7.31

SSC-A / FSC-A

singlets

95.3

FSC-H / FSC-A

T cells

5.26

Dump / CD3

CD4 Tet+

38   21.9

40.1   0.0528

CD8 Tet+

28.4   0

71.6   0

CD44 / Tetramer

CD4s and CD8s

62.4

33.9
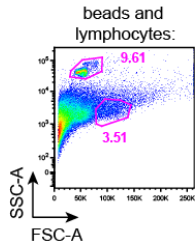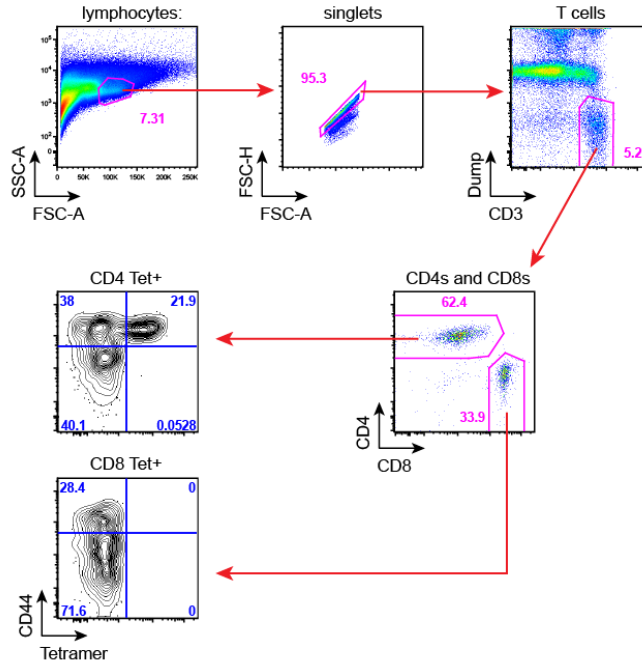
CD4 / CD8

% singlets
% T cells
% CD4+
% CD4+ CD44hi Tet+
% CD8+
% CD8+ CD44hi Tet+

Reagents and Materials for Immunization/Tetramer Analysis

Peptide/CFA

IRBP P2 peptide = PLGGG GQTWE GSGVL PCVGT, >80% purity
Resuspend lyophilized peptide in DMSO at 20mg/ml, freeze aliquots
IFA = Incomplete Freund's Adjuvant (BD Difco, #263910)
M. Tuberculosis H37 Ra (BD Difco, #231141)

Ketamine/Xylaxine

Inject 50-75ul intramuscularly depending on degree of desired sedation and
weight of the mouse
Ketamine stock = 100mg/ml
Xylaxine stock = 20mg/ml
To make 1ml working stock:
      200ul Ketamine
      125ul Xylaxine
      675ul sterile saline

Tetramer Block

20ml FACS buffer
400ul FBS
400ul Rat/Mouse serum (we typically use only rat, but can use half and half)
400ul 2.4G2 (from a 1ug/ul stock)

Antibody Mix (per 100ul stain/sample)

2.5ul CD3-PerCP
1ul CD4- APC-Cy7
1ul CD8-A700
1ul CD44- FITC
5ul Dump-PacBlue (CD11b, CD11c, F4/80, NK1.1, B220)
(DAPI)

Anti-APC microbeads (Miltenyi, 130-090-855)

MACS LS Separation Columns (Miltenyi, 130-042-401)

70um Cell strainer (Fisher, 352350)

CountBright absolute counting beads (Invitrogen, C36950)

microRNA *in situ* Hybridization

Protocol Adapted from Anastasia Mavropoulos and Helene Favre, optimized for the mouse thymus with the use of LNA-probes from Exiqon

Tissue Preparation

1. Harvest tissue, soak in 4% PFA/DEPC-PBS in 15mL conical, agitate overnight at 4°C (agitation on the slow rocker in the cold room is fine, just keep it moving around)
2. In the morning wash once with DEPC-PBS and then soak in 30% sucrose/DEPC-PBS
3. Continue agitation at 4°C, bring up to 24 hours total
   a. **Alternatively**, harvest tissue into 4% PFA for 2 hours at 4°C with agitation
   b. Fixation time may vary by size of tissue, 2 hours works fine for the thymus and prevents over-fixation which can cause the tissue to become brittle and crack during the sectioning
   c. Wash quickly with DEPC-PBS and then incubate with 30% sucrose/DEPC-PBS for 7-8 hours at 4°C with agitation
4. Freeze down in OCT
5. Sections can be cut and kept frozen at -80°C for several months, or cut fresh before starting. For the thymus, 8-10 µm sections work fine.

Pre-treatment of Sections

1. Warm slides @RT for 1 hour
2. Add 1mL 4%PFA/DEPC-PBS across the sections for additional fixation, incubate 10 min @RT
3. Wash 3x with DEPC-PBS. Set up Acetylation. [wash = incubate, no agitation]
4. Acetylation: Set up in fume hood using a magnetic stir plate. Use a 1 Liter glass beaker to immerse slide holder. You will need to angle the

slide holder such that it is submerged in solution and gives clearance for the magnetic stir bar

    a. 500mL DEPC-H2O + 6.8mL triethanolamine + 900ul conc. HCL, mix with stir bar.

    b. Immerse slides and add 2 x 640ul acetic anhydride dropwise with constant stirring. Leave for 10 mins. [Do not drip too close to the tissue, don't want it to touch the tissues directly. Not all of it will go into solution and this is normal]

5. Wash slides in DEPC-PBS for 5 mins @RT.

6. Add 1mL Proteinase-K solution across the slides, incubate 10 min @ RT

7. Wash 3x with DEPC-PBS

8. Place slides in humidified chamber→Set up near incubator.

    a. Soak paper towels in the chamber with 50% Formamide/5xSSC [final concentrations]

    b. Add 1mL hyb solution across the tissue sections

    c. Pre-hybridize for 3 hours @57°C [hyb temp of probe being used]

9. Prepare probe

    a. Add 1ul probe to 100ul hyb solution per slide, denature at 80°C for 10 mins, then store on ice for another 2 mins

    b. Dab off the pre-hyb solution from the slides without touching the tissues. Use a kimwipe to dry off extra solution from around the tissues. Add 100ul hyb solution across slide

    c. Place small and medium coverslips across the tissues to ensure that the entire slide is completely covered. Incubate 12-16 hours @57°C. [hyb temp for your probe]

    d. Set up 2x and 0.1x SSC in incubator o/n so they are at the appropriate temperature for the stringency washes tomorrow

Stringency Washes and Antibody Incubation

1. Set up glass trough with pre-heated 2x SSC

2. Immerse each slide one by one into the trough and lightly shake it around while holding the edge to help the cover slip slide off on its own
3. Wash in 2x SSC at 57°C for 60 mins. [hyb temp for probe]
4. Wash in 1x SSC @RT for 10 mins
5. Wash in 0.5x SSC @RT for 10 mins
6. Wash in 0.1x SSC @57°C for 45 mins
7. Block in 1% goat serum in PBST for 2 hours [either 1mL across the slide or in slide mailer]
8. Incubate w/ 1:5000 dil. anti-DIG-AP antibody diluted in blocking buffer
    a. Can use 100ul + coverslip or 10-20mL in slide mailer to avoid tissue tearing
    b. Incubate overnight at 4°C

Visualization of Digoxigenin
1. Wash three times in PBST @RT for 30 mins each [minimum time, can leave overnight each time]
2. Wash twice with Alk Phos Buffer @RT for 5 mins
    a. First wash without levimasole, and then add in levimasole for second wash
3. For every mL of Alk Phos buffer add 20ul of NBT/BCIP solution.
4. Develop in the dark for 0.5-20 hours and check frequently for development
    a. Immerse slides in PBST to pause development, and switch back to NBT/BCIP to continue development later as needed
    b. Can develop at 37°C to speed up development, but err on the side of caution as you proceed with the development because you can always continue the development, but you can't unstain the tissue once it's done
    c. You should be checking the scramble probe's staining to make you're your background is not getting too high. The double-DIG labeled probes will develop much faster than single-labled probes

Reagents and Materials for *in situ* hybridization protocol

Materials

- Glass staining trough with slide holder/rack
- Large glass beaker (1-2L, autoclaved)
- Plastic slide mailers
- Stir-bars
- Hybridization chamber: we use the plastic Tupperware-like boxes because they create a tight seal when closed and will not allow evaporation
- Formamide (cheap kind to soak paper towels in hyb. chamber)
- For glass items that cannot be autoclaved or obtained as RNase-free, incubate them overnight in 1% SDS or clean with RNase-ZAP and DEPC-H2O

Tissue Preparation

- 4% PFA in DEPC-PBS
- DEPC PBS = 500ml DEPC bottle + 55mL 10x PBS
- 30% Sucrose in DEPC-PBS, filter sterilized
- Proteinase-K: 5µg/ml final working concentration
    - Roche 03115879001, UCSF CCF ROCZR160
    - Resuspend in DEPC-PBS

Acetylation

Makes ~500mL, scale up as needed:

6.8mL	Triethanolamine
900ul	Conc. HCl
1280ul	Acetic anhydride
500mL	DEPC-H2O

Hybridization Buffer

25mL	Formamide (Ambion AM9342)
12.5mL	20x SSC
0.5mL	500mM EDTA
1mL	50x Denhardts
50ul	Tween-20
100ul	50ug/ul Heparin
500ul	100ug/ul CHAPS
1mL	50mg/ml torula RNA
10mL	DEPC-H2O

Stringency Washes and Antibody Incubation

- 20x SSC, Invitrogen 4L box from UCSF CCF is fine
- PBST = D-PBS (UCSF CCF: CCFAL003) w/ 0.1% Tween-20 (500ul into 500mL bottle)
- Goat Serum
- Anti-DIG-AP (UCSF CCF ROCZR223)

Visualization of Digoxigenin

- Alkaline Phosphatase buffer:
  100mM Tris pH9.5
  50mM MgCl2
  100mM NaCl
  0.1% Tween-20
- Levimasole (Sigma L9756 tetramisole hydrochloride), use 1-2mM final
  - Dissolve 250mg in 10.38mL diH2O for 100mM stock, stable ~1 mo. at 4°C
- NBT/BCIP solution (UCSF CCF ROCZR263)

Immunofluorescence: Aire, Cytokeratins, and tdTomato

Prepare Tissue

1. Harvest thymi carefully so as not to squeeze the tissue and create internal creases and tears of epithelial tissue
2. If there is no cytosolic protein to detect, freeze down thymi in OCT
   a. For cytosolic proteins such as RFP (driven by the Rosa26 in many of our fate-mapping lines), it is critical to harvest thymi into 2% PFA
   b. Harvest into 5mL of 2% in a 15mL conical
   c. Wrap tubes in foil and lay them horizontally on the cold room rocker for 2-3 hours
   d. Pour off the PFA and quickly rinse tissue in PBS
   e. Transfer tissue to 30% Sucrose/PBS solution and return to the cold room rocker for 2-3 hours
   f. For the last hour, transfer tubes to the 4-degree fridge in a vertical orientation so you can see whether the thymi are still floating, or whether they have equilibrated with the sucrose and sink to the bottom
   g. Pour off sucrose solution once equilibrated and freeze down in OCT
3. Use cryostat to cut 8µm sections and air dry for about 30 minutes.
4. For "standard" staining which do not require PFA perfusion (Aire, K5, K8, etc.), fix the slides now in ice-cold 100% Acetone (Stored in Coplin Jar in the -20) for 10 minutes.
5. Air dry slides for 1 hour after fixation.
6. Can either use immediately or store in -80 for later use. Can also store in 4-degree fridge to be used within a day.

Antibody Staining

1. If removing slides from freezer, air dry for 30 mins.
2. Clean off the excess OCT from the edges of the slide and use the ImmunoPen to draw a boundary around each section.
3. Once the pen has dried, wash in PBS for 3 x 5 mins to remove excess OCT.

4. Block sections in 10% Goat serum in PBS.

5. Place slides in humid staining chamber. Incubate 30 min at RT.

6. Dilute primary antibodies in 3%BSA/PBS.

7. Add antibody mix to the slides in a 1:1 ratio. Incubate for 1 hour at RT or overnight in the cold room.

8. Wash 3 x 5 mins with PBS.

9. Dilute secondary antibodies in 3%BSA/PBS. Add antibody mix to slides and incubate 45-60 min at RT, covered and protected from light.

10. Wash 2 x 5 mins with PBS.

    a. Add 1:2000 dilution of DAPI in PBS to the slides, incubate 5 mins at RT (optional)

11. Wash 1 x 5 mins with PBS.

12. Mount slides using CalBiochem FluorSave reagent and coverslips.

Antibodies

Rabbit anti-DsRed (Clontech, Living colors DsRed polyclonal, 632496)- 1:500 final

Rat Anti-Aire unconjugated (eBioscience, clone 5H12, 14-5934-82)- 1:200 final

Rabbit anti-K5 (abcam, ab53121)- 1:500 – 1:1000 final

Chicken anti-K8 (abcam, ab107115) 1:500 final

Secondaries: all are goat antibodies from Invitrogen, all used 1:500 final

Preparation of Splenocytes for Adoptive Transfer

Reagents

DMEM (High glucose)

ACK lysis buffer

HBSS

Anti-CD25 hybridoma supernatant (clone 7D4)

Rabbit Complement, 3-4wk old (Pel-Freeze Biologicals, 31061-3)

1. Set up Petri dishes with a cell strainer and 5mL DMEM.
2. Harvest 2-3 donor spleens per Petri dish. Transfer everything from bench to the cell culture hood.
3. In hood, use the base of a syringe to mash the spleens. Mix vigorously to disrupt any clumps and transfer solution to a 15mL conical. Wash the dish with another 5mL DMEM and transfer.
4. Spin down tubes 1200 rpm for 5 min at 4ºC
5. Carefully aspirate supernatant and add 2mL sterile ACK lysis buffer. Incubate at RT for a few minutes with gentle agitation until RBC lysis is evident.
6. Add 8mL of sterile DMEM to quench the reaction and spin down.
7. Resuspend cells in 2mL DMEM (without FCS).
    a. Remove a small aliquot for FACS analysis of pre-depletion cells
8. Add 2 mL of anti-CD25 supe. Incubate on ice 25 min, mixing every 5 min.
    a. Place 10mL sterile DMEM into 37ºC water bath to pre-heat
9. Add 10mL pre-warmed DMEM and 1mL Rabbit Complement to cells. Incubate in either 37ºC incubator with rotator, or in 37ºC water bath for 50 min. If using water bath invert the tubes every 5 min.
10. Spin down cells after 50 min incubation.
11. Resuspend in 10mL HBSS, pass cells through a cell strainer
12. Spin down cells again, resuspend in 10mL HBSS.

      a. Take aliquots for counting and FACS analysis.

13. Spin down cells again and resuspent in desired volume of HBSS for injections

14. For injections, anesthetize mice using 50-70uL Ketamine/Xylaxine intramuscularly

      a. Inject 100-200uL cells via retro-orbital injection using an insulin syringe

References

1   Starr, T. K., Jameson, S. C. and Hogquist, K. A., Positive and negative selection of T cells. *Annu Rev Immunol* 2003. 21: 139-176.

2   Petrie, H. T. and Zuniga-Pflucker, J. C., Zoned out: functional mapping of stromal signaling microenvironments in the thymus. *Annu Rev Immunol* 2007. 25: 649-679.

3   Fehling, H. J., Krotkova, A., Saint-Ruf, C. and von Boehmer, H., Crucial role of the pre-T-cell receptor alpha gene in development of alpha beta but not gamma delta T cells. *Nature* 1995. 375: 795-798.

4   Rothenberg, E. V. and Dionne, C. J., Lineage plasticity and commitment in T-cell development. *Immunol Rev* 2002. 187: 96-115.

5   Sebzda, E., Mariathasan, S., Ohteki, T., Jones, R., Bachmann, M. F. and Ohashi, P. S., Selection of the T cell repertoire. *Annu Rev Immunol* 1999. 17: 829-874.

6   von Boehmer, H., Positive selection of lymphocytes. *Cell* 1994. 76: 219-228.

7   Hinterberger, M., Aichinger, M., Prazeres da Costa, O., Voehringer, D., Hoffmann, R. and Klein, L., Autonomous role of medullary thymic epithelial cells in central CD4(+) T cell tolerance. *Nat Immunol* 2010. 11: 512-519.

8   Gallegos, A. M. and Bevan, M. J., Central tolerance to tissue-specific antigens mediated by direct and indirect antigen presentation. *J Exp Med* 2004. 200: 1039-1049.

9   Millet, V., Naquet, P. and Guinamard, R. R., Intercellular MHC transfer between thymic epithelial and dendritic cells. *Eur J Immunol* 2008. 38: 1257-1263.

10   Koble, C. and Kyewski, B., The thymic medulla: a unique microenvironment for intercellular self-antigen transfer. *J Exp Med* 2009. 206: 1505-1513.

11   Liston, A., Lesage, S., Wilson, J., Peltonen, L. and Goodnow, C. C., Aire regulates negative selection of organ-specific T cells. *Nat Immunol* 2003. 4: 350-354.

12   Anderson, M. S., Venanzi, E. S., Chen, Z., Berzins, S. P., Benoist, C. and Mathis, D., The cellular mechanism of Aire control of T cell tolerance. *Immunity* 2005. 23: 227-239.

13   DeVoss, J., Hou, Y., Johannes, K., Lu, W., Liou, G. I., Rinn, J., Chang, H. et al., Spontaneous autoimmunity prevented by thymic expression of a single self-antigen. *J Exp Med* 2006. 203: 2727-2735.

14   Shum, A. K., DeVoss, J., Tan, C. L., Hou, Y., Johannes, K., O'Gorman, C. S., Jones, K. D. et al., Identification of an autoantigen demonstrates a link between interstitial lung disease and a defect in central tolerance. *Sci Transl Med* 2009. 1: 9ra20.

15   Taniguchi, R. T., DeVoss, J. J., Moon, J. J., Sidney, J., Sette, A., Jenkins, M. K. and Anderson, M. S., Detection of an autoreactive T-cell population within the polyclonal repertoire that undergoes distinct autoimmune regulator (Aire)-mediated selection. *Proc Natl Acad Sci U S A* 2012. 109: 7847-7852.

16   Malchow, S., Leventhal, D. S., Nishi, S., Fischer, B. I., Shen, L., Paner, G. P., Amit, A. S. et al., Aire-dependent thymic development of tumor-associated regulatory T cells. *Science* 2013. 339: 1219-1224.

17   DeVoss, J. J., LeClair, N. P., Hou, Y., Grewal, N. K., Johannes, K. P., Lu, W., Yang, T. et al., An autoimmune response to odorant binding protein 1a is associated with dry eye in the Aire-deficient mouse. *J Immunol* 2010. 184: 4236-4246.

18   Derbinski, J., Schulte, A., Kyewski, B. and Klein, L., Promiscuous gene expression in medullary thymic epithelial cells mirrors the peripheral self. *Nat Immunol* 2001. 2: 1032-1039.

19   Aschenbrenner, K., D'Cruz, L. M., Vollmann, E. H., Hinterberger, M., Emmerich, J., Swee, L. K., Rolink, A. and Klein, L., Selection of Foxp3+ regulatory T cells specific for self antigen expressed and presented by Aire+ medullary thymic epithelial cells. *Nat Immunol* 2007. 8: 351-358.

20   Heino, M., Peterson, P., Sillanpaa, N., Guerin, S., Wu, L., Anderson, G., Scott, H. S. et al., RNA and protein expression of the murine autoimmune regulator gene (Aire) in normal, RelB-deficient and in NOD mouse. *Eur J Immunol* 2000. 30: 1884-1893.

21   Weih, F., Carrasco, D., Durham, S. K., Barton, D. S., Rizzo, C. A., Ryseck, R. P., Lira, S. A. and Bravo, R., Multiorgan inflammation and hematopoietic abnormalities in mice with a targeted disruption of RelB, a member of the NF-kappa B/Rel family. *Cell* 1995. 80: 331-340.

22   Burkly, L., Hession, C., Ogata, L., Reilly, C., Marconi, L. A., Olson, D., Tizard, R. et al., Expression of relB is required for the development of thymic medulla and dendritic cells. *Nature* 1995. 373: 531-536.

23   Danzl, N. M., Jeong, S., Choi, Y. and Alexandropoulos, K., Identification of Novel Thymic Epithelial Cell Subsets Whose Differentiation Is Regulated by RANKL and Traf6. *PLoS One* 2014. 9: e86129.

24   Akiyama, T., Maeda, S., Yamane, S., Ogino, K., Kasai, M., Kajiura, F., Matsumoto, M. and Inoue, J., Dependence of self-tolerance on TRAF6-directed development of thymic stroma. *Science* 2005. 308: 248-251.

25   Bonito, A. J., Aloman, C., Fiel, M. I., Danzl, N. M., Cha, S., Weinstein, E. G., Jeong, S. et al., Medullary thymic epithelial cell depletion leads to autoimmune hepatitis. *J Clin Invest* 2013. 123: 3510-3524.

26   Consortium, F.-G. A., An autoimmune disease, APECED, caused by mutations in a novel gene featuring two PHD-type zinc-finger domains. *Nat Genet* 1997. 17: 399-403.

27   Nagamine, K., Peterson, P., Scott, H. S., Kudoh, J., Minoshima, S., Heino, M., Krohn, K. J. et al., Positional cloning of the APECED gene. *Nat Genet* 1997. 17: 393-398.

28   Waterfield, M. and Anderson, M. S., Clues to immune tolerance: the monogenic autoimmune syndromes. *Ann N Y Acad Sci* 2010. 1214: 138-155.

29   Zuklys, S., Balciunaite, G., Agarwal, A., Fasler-Kan, E., Palmer, E. and Hollander, G. A., Normal thymic architecture and negative selection are associated with Aire expression, the gene defective in the autoimmune-

polyendocrinopathy-candidiasis-ectodermal dystrophy (APECED). *J Immunol* 2000. 165: 1976-1983.

30   Heino, M., Peterson, P., Kudoh, J., Nagamine, K., Lagerstedt, A., Ovod, V., Ranki, A. et al., Autoimmune regulator is expressed in the cells regulating immune tolerance in thymus medulla. *Biochem Biophys Res Commun* 1999. 257: 821-825.

31   Ramsey, C., Winqvist, O., Puhakka, L., Halonen, M., Moro, A., Kampe, O., Eskelin, P. et al., Aire deficient mice develop multiple features of APECED phenotype and show altered immune response. *Hum Mol Genet* 2002. 11: 397-409.

32   Anderson, M. S., Venanzi, E. S., Klein, L., Chen, Z., Berzins, S. P., Turley, S. J., von Boehmer, H. et al., Projection of an immunological self shadow within the thymus by the aire protein. *Science* 2002. 298: 1395-1401.

33   Shum, A. K., Alimohammadi, M., Tan, C. L., Cheng, M. H., Metzger, T. C., Law, C. S., Lwin, W. et al., BPIFB1 is a lung-specific autoantigen associated with interstitial lung disease. *Sci Transl Med* 2013. 5: 206ra139.

34   Gray, D., Abramson, J., Benoist, C. and Mathis, D., Proliferative arrest and rapid turnover of thymic epithelial cells expressing Aire. *J Exp Med* 2007. 204: 2521-2528.

35   Gabler, J., Arnold, J. and Kyewski, B., Promiscuous gene expression and the developmental dynamics of medullary thymic epithelial cells. *Eur J Immunol* 2007. 37: 3363-3372.

36   Derbinski, J., Gabler, J., Brors, B., Tierling, S., Jonnakuty, S., Hergenhahn, M., Peltonen, L. et al., Promiscuous gene expression in thymic epithelial cells is regulated at multiple levels. *J Exp Med* 2005. 202: 33-45.

37   Metzger, T. C., Khan, I. S., Gardner, J. M., Mouchess, M. L., Johannes, K. P., Krawisz, A. K., Skrzypczynska, K. M. and Anderson, M. S., Lineage tracing and cell ablation identify a post-Aire-expressing thymic epithelial cell population. *Cell Rep* 2013. 5: 166-179.

38   Nishikawa, Y., Nishijima, H., Matsumoto, M., Morimoto, J., Hirota, F., Takahashi, S., Luche, H. et al., Temporal Lineage Tracing of Aire-Expressing Cells Reveals a Requirement for Aire in Their Maturation Program. *J Immunol* 2014.

39   Wang, X., Laan, M., Bichele, R., Kisand, K., Scott, H. S. and Peterson, P., Post-Aire maturation of thymic medullary epithelial cells involves selective expression of keratinocyte-specific autoantigens. *Front Immunol* 2012. 3: 19.

40   Naspetti, M., Aurrand-Lions, M., DeKoning, J., Malissen, M., Galland, F., Lo, D. and Naquet, P., Thymocytes and RelB-dependent medullary epithelial cells provide growth-promoting and organization signals, respectively, to thymic medullary stromal cells. *Eur J Immunol* 1997. 27: 1392-1397.

41   Surh, C. D., Ernst, B. and Sprent, J., Growth of epithelial cells in the thymic medulla is under the control of mature T cells. *J Exp Med* 1992. 176: 611-616.

42   Shores, E. W., Van Ewijk, W. and Singer, A., Disorganization and restoration of thymic medullary epithelial cells in T cell receptor-negative scid mice: evidence

that receptor-bearing lymphocytes influence maturation of the thymic microenvironment. *Eur J Immunol* 1991. 21: 1657-1661.

43   Negishi, I., Motoyama, N., Nakayama, K., Nakayama, K., Senju, S., Hatakeyama, S., Zhang, Q. et al., Essential role for ZAP-70 in both positive and negative selection of thymocytes. *Nature* 1995. 376: 435-438.

44   Ueno, T., Saito, F., Gray, D. H., Kuse, S., Hieshima, K., Nakano, H., Kakiuchi, T. et al., CCR7 signals are essential for cortex-medulla migration of developing thymocytes. *J Exp Med* 2004. 200: 493-505.

45   Kurobe, H., Liu, C., Ueno, T., Saito, F., Ohigashi, I., Seach, N., Arakaki, R. et al., CCR7-dependent cortex-to-medulla migration of positively selected thymocytes is essential for establishing central tolerance. *Immunity* 2006. 24: 165-177.

46   Nitta, T., Nitta, S., Lei, Y., Lipp, M. and Takahama, Y., CCR7-mediated migration of developing thymocytes to the medulla is essential for negative selection to tissue-restricted antigens. *Proc Natl Acad Sci U S A* 2009. 106: 17129-17133.

47   Hikosaka, Y., Nitta, T., Ohigashi, I., Yano, K., Ishimaru, N., Hayashi, Y., Matsumoto, M. et al., The cytokine RANKL produced by positively selected thymocytes fosters medullary thymic epithelial cells that express autoimmune regulator. *Immunity* 2008. 29: 438-450.

48   Desanti, G. E., Cowan, J. E., Baik, S., Parnell, S. M., White, A. J., Penninger, J. M., Lane, P. J. et al., Developmentally regulated availability of RANKL and CD40 ligand reveals distinct mechanisms of fetal and adult cross-talk in the thymus medulla. *J Immunol* 2012. 189: 5519-5526.

49   Irla, M., Hugues, S., Gill, J., Nitta, T., Hikosaka, Y., Williams, I. R., Hubert, F. X. et al., Autoantigen-specific interactions with CD4+ thymocytes control mature medullary thymic epithelial cell cellularity. *Immunity* 2008. 29: 451-463.

50   Boehm, T., Scheu, S., Pfeffer, K. and Bleul, C. C., Thymic medullary epithelial cell differentiation, thymocyte emigration, and the control of autoimmunity require lympho-epithelial cross talk via LTbetaR. *J Exp Med* 2003. 198: 757-769.

51   White, A. J., Withers, D. R., Parnell, S. M., Scott, H. S., Finke, D., Lane, P. J., Jenkinson, E. J. and Anderson, G., Sequential phases in the development of Aire-expressing medullary thymic epithelial cells involve distinct cellular input. *Eur J Immunol* 2008. 38: 942-947.

52   Rossi, S. W., Kim, M. Y., Leibbrandt, A., Parnell, S. M., Jenkinson, W. E., Glanville, S. H., McConnell, F. M. et al., RANK signals from CD4(+)3(-) inducer cells regulate development of Aire-expressing epithelial cells in the thymic medulla. *J Exp Med* 2007. 204: 1267-1272.

53   Akiyama, T., Shimo, Y., Yanai, H., Qin, J., Ohshima, D., Maruyama, Y., Asaumi, Y. et al., The tumor necrosis factor family receptors RANK and CD40 cooperatively establish the thymic medullary microenvironment and self-tolerance. *Immunity* 2008. 29: 423-437.

54   Roberts, N. A., White, A. J., Jenkinson, W. E., Turchinovich, G., Nakamura, K., Withers, D. R., McConnell, F. M. et al., Rank signaling links the development of

invariant gammadelta T cell progenitors and Aire(+) medullary epithelium. *Immunity* 2012. 36: 427-437.

55   Boehm, T. and Swann, J. B., Thymus involution and regeneration: two sides of the same coin? *Nat Rev Immunol* 2013. 13: 831-838.

56   Dooley, J. and Liston, A., Molecular control over thymic involution: from cytokines and microRNA to aging and adipose tissue. *Eur J Immunol* 2012. 42: 1073-1079.

57   Sutherland, J. S., Goldberg, G. L., Hammett, M. V., Uldrich, A. P., Berzins, S. P., Heng, T. S., Blazar, B. R. et al., Activation of thymic regeneration in mice and humans following androgen blockade. *J Immunol* 2005. 175: 2741-2753.

58   Tibbetts, T. A., DeMayo, F., Rich, S., Conneely, O. M. and O'Malley, B. W., Progesterone receptors in the thymus are required for thymic involution during pregnancy and for normal fertility. *Proc Natl Acad Sci U S A* 1999. 96: 12021-12026.

59   Zoller, A. L., Schnell, F. J. and Kersh, G. J., Murine pregnancy leads to reduced proliferation of maternal thymocytes and decreased thymic emigration. *Immunology* 2007. 121: 207-215.

60   Anz, D., Thaler, R., Stephan, N., Waibler, Z., Trauscheid, M. J., Scholz, C., Kalinke, U. et al., Activation of melanoma differentiation-associated gene 5 causes rapid involution of the thymus. *J Immunol* 2009. 182: 6044-6050.

61   Dudakov, J. A., Hanash, A. M., Jenq, R. R., Young, L. F., Ghosh, A., Singer, N. V., West, M. L. et al., Interleukin-22 drives endogenous thymic regeneration in mice. *Science* 2012. 336: 91-95.

62   Fletcher, A. L., Lowen, T. E., Sakkal, S., Reiseger, J. J., Hammett, M. V., Seach, N., Scott, H. S. et al., Ablation and regeneration of tolerance-inducing medullary thymic epithelial cells after cyclosporine, cyclophosphamide, and dexamethasone treatment. *J Immunol* 2009. 183: 823-831.

63   Goldberg, G. L., Dudakov, J. A., Reiseger, J. J., Seach, N., Ueno, T., Vlahos, K., Hammett, M. V. et al., Sex steroid ablation enhances immune reconstitution following cytotoxic antineoplastic therapy in young mice. *J Immunol* 2010. 184: 6014-6024.

64   Billard, M. J., Gruver, A. L. and Sempowski, G. D., Acute endotoxin-induced thymic atrophy is characterized by intrathymic inflammatory and wound healing responses. *PLoS One* 2011. 6: e17940.

65   Ross, E. A., Coughlan, R. E., Flores-Langarica, A., Lax, S., Nicholson, J., Desanti, G. E., Marshall, J. L. et al., Thymic function is maintained during Salmonella-induced atrophy and recovery. *J Immunol* 2012. 189: 4266-4274.

66   Purton, J. F., Monk, J. A., Liddicoat, D. R., Kyparissoudis, K., Sakkal, S., Richardson, S. J., Godfrey, D. I. and Cole, T. J., Expression of the glucocorticoid receptor from the 1A promoter correlates with T lymphocyte sensitivity to glucocorticoid-induced cell death. *J Immunol* 2004. 173: 3816-3824.

67   Heng, T. S., Goldberg, G. L., Gray, D. H., Sutherland, J. S., Chidgey, A. P. and Boyd, R. L., Effects of castration on thymocyte development in two different models of thymic involution. *J Immunol* 2005. 175: 2982-2993.

68   Gray, D. H., Seach, N., Ueno, T., Milton, M. K., Liston, A., Lew, A. M., Goodnow, C. C. and Boyd, R. L., Developmental kinetics, turnover, and stimulatory capacity of thymic epithelial cells. *Blood* 2006. 108: 3777-3785.

69   Rode, I. and Boehm, T., Regenerative capacity of adult cortical thymic epithelial cells. *Proc Natl Acad Sci U S A* 2012. 109: 3463-3468.

70   Alpdogan, O., Hubbard, V. M., Smith, O. M., Patel, N., Lu, S., Goldberg, G. L., Gray, D. H. et al., Keratinocyte growth factor (KGF) is required for postnatal thymic regeneration. *Blood* 2006. 107: 2453-2460.

71   Min, D., Taylor, P. A., Panoskaltsis-Mortari, A., Chung, B., Danilenko, D. M., Farrell, C., Lacey, D. L. et al., Protection from thymic epithelial cell injury by keratinocyte growth factor: a new approach to improve thymic and peripheral T-cell reconstitution after bone marrow transplantation. *Blood* 2002. 99: 4592-4600.

72   Blanpain, C., Horsley, V. and Fuchs, E., Epithelial stem cells: turning over new leaves. *Cell* 2007. 128: 445-458.

73   Osada, M., Singh, V. J., Wu, K., Sant'angelo, D. B. and Pezzano, M., Label retention identifies a multipotent mesenchymal stem cell-like population in the postnatal thymus. *PLoS One* 2013. 8: e83024.

74   Tumbar, T., Guasch, G., Greco, V., Blanpain, C., Lowry, W. E., Rendl, M. and Fuchs, E., Defining the epithelial stem cell niche in skin. *Science* 2004. 303: 359-363.

75   Dumont-Lagace, M., Brochu, S., St-Pierre, C. and Perreault, C., Adult Thymic Epithelium Contains Nonsenescent Label-Retaining Cells. *J Immunol* 2014.

76   Rossi, S. W., Jenkinson, W. E., Anderson, G. and Jenkinson, E. J., Clonal analysis reveals a common progenitor for thymic cortical and medullary epithelium. *Nature* 2006. 441: 988-991.

77   Bleul, C. C., Corbeaux, T., Reuter, A., Fisch, P., Monting, J. S. and Boehm, T., Formation of a functional thymus initiated by a postnatal epithelial progenitor cell. *Nature* 2006. 441: 992-996.

78   Bartel, D. P., MicroRNAs: genomics, biogenesis, mechanism, and function. *Cell* 2004. 116: 281-297.

79   Bartel, D. P., MicroRNAs: target recognition and regulatory functions. *Cell* 2009. 136: 215-233.

80   Kim, V. N., Han, J. and Siomi, M. C., Biogenesis of small RNAs in animals. *Nat Rev Mol Cell Biol* 2009. 10: 126-139.

81   Khan, I. S., Taniguchi, R. T., Fasano, K. J., Anderson, M. S. and Jeker, L. T., Canonical microRNAs in thymic epithelial cells promote central tolerance. *Eur J Immunol* 2014.

82   Papadopoulou, A. S., Dooley, J., Linterman, M. A., Pierson, W., Ucar, O., Kyewski, B., Zuklys, S. et al., The thymic epithelial microRNA network elevates the threshold for infection-associated thymic involution via miR-29a mediated suppression of the IFN-alpha receptor. *Nat Immunol* 2012. 13: 181-187.

83   Ucar, O., Tykocinski, L. O., Dooley, J., Liston, A. and Kyewski, B., An evolutionarily conserved mutual interdependence between Aire and microRNAs in promiscuous gene expression. *Eur J Immunol* 2013. 43: 1769-1778.

84   Zuklys, S., Mayer, C. E., Zhanybekova, S., Stefanski, H. E., Nusspaumer, G., Gill, J., Barthlott, T. et al., MicroRNAs control the maintenance of thymic epithelia and their competence for T lineage commitment and thymocyte selection. *J Immunol* 2012. 189: 3894-3904.

85   Kyewski, B. and Klein, L., A central role for central tolerance. *Annu Rev Immunol* 2006. 24: 571-606.

86   Trager, U., Sierro, S., Djordjevic, G., Bouzo, B., Khandwala, S., Meloni, A., Mortensen, M. and Simon, A. K., The immune response to melanoma is limited by thymic selection of self-antigens. *PLoS One* 2012. 7: e35005.

87   Bos, R., van Duikeren, S., van Hall, T., Kaaijk, P., Taubert, R., Kyewski, B., Klein, L. et al., Expression of a natural tumor antigen by thymic epithelial cells impairs the tumor-protective CD4+ T-cell repertoire. *Cancer Res* 2005. 65: 6443-6449.

88   Zhu, M. L., Nagavalli, A. and Su, M. A., Aire deficiency promotes TRP-1-specific immune rejection of melanoma. *Cancer Res* 2013. 73: 2104-2116.

89   Cloosen, S., Arnold, J., Thio, M., Bos, G. M., Kyewski, B. and Germeraad, W. T., Expression of tumor-associated differentiation antigens, MUC1 glycoforms and CEA, in human thymic epithelial cells: implications for self-tolerance and tumor therapy. *Cancer Res* 2007. 67: 3919-3926.

90   Tykocinski, L. O., Sinemus, A. and Kyewski, B., The thymus medulla slowly yields its secrets. *Ann N Y Acad Sci* 2008. 1143: 105-122.

91   Metzger, T. C. and Anderson, M. S., Control of central and peripheral tolerance by Aire. *Immunol Rev* 2011. 241: 89-103.

92   Chen, D. S. and Mellman, I., Oncology meets immunology: the cancer-immunity cycle. *Immunity* 2013. 39: 1-10.

93   Swann, J. B. and Smyth, M. J., Immune surveillance of tumors. *J Clin Invest* 2007. 117: 1137-1146.

94   Kearns, A. E., Khosla, S. and Kostenuik, P. J., Receptor activator of nuclear factor kappaB ligand and osteoprotegerin regulation of bone remodeling in health and disease. *Endocr Rev* 2008. 29: 155-192.

95   Lee, E. N., Park, J. K., Lee, J. R., Oh, S. O., Baek, S. Y., Kim, B. S. and Yoon, S., Characterization of the expression of cytokeratins 5, 8, and 14 in mouse thymic epithelial cells during thymus regeneration following acute thymic involution. *Anat Cell Biol* 2011. 44: 14-24.

96   Su, M. A., Giang, K., Zumer, K., Jiang, H., Oven, I., Rinn, J. L., Devoss, J. J. et al., Mechanisms of an autoimmunity syndrome in mice caused by a dominant mutation in Aire. *J Clin Invest* 2008. 118: 1712-1726.

97   Guerau-de-Arellano, M., Martinic, M., Benoist, C. and Mathis, D., Neonatal tolerance revisited: a perinatal window for Aire control of autoimmunity. *J Exp Med* 2009. 206: 1245-1252.

98   Muranski, P., Boni, A., Antony, P. A., Cassard, L., Irvine, K. R., Kaiser, A., Paulos, C. M. et al., Tumor-specific Th17-polarized cells eradicate large established melanoma. *Blood* 2008. 112: 362-373.

99   Xie, Y., Akpinarli, A., Maris, C., Hipkiss, E. L., Lane, M., Kwon, E. K., Muranski, P. et al., Naive tumor-specific CD4(+) T cells differentiated in vivo eradicate established melanoma. *J Exp Med* 2010. 207: 651-667.

100   Pardoll, D. M., Immunology beats cancer: a blueprint for successful translation. *Nat Immunol* 2012. 13: 1129-1132.

101   Simpson, T. R., Li, F., Montalvo-Ortiz, W., Sepulveda, M. A., Bergerhoff, K., Arce, F., Roddie, C. et al., Fc-dependent depletion of tumor-infiltrating regulatory T cells co-defines the efficacy of anti-CTLA-4 therapy against melanoma. *J Exp Med* 2013. 210: 1695-1710.

102   van Elsas, A., Hurwitz, A. A. and Allison, J. P., Combination immunotherapy of B16 melanoma using anti-cytotoxic T lymphocyte-associated antigen 4 (CTLA-4) and granulocyte/macrophage colony-stimulating factor (GM-CSF)-producing vaccines induces rejection of subcutaneous and metastatic tumors accompanied by autoimmune depigmentation. *J Exp Med* 1999. 190: 355-366.

103   Cummings, S. R., San Martin, J., McClung, M. R., Siris, E. S., Eastell, R., Reid, I. R., Delmas, P. et al., Denosumab for prevention of fractures in postmenopausal women with osteoporosis. *N Engl J Med* 2009. 361: 756-765.

104   Gardner, J. M., Devoss, J. J., Friedman, R. S., Wong, D. J., Tan, Y. X., Zhou, X., Johannes, K. P. et al., Deletional tolerance mediated by extrathymic Aire-expressing cells. *Science* 2008. 321: 843-847.

105   Moon, J. J., Chu, H. H., Hataye, J., Pagan, A. J., Pepper, M., McLachlan, J. B., Zell, T. and Jenkins, M. K., Tracking epitope-specific T cells. *Nat Protoc* 2009. 4: 565-581.

106   Babiarz, J. E., Hsu, R., Melton, C., Thomas, M., Ullian, E. M. and Blelloch, R., A role for noncanonical microRNAs in the mammalian brain revealed by phenotypic differences in Dgcr8 versus Dicer1 knockouts and small RNA sequencing. *RNA* 2011. 17: 1489-1501.

107   Babiarz, J. E., Ruby, J. G., Wang, Y., Bartel, D. P. and Blelloch, R., Mouse ES cells express endogenous shRNAs, siRNAs, and other Microprocessor-independent, Dicer-dependent small RNAs. *Genes Dev* 2008. 22: 2773-2785.

108   Suh, N., Baehner, L., Moltzahn, F., Melton, C., Shenoy, A., Chen, J. and Blelloch, R., MicroRNA function is globally suppressed in mouse oocytes and early embryos. *Curr Biol* 2010. 20: 271-277.

109   Baumjohann, D., Kageyama, R., Clingan, J. M., Morar, M. M., Patel, S., de Kouchkovsky, D., Bannard, O. et al., The microRNA cluster miR-17~92 promotes TFH cell differentiation and represses subset-inappropriate gene expression. *Nat Immunol* 2013. 14: 840-848.

110   Jeker, L. T. and Bluestone, J. A., Small RNA regulators of T cell-mediated autoimmunity. *J Clin Immunol* 2010. 30: 347-357.

111   Jeker, L. T. and Bluestone, J. A., MicroRNA regulation of T-cell differentiation and function. *Immunol Rev* 2013. 253: 65-81.

112   Jeker, L. T., Zhou, X., Blelloch, R. and Bluestone, J. A., DGCR8-Mediated Production of Canonical Micrornas Is Critical for Regulatory T Cell Function and Stability. *PLoS One* 2013. 8: e66282.

113   Zhou, X., Jeker, L. T., Fife, B. T., Zhu, S., Anderson, M. S., McManus, M. T. and Bluestone, J. A., Selective miRNA disruption in T reg cells leads to uncontrolled autoimmunity. *J Exp Med* 2008. 205: 1983-1991.

114   Rao, P. K., Toyama, Y., Chiang, H. R., Gupta, S., Bauer, M., Medvid, R., Reinhardt, F. et al., Loss of cardiac microRNA-mediated regulation leads to dilated cardiomyopathy and heart failure. *Circ Res* 2009. 105: 585-594.

115   Gordon, J., Xiao, S., Hughes, B., 3rd, Su, D. M., Navarre, S. P., Condie, B. G. and Manley, N. R., Specific expression of lacZ and cre recombinase in fetal thymic epithelial cells by multiplex gene targeting at the Foxn1 locus. *BMC Dev Biol* 2007. 7: 69.

116   Klug, D. B., Carter, C., Gimenez-Conti, I. B. and Richie, E. R., Cutting edge: thymocyte-independent and thymocyte-dependent phases of epithelial patterning in the fetal thymus. *J Immunol* 2002. 169: 2842-2845.

117   Jeker, L. T., Barthlott, T., Keller, M. P., Zuklys, S., Hauri-Hohl, M., Deng, C. X. and Hollander, G. A., Maintenance of a normal thymic microenvironment and T-cell homeostasis require Smad4-mediated signaling in thymic epithelial cells. *Blood* 2008. 112: 3688-3695.

118   Nurieva, R. I., Liu, X. and Dong, C., Molecular mechanisms of T-cell tolerance. *Immunol Rev* 2011. 241: 133-144.

119   Hogquist, K. A., Baldwin, T. A. and Jameson, S. C., Central tolerance: learning self-control in the thymus. *Nat Rev Immunol* 2005. 5: 772-782.

120   Hanahan, D., Peripheral-antigen-expressing cells in thymic medulla: factors in self-tolerance and autoimmunity. *Curr Opin Immunol* 1998. 10: 656-662.

121   Rothenberg, E. V. and Taghon, T., Molecular genetics of T cell development. *Annu Rev Immunol* 2005. 23: 601-649.

122   Park, C. Y., Jeker, L. T., Carver-Moore, K., Oh, A., Liu, H. J., Cameron, R., Richards, H. et al., A resource for the conditional ablation of microRNAs in the mouse. *Cell Rep* 2012. 1: 385-391.

123   Siomi, H. and Siomi, M. C., Posttranscriptional regulation of microRNA biogenesis in animals. *Mol Cell* 2010. 38: 323-332.

124   Yano, M., Kuroda, N., Han, H., Meguro-Horike, M., Nishikawa, Y., Kiyonari, H., Maemura, K. et al., Aire controls the differentiation program of thymic epithelial cells in the medulla for the establishment of self-tolerance. *J Exp Med* 2008. 205: 2827-2838.

125   Matsumoto, M., Contrasting models for the roles of Aire in the differentiation program of epithelial cells in the thymic medulla. *Eur J Immunol* 2011. 41: 12-17.

126   Gregory, P. A., Bert, A. G., Paterson, E. L., Barry, S. C., Tsykin, A., Farshid, G., Vadas, M. A. et al., The miR-200 family and miR-205 regulate epithelial to mesenchymal transition by targeting ZEB1 and SIP1. *Nat Cell Biol* 2008. 10: 593-601.

127   Gregory, P. A., Bracken, C. P., Bert, A. G. and Goodall, G. J., MicroRNAs as regulators of epithelial-mesenchymal transition. *Cell Cycle* 2008. 7: 3112-3118.

128   Matsushima, K., Isomoto, H., Yamaguchi, N., Inoue, N., Machida, H., Nakayama, T., Hayashi, T. et al., MiRNA-205 modulates cellular invasion and migration via regulating zinc finger E-box binding homeobox 2 expression in esophageal squamous cell carcinoma cells. *J Transl Med* 2011. 9: 30.

129   Sleeman, J. P. and Thiery, J. P., SnapShot: The epithelial-mesenchymal transition. *Cell* 2011. 145: 162 e161.

130   Savagner, P., Leaving the neighborhood: molecular mechanisms involved during epithelial-mesenchymal transition. *Bioessays* 2001. 23: 912-923.

131   Hamazaki, Y., Fujita, H., Kobayashi, T., Choi, Y., Scott, H. S., Matsumoto, M. and Minato, N., Medullary thymic epithelial cells expressing Aire represent a unique lineage derived from cells expressing claudin. *Nat Immunol* 2007. 8: 304-311.

132   Park, C. Y., Choi, Y. S. and McManus, M. T., Analysis of microRNA knockouts in mice. *Hum Mol Genet* 2010. 19: R169-175.

133   Bandiera, S., Hatem, E., Lyonnet, S. and Henrion-Caude, A., microRNAs in diseases: from candidate to modifier genes. *Clin Genet* 2010. 77: 306-313.

134   Sayed, D. and Abdellatif, M., MicroRNAs in development and disease. *Physiol Rev* 2011. 91: 827-887.

135   Leung, A. K. and Sharp, P. A., MicroRNA functions in stress responses. *Mol Cell* 2010. 40: 205-215.

136   Mendell, J. T. and Olson, E. N., MicroRNAs in stress signaling and human disease. *Cell* 2012. 148: 1172-1187.

137   Dar, A. A., Majid, S., de Semir, D., Nosrati, M., Bezrookove, V. and Kashani-Sabet, M., miRNA-205 suppresses melanoma cell proliferation and induces senescence via regulation of E2F1 protein. *J Biol Chem* 2011. 286: 16606-16614.

138   Xie, H., Zhao, Y., Caramuta, S., Larsson, C. and Lui, W. O., miR-205 expression promotes cell proliferation and migration of human cervical cancer cells. *PLoS One* 2012. 7: e46990.

139   Greene, S. B., Gunaratne, P. H., Hammond, S. M. and Rosen, J. M., A putative role for microRNA-205 in mammary epithelial cell progenitors. *J Cell Sci* 2010. 123: 606-618.

140   Gandellini, P., Folini, M., Longoni, N., Pennati, M., Binda, M., Colecchia, M., Salvioni, R. et al., miR-205 Exerts tumor-suppressive functions in human prostate through down-regulation of protein kinase Cepsilon. *Cancer Res* 2009. 69: 2287-2295.

141   Nitta, T., Ohigashi, I., Nakagawa, Y. and Takahama, Y., Cytokine crosstalk for thymic medulla formation. *Curr Opin Immunol* 2011. 23: 190-197.

142   Farmer, D. T., Shariat, N., Park, C. Y., Liu, H. J., Mavropoulos, A. and McManus, M. T., Partially penetrant postnatal lethality of an epithelial specific MicroRNA in a mouse knockout. *PLoS One* 2013. 8: e76634.
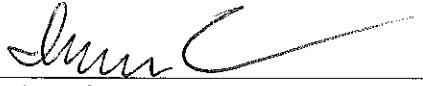
143   Ryan, D. G., Oliveira-Fernandes, M. and Lavker, R. M., MicroRNAs of the mammalian eye display distinct and overlapping tissue specificity. *Mol Vis* 2006. 12: 1175-1184.

144   Yi, R., O'Carroll, D., Pasolli, H. A., Zhang, Z., Dietrich, F. S., Tarakhovsky, A. and Fuchs, E., Morphogenesis in skin is governed by discrete sets of differentially expressed microRNAs. *Nat Genet* 2006. 38: 356-362.

145   Balciunaite, G., Keller, M. P., Balciunaite, E., Piali, L., Zuklys, S., Mathieu, Y. D., Gill, J. et al., Wnt glycoproteins regulate the expression of FoxN1, the gene defective in nude mice. *Nat Immunol* 2002. 3: 1102-1108.

146   Nowell, C. S., Bredenkamp, N., Tetelin, S., Jin, X., Tischner, C., Vaidya, H., Sheridan, J. M. et al., Foxn1 regulates lineage progression in cortical and medullary thymic epithelial cells but is dispensable for medullary sublineage divergence. *PLoS Genet* 2011. 7: e1002348.

147   Seach, N., Wong, K., Hammett, M., Boyd, R. L. and Chidgey, A. P., Purified enzymes improve isolation and characterization of the adult thymic epithelium. *J Immunol Methods* 2012. 385: 23-34.

148   Jeker, L. T., Zhou, X., Gershberg, K., de Kouchkovsky, D., Morar, M. M., Stadthagen, G., Lund, A. H. and Bluestone, J. A., MicroRNA 10a marks regulatory T cells. *PLoS One* 2012. 7: e36684.

Publishing Agreement

It is the policy of the University to encourage the distribution of all theses, dissertations, and manuscripts. Copies of all UCSF theses, dissertations, and manuscripts will be routed to the library via the Graduate Division. The library will make all theses, dissertations, and manuscripts accessible to the public and will preserve these to the best of their abilities, in perpetuity.

Please sign the following statement:

I hereby grant permission to the Graduate Division of the University of California, San Francisco to release copies of my thesis, dissertation, or manuscript to the Campus Library to provide access and preservation, in whole or in part, in perpetuity.

_____   3/20/14
Author Signature   Date